Nickel-Oxide-Based Electrodes for Energy Storage Applications

by

Abraham Gomez Vidales

A thesis submitted to McGill University in partial fulfillment of the requirements of the degree of Doctor of Philosophy

at

Department of Chemical Engineering
McGill University
Montreal, Canada
March 2019

"When the world says: "give up,"
Hope whispers: "try it one more time."

Dedicated to María Guadalupe Vidales Ramos and Paulino Gómez González, the people who have taught me good and bad, how to win, how to lose, how to love, how to keep going, how to achieve my dreams. My parents. I'm so thankful that God chose you to bring me into this world.

Abstract

This Ph.D. thesis presents a comprehensive study on the use of nickel-oxide-based electrodes for energy storage applications, focusing specifically on cathodes for production of hydrogen by water electrolysis and electrodes for electrochemical supercapacitors. The main objective of this research was to develop Ni-oxide-based materials (Ni-Co-oxide, Ni-Mo-oxide, and Ni-Mo-Ir-oxide) to achieve (i) high electrocatalytic activity and long-term performance stability in the hydrogen evolution reaction (HER), and (ii) high energy storage capacity under various operating conditions (i.e. metal oxide composition, electrolyte type, pH, and temperature).

The Ni-oxide based coatings of various compositions were fabricated on a titanium substrate through a thermal-salt decomposition method. The coatings were characterized by several surface-characterization techniques, such as X-ray photoelectron spectroscopy (XPS), energy dispersive spectroscopy (EDS), X-ray diffraction (XRD), and scanning electron microscopy (SEM), to know their chemical composition, structure, and morphology. At the same time, electrochemical techniques such as linear Tafel polarization (LTP), cyclic voltammetry (CV), chronoamperometry (CA), chronopotentiometry (CP), and galvanostatic charge-discharge (GCD) were employed to determine their electrochemical activity, active surface area, long-term stability, and charge-discharge capacity.

First, the electrocatalytic activity of Ni-Co-oxide cathodes of various compositions for HER in acidic and alkaline media was studied. The electrodes were found to be of a semi-crystalline structure, yielding a surface morphology characterized by a relatively high surface roughness factor (up to 25). The $Ni_{0.2}Co_{0.8}$-oxide was identified as the best electrode material candidate, due to the surface-area effect. Furthermore, it showed a significantly higher electrocatalytic stability compared to Ni. However, its intrinsic activity was found to be lower than that of the control sample (pure metal nickel).

The electrocatalytic properties of Ni-Mo-oxides for hydrogen production in acidic, alkaline, and neutral electrolytes were studied next. These oxides showed a better performance than pure nickel, and they were stable in the whole pH scale, even during long-term electrolysis in an acidic medium. The most extrinsically active coating was found to be $Ni_{0.6}Mo_{0.4}$-oxide (in all three electrolytes), and this coating showed the highest intrinsic activity in the neutral electrolyte. In the acidic and alkaline electrolytes, the $Ni_{0.8}Mo_{0.2}$-oxide coating was found to be the most intrinsically active. This superior performance was attributed to an increase in the electrochemically active surface area, as well as the electrochemical activity of the material.

Considering the excellent results obtained with the Ni-Mo-oxide electrodes (specifically the $Ni_{0.6}$-$Mo_{0.4}$-oxide coating, which was the best performing composition), the addition of iridium (an excellent but expensive catalyst) was investigated for hydrogen production and in the development of electrodes for supercapacitors.

In all the cases, the Ni-Mo-Ir-oxide showed a better performance in an acidic medium when compared to nickel for HER. These results were attributed to both the increase of surface area and a possible modification of the electronic structure of the coatings. In addition, deactivation/re-activation experiments were done in the presence of the most common impurities found in commercial electrolytes during hydrogen production (Cu, Fe, Cu + Fe). These experiments showed that the Ni-Mo-Ir- electrodes were much more resistant to deactivation and can be, in addition, reactivated to a higher activity degree than pure nickel cathodes.

Finally, Ni-Mo-Ir-oxides electrodes were employed as electrodes for electrochemical supercapacitors. The electrodes yielded a high specific capacitance, excellent cycling stability, and a fast charge-discharge rate in both acidic and alkaline environments. The highest capacitance (108 ± 2 $mF\,cm^{-2}$) was obtained for the composition containing 40 mol.% of Ir ($Ni_{0.36}Mo_{0.24}Ir_{0.4}$-oxide coating). This composition was also found to retain ca. 86% of its initial capacitance after 2500 charging/discharging cycles.

Based on the results of this thesis, it was concluded that nickel-oxide-based electrodes are excellent candidates for alternative electrochemical energy storage systems (hydrogen production by water electrolysis and electricity storage in supercapacitors).

Abrégé

Cette thèse présente une étude compréhensive de l'utilisation d'électrodes d'oxyde de nickel pour des applications de stockage d'énergie, en se concentrant spécifiquement sur des cathodes pour la production d'hydrogène par l'électrolyse de l'eau et des électrodes pour des supercondensateurs électrochimiques. L'objectif de cette recherche est de développer des matériaux à base de Ni-oxyde (Ni-Co-oxyde, Ni-Mo-oxyde, et Ni-Mo-Ir-oxyde) pour obtenir (i) une haute activité électrocatalytique et une stabilité à long terme dans la performance de la réaction de dégagement d'hydrogène (HER), et (ii) une haute capacité de stockage d'énergie dans une variété de conditions d'opération (c'est à dire, composition d'oxyde métallique, type d'électrolyte, pH, et température).

Les différentes variétés de couches à base d'oxyde de nickel ont été fabriqué sur un substrat de titanium en utilisant une méthode de décomposition de sel thermique. Les couches ont été caractérisé par plusieurs techniques de caractérisation de surface, tel que la spectroscopie de photoélectrons X (XPS), la spectroscopie dispersive d'énergie (EDS), la diffractions de rayons X (XRD), et la microscopie électronique à balayage (SEM), pour connaître leur composition chimique, structure, et morphologie. En même temps, des techniques électrochimiques, tel que la polarisation linéaire de Tafel (LTP), voltampérométrie cyclique (CV), chronoampérométrie (CA), chronopotentiométrie (CP), et la décharge galvanostatique (GCD) ont été employé pour déterminer l'activité électrochimique, la surface active, la stabilité à long terme, et la capacité de charge-décharge des couches.

En premier, l'activité électrocatalytique de cathodes de différentes variétés de Ni-Co-oxyde pour la HER a été étudié dans des médias acides et alcalins. Les électrodes se sont révélés être d'une structure semi-crystalline, donnant une morphologie de surface caractérisé par un facteur de rugosité plutôt élevé (jusqu'à 25). Le $Ni_{0.2}Co_{0.8}$-oxyde a été identifié comme le meilleure candidat de matériel d'électrode, ce qui est liée à l'effet de

surface. De plus, il a montré une stabilité éléctrocatalytique beaucoup plus élevé que celle des autres matériaux. Cependant, son activité intrinsèque s'est révélé être bien plus basse que celle de l'échantillon de contrôle (un métal de nickel pure).

Les propriétés électrocatalytiques de Ni-Mo-oxyde pour la production d'hydrogène dans des électrolytes acides, alcalis et neutres ont ensuite été étudiées. Ces oxydes ont démontré de meilleures performances que le nickel pur, ainsi qu'une stabilité sur toute l'échelle de pH, même pendant l'électrolyses à long terme dans des médias acides. La recherche a démontré que le revêtement le plus extrinsèquement actif était le $Ni_{0.6}Mo_{0.4}$-oxyde (dans les trois cas d'électrolytes). De plus, ce revêtement avait la plus haute activité intrinsèque dans l'électrolyte neutre. Dans les électrolytes acides et alcalis, le revêtement de $Ni_{0.8}Mo_{0.2}$-oxyde a démontré la plus haute activité intrinsèque. Cette performance supérieure a été attribuée à une augmentation de la surface électrochimiquement active, ainsi que l'activité électrochimique du matériel.

Considérant les excellents résultats obtenus avec les électrodes de Ni-Mo-oxyde (spécifiquement le revêtement de $Ni_{0.6}$-$Mo_{0.4}$-oxiyde qui a démontré la meilleur performance) , l'ajout d'iridium (un excellent mais dispendieux catalyste) a été étudié pour la production d'hydrogène et le development d'electrodes de supercondensateurs.

Dans tous les cas, les électrodes de Ni-Mo-Ir-oxyde ont démontré de meilleures performances dans des électrolytes acides comparées aux électrodes de nickel pur pour la RDH. Ces résultats ont été attribué à une augmentation de la surface des électrodes ainsi que la modification possible de la structure électronique des revêtements. De plus, des expériences de désactivation/réactivation ont été entreprises en présence des impuretés les plus communes dans les électrolytes commerciaux utilisés pour la production d'hydrogène (Cu, Fe, Cu + Fe). Ces expériences ont démontré que l'ajout d'iridium aux revêtements augmente la résistance à la désactivation et améliore la réactivation des cathodes comparé au contrôle.

Finalement, des électrodes de Ni-Mo-Ir-oxydes ont été utilisées pour fabriquer des supercondensateurs électrochimiques. Les électrodes ont produit une capacité spécifique élevée, une excellente stabilité cyclique et une vitesse élevée de charge-décharge dans des médias acides et alcalis. La plus haute capacité (108 ± 2 $\mathrm{mF\,cm^{-2}}$) a été obtenue en utilisant une composition de 40 mol.% d'iridium (revêtement de $Ni_{0.36}Mo_{0.24}Ir_{0.4}$-oxyde). Cette composition a aussi retenue 86% de sa capacité initiale après 2500 cycles de charge/décharge.

Selon les résultats de la thèse présentée, il a été conclu que les électrodes à base d'oxyde de nickel représentent d'excellents candidats pour le stockage d'énergie électrochimique pour la production d'hydrogène à partir d'électrolyse de l'eau et pour le stockage d'électricité dans des supercondensateurs.

Acknowledgments

Completing a Ph.D. is a very significant event in my life and represents an opportunity to remember all the experiences that I have lived in these almost four years since I arrived in Canada. It also represents an excellent opportunity to thank all those people who have been with me on this journey. I look back, and I remember when I started this Ph.D., Prof. **Sasha Omanovic** gave me the opportunity to start this research project in his laboratory. Sasha, thank you for all your trust, and your patience, your guidance, your advice and your support in easy and challenging times, both scientific and in my personal life. I am extremely thankful for your scientific advice and the critical but always positive discussion about my project. Your suggestions and the valuable discussions about the experimental methods and results made possible the successful completion of this thesis. I really appreciate all your effort and encouragement to finish this thesis on time. All your support made this research journey a very enriching experience.

I want to thank all the members of my graduation committee: Prof. **Jan Kopyscinski**, Prof. **Rolf Wüthrich,** Prof. **Viviane Yargeau,** Prof. **Phillip Servio,** and **Prof. Tomislav Friscic** for reading this thesis, for their suggestions, and comments, for all their contributions for its improvement and for approving to defend it. Dear professors, it is an honor for me that you are part of my committee.

During these more than three years, I have been working in the Electrochemistry and Corrosion Laboratory. I would like to thank my former and current colleagues from this research group: **Mario, Nehar, Mark, Saloumeh, Jacob, Emmanuel, Aqeel, Hawa, Remi, Ahmad, Amir, Deepak, Elmira, Ipsita, Logan, Xingge, Mahmoud, Ahmad, Rihab, Kanghoon, Hao, Zhuoya, Ruben, Jorge, Dayana, Vincent, Lalita, Melvin, Mark,** and **Sogol** for their support and advice, for the stimulating discussions and for all the good times we shared during the past years. I would like to thank all my colleagues for providing a friendly working environment. This was undoubtedly a friendly group to work with. I also wish to thank **Mario** for giving useful preliminary guidance at the begging of my project. I want to thank **Alais Hewes** and **Jean-Christophe Goulet** for her help to translate the abstract into French. My appreciation is extended to the staff members in the Chemical Engineering Department: **Lou, Anna, Frank, Ranjan, Andrew, Gerald, Lisa, Jo-Ann,** and **Louise** for all their help and support.

Thank you to **Kanghoon Choi**, **Jenny Hsu**, **Liem Dam-Quang**, **Mathias Semai,** and **Anlan Wong** the undergraduate students who contributed to this project, through our work together, I learned a lot from you and your research. Thank you for your ideas, your motivation, and the time invested. You were a great addition to this work, and it was a pleasure working with you. I wish you all the best in your personal and professional projects. I am sure that you will be great engineers shortly.

During my Ph.D., I took the opportunity to do a research collaboration at the Federal University of Rio de Janeiro. I would like to express my deepest appreciation to professor **José Antônio da Cunha Ponciano Gomes** for his kindness and for taking care of all the arrangements during my stay in his research group.

I would also like to extend my deepest gratitude to the **National Council of Science and Technology from Mexico (CONACYT)** for the scholarship that allowed me to pursue my doctoral studies in Chemical Engineering at McGill University over these years. I gratefully acknowledge the financial support from the **Natural Science and Engineering Research Council of Canada (NSERC)**, the **Eugene Ulmer Lamothe Fellowship,** the **McGill Engineering Faculty,** and the **Mitacs Globalink program**.

During my Ph.D. studies, I belonged to several student associations which were such as the **McGill Mexican Students' Association (MMSA)**, **Red Global Capitulo**

Montreal and the **Chemical Engineering Graduate Student Society (CheGSS)**. Thank you to the MMSA members: **Paul, Pablo, Santiago, Mara, Sofia, Matas, Alex Frias, Mariel, Julio, Miguel, Sebastian, Alfredo,** and **Carolina** for sharing the Mexican culture, values, and traditions throughout the different events that we organized. Special thanks to **Alex Frias**, for his personal and professional advice, for his help, and for coming to my office to study or just to talk. Thank you to the members of the Red Global: **Jose Miguel, Norma, Pablo, Mario, Laura,** and **Enrique** for all the projects and events that we organized together. Thanks to the members of ChEGSS, especially to **Thomas, Laura, Elena, Jennifer, Sanya,** and **Roya,** for organizing the BBQs, the soirée gourmands and other events in the Chemical Engineering Department. Thanks to all of you guys, I learned a lot about you. We did excellent teamwork, and we organized successful events and projects on time. It was a pleasure to work with you, and I wish you the best.

I would like to thanks to my Mexican and Latin-American friends, we are more every time and I really hope not to forget anybody, **Oscar Aguilar, Karla, Oscar Matus, Paulina, Oscar Marin, Norma, Charlie, Mario, Jennifer, Alejandro, Jose, Cindy,** and **Evelyn** that I have known since I arrived here in Montreal, for all the good times that we had together, for all the crazy parties, for all the dinners and the BBQ, for sharing their friendship with me. Thank you, **Mario**, for being so kind to me before I arrived in Montreal, for introducing me to all the Mexican community in the Chemical Engineering Department, and for your support in all these years, you become a good friend. Thank you, **Norma** and **Charlie**, for your hospitality, for all the delicious cochinita and the tacos árabes, for fixing my bike, and for making me feel at home and for keeping the doors of your home always open for me, especially when I needed it the most. Thank you, **Oscar** and **Paulina**, for getting me dinner several times when I was sick. Thank you, **Alejandro**, for the coffee breaks in winter. Thank you, **Oscar Marin**, for our dinners, for cooking several times and for coming to my apartment when I needed. Thank you to **Evelyn** for being so lovely, and always smiling at me in the hallways. Thank you, Javier and Karina for invite me for dinner, for choosing my apartment and for being so nice with me since I arrived in Canada. I would like to extend my sincere thanks to **Kevin Kofler**, **Aaron Roberts**, and **Karter Romeo**, thank you guys for being my gym buddies and friends. If it had not been for you, I would be > 10 kilos fatter now. Special thanks to **Karter Romeo**, for being so gentle with me since we met, for his friendship, his support, for cheering me up at the end of my Ph.D., and for being a so refreshing person in my life.

In my four years of Ph.D., I shared my apartment and part of my life with several people. Thank you, **Michael Dougan**, **Christian Both**, **Tobias Priemel**, and **Matthieu Cadiot**. Thanks for being good roommates and for sharing part of your life with me. I want to thank in particular my German friend **Christian Both**. Thank you for our dinners together and of course our talks and the tea ceremony afterward. I am surprised how Mexican you have become. Thank you also to **Jennifer** for taking care of me during those awful days after my treatment and for taking care of my plans during my trips and holidays.

Thank you to the Frente FTR members: **Alex, Mayra, Pablo, Felipe, Lore, Yasser, Natalia, Paula,** and **Luciano** thanks for the fun we had during our Latin nights and for all the crazy parties, for all the BBQs that lasted until 6 am or later…, you knew exactly the best way to cheer me up all the time. For being so unique and so much fun. Thank you for being my family in Montreal and for the unconditional support and motivation. My time in Montreal would certainly not have been the same without you.

I would like to thank my friends that not only make every holiday in Mexico a special one, but that from afar have been following my steps all this time and given me their support during my Ph.D. My friends from the university; time passes by, and it feels like yesterday when we were studying the bachelor together. Thank you, **Juan, Jorge, Octavio** and **Alejandro** the "LORDS" For always welcoming with open arms. For never understanding why I decided to do a Ph.D. but still supporting me all the time.

For showing me a positive e perspective of what I can become, for their advice in my personal and professional decisions. Guys, thanks for being in the last 14 years part of my life and being always present in one way or another by a call, chat. To **Guillermo**, for always being available to talk to me, for his advice and many years of friendship. Having met you all those years ago was a highlight in my life, and now, so many years later, you still inspire me.

Thank you, **Zamira**, **Carolina,** and **Maximiliano**, for always welcoming in Monterrey. Every time that I come back from Mexico I remember that saying goodbye to cool people is always bad, but having shared nice moments together is worth it, especially when those moments make you laugh out loud. Thank you, **Natalia**, you are very assertive, perseverant and straightforward person. I am happy to have you as a friend. I wish you lots of success and happiness in your career and your personal life. Thank you, **Sergio**, for being so kind, for giving me a place where to stay in Holland, thank you for your advice, for the trips to Portugal and Turkey that we made together, for the visits to the spa with me, and for your support. Thank you for being such a responsible person in all senses. Thank you, **Mariella,** my ex-roommate, my Italian friend who is always smiling, you are one of my favorite persons in the whole world and an excellent friend, it was fun to see you again in Lisbon after some time. Thank you, **Sander**, for hosting me in Estonia, it was really lovely to visit your country and being in touch after all these years.

Mayra Rosario Martinez Gonzalez, I still remember that when we met, you didn’t stop talking and dancing all night. You seemed like a really good person from the beginning, and you became an excellent friend. Thank you for inviting me for dinners, for taking care of me in difficult times, for sharing important things in our lives, for your advice and support. No matter the circumstances you kept smiling and stayed positive. I admire your will, your strength, and your never-ending happiness.

Pablo Diaz Gomez Maqueo, I am happy to celebrate my birthday on the exact day as you. Thank you for always listening and for sharing our frustrations, and difficulties, our achievements, and plans or simply going to your office and greeting us every day. I am glad we shared nice moments, parties and talks together. I hope our friendship continues growing and since you are one of the persons that know me the most, for good and bad.

Michael Patrick Dougan, my dear Canadian friend, ex-roommate, and ex-gym buddy you are a great listener and great talker. I would have lost without you at the start, and probably I would still be. Thank you for giving me courage in difficult moments, your advice has always been welcome. You have wise words to make me feel better on the most difficult days that I have had in my life. Honest, funny, dedicated, and smart person you certainly made me feel better. My dear friend, thank you for the time, for offering your help. Thank you for being always being willing to help everybody in any situation no matter what. I have learned a lot from you.

Jose Alberto Gomez Roldan even when going through difficult times you were always willing to help me by giving me some tips and tricks to keep everything running. I am blessed to have you in my life. Thanks for being there all these years. Have I ever told you how much I admire you? Moreover, how much you deserve to be as happy as you want. You deserve the best, and I wish you all the happiness in the world. Thanks for always being present to listen to me, for your constant support in professional and personal matters, for encouraging me to grow and be a better person.

Me gustaría agradecer a mi familia, las personas más importantes de mi vida, por su amor, apoyo y comprensión en todas las decisiones que he tomado. A mi hermana **Angelica** le quiero dar las gracias por su tenacidad ante los desafíos y por ayudarme a ser una mejor persona. Quiero agradecer el apoyo incansable de mis padres, **María Guadalupe** y **Paulino**, gracias por criarnos con amor y por enseñarnos el valor de la familia. Mi más profunda gratitud a ellos por ser mi inspiración y mi fortaleza, por ser un ejemplo para mí, por todas sus enseñanzas, valores y consejos que me han inculcado siempre y que me han permitido llegar hasta aquí.

Finalmente quiero agradecer a Dios y a la vida por todas las experiencias que he vivido. Estas experiencias me han ayudado a madurar y a comprender de una mejor forma la vida y me han permitido cumplir uno de mis grandes anhelos que es culminar este doctorado. He aprendido mucho en estos últimos meses de mi doctorado, los cuales no han sido del todo fáciles y en los que he vivido experiencias retadoras en el ámbito profesional y personal. Sin embargo, en todo momento he encontrado apoyo de diferentes personas, a las cuales agradezco y de una humilde manera hago un reconocimiento en esta sección de mi tesis. Simplemente les quiero decir nuevamente:

¡¡¡Mil gracias a todos!!!

Abraham Gomez Vidales
October 2018

Table of Contents

List of Figures

List of Tables

List of Abbreviations and Symbols Used

A	surface area (cm^2)
AEASA	apparent electrochemically-active surface area (cm^2)
b_C	cathodic Tafel slope (V dec^{-1})
C	capacitance (F cm^{-2})
CA	areal capacitance (F cm^{-2})
CF	Faradaic capacitance (F g^{-1})
C_{sp}	specific capacitance (F g^{-1})
Cdl	double-layer capacitance (F cm^{-2})
CE	counter electrode
CSC	charge storage capacity (C cm^{-2})
CV	cyclic voltammetry
E	potential (V)
EDS	energy dispersive spectroscopy
EDL	electrochemical double-layer
EDLC	electrochemical double-layer capacitor
EEC	electrical equivalent circuit
EIS	electrochemical impedance spectroscopy
F	Faraday constant (96485 C mol^{-1})
fcc	face-centred cubic
H_{ads}	adsorbed hydrogen atom
HER	hydrogen evolution reaction
J	current (A)
j	current density (A cm^{-2})
j_0	exchange current density (A cm^{-2})
LTP	linear Tafel polarization

LSV	linear sweep voltammetry
M	metal catalyst
MMO	mixed metal oxide
PEM	polymer exchange membrane
Q	charge (C)
R	resistance (Ω cm^2)
RE	reference electrode
SCE	saturated calomel electrode
SCs	supercapacitance
SEM	scanning electron microscopy
SHE	standard hydrogen electrode
sr	scan rate (V s^{-1})
t	time (s)
T	temperature (°C or K)
XPS	X-ray photoelectric spectroscopy
XRD	X-ray diffraction
2D	two-dimensional
3D	three-dimensional
ΔG	change in Gibbs free energy (J mol^{-1})
ΔH	change in enthalpy (J mol^{-1})
ΔS	change in entropy (J mol^{-1} K−1)
η	overpotential (V)

Chapter 1

1 Introduction

1.1 Preface

According to the Intergovernmental Panel on Climate Change (IPCC), since the industrial revolution, global warming has been rapidly increasing and the record set of temperatures reached in the last 25 years is a tangible proof of this. Furthermore, the IPCC estimates that the increase in temperatures can reach between 1.4^{o}C and 5.8^{o}C at the end of this century if no action is taken in this regard [1]. The dependence on fossil energies results in emissions of greenhouse gases, with CO_2 (80% of contribution) as the product of combustion. As global energy demand continues to grow, CO_2 emissions are expected to increase by 1.3% annually, so the use of fossil fuels for energy needs will rapidly result in critical environmental problems in the world.

In the same context, it is well known that fossil fuels are rapidly being depleted. The most optimistic estimates show that there are oil reserves for another 100 years [1]. Furthermore, as CO_2 increases, environmental risk such as climate change rises as well [2, 3]. As a result, new energy resources, techniques, and technologies are rapidly being designed to reduce the amount of unbalanced anthropogenic CO_2 and avoid possible detriments from our current standard of living. With this regard, energy industries have sought ways to decrease the reliance on fossil fuels by trying to find alternative energy sources. The field of electrochemistry can contribute to the development of greener energy production and storage devices. In this thesis, the use of mixed metal oxides (MMOs) as electrodes is considered for application in hydrogen generators (electrolyzers) and electrochemical supercapacitors (ESs), as green ways of storing electricity.

Hydrogen, the most abundant element in the universe, is considered to be the best alternative to the current fossil fuel energy economy [4-6]. In addition, hydrogen has the highest specific energy density (per mass), its chemical energy can be converted directly into electrical energy using fuel cells or can also be burned, in both cases producing pure water. For these reasons, hydrogen is expected to provide a solution to our needs as a sustainable fuel (vector) for our future transport requirements and also an approach to large-scale storage of energy [7]. However, only 4% of hydrogen is currently produced by renewable avenues, and the other 96% comes from hydrocarbon reforming [8, 9]. As such, environmental savings/benefits to produce hydrogen gas are minimal considering a great deal of fossil fuels required and amount of CO_2 produced by their reformation. Hence, renewable techniques for hydrogen production must be employed instead [10].

Water electrolysis can be the proper technology to address these issues. In water electrolysis, an electrical current is used to separate (split) water into its components, oxygen, and hydrogen [8]. Moreover, when used in combination with solar/wind/hydroelectricity-producing systems, water electrolysis provides a clean route to hydrogen, without the consumption of fossil fuels or the emission of carbon dioxide. In consequence, there is much interest in this technology [7]. Unfortunately, among the industrial methods of hydrogen production, water electrolysis is not yet cost-competitive due to its high operating costs.

A significant portion of these costs is associated with the poor performance, fouling susceptibility and insufficient durability of current electrocatalyst materials (electrodes) on which the hydrogen evolution reaction (HER) is conducted [11]. The state-of-the-art electrocatalyst materials are noble metals such as platinum, iridium, and ruthenium, which show the highest electrocatalytic activity for the HER, but the scarcity and high cost, unfortunately, limits their large-scale applications [12]. To overcome these significant barriers without significantly sacrificing catalytic performance, numerous research efforts have been devoted to reducing the Pt usage or the replacement of Pt with other inexpensive materials [12-15].

In this context, certain non-noble transition metals, especially Ni and Ni-based alloys, have shown to possess many properties to suit this application [12-15]. In this Ph.D. thesis, Ni is chosen as the base material because it has relatively high intrinsic electrocatalytic activity in the HER and it is relatively inexpensive. Ni alloyed with other transition metals, including Mo, Fe, and Co, has been shown to increase the electrolytic activity of the HER by apparently modifying the *d*-shell electronic configuration [12]. Moreover, the electrocatalytic activity can be further improved by modifying the geometry of the surface to increase the electroactive surface area and surface roughness of the catalyst, which introduces a higher number of active sites.

Nonetheless, Ni and its alloys are susceptible to deactivation by electrodeposition of metallic impurities presented in the electrolyte, and their long-term stability and activity are not optimum [16]. Furthermore, they are not suitable for the operation in acidic environments that are present in polymer-electrolyte-membrane (PEM) electrolyzers, due to the poor corrosion resistance of Ni at low pH (in PEMs, pH is around zero), which is of issue when the PEM cell is at open circuit.

In the search for new materials, certain metal oxide electrodes have demonstrated good performances in the cathodic evolution of hydrogen, but they have not been widely studied [16-19]. These electrodes have also shown their activity for some other common electrocatalytic reactions such as O_2 evolution and O_2 reduction [20]. Nevertheless, a relatively small number of scientific report research on hydrogen evolution at oxide electrodes [10, 16-26]. Two aspects make metal oxides interesting for applications as a hydrogen evolution cathode material: their better corrosion stability and fouling resistance. As a consequence of the different surface chemistry of oxides, compared to the respective pure metals, oxides are more resistant to deactivation caused by the (electro)deposition of ions (impurities) dissolved in the electrolyte [16]. Additionally, some research studies claim that the oxidative treatment of the cathode material could lead to a relative improvement of cathode performance [16-19]. Considering this information, and the fact that metal oxides have shown to be promising cathode materials, the goal of this project is to develop novel mixed-metal oxide (MMO) cathode materials for HER, in order to achieve high electrocatalytic activity and fouling resistance (better long-term electrocatalytic stability).

Mixed metal oxides can also be used as electrodes in electrochemical supercapacitors. Electrochemical supercapacitors store potential energy in an electric field. They are considered to be the bridge gap between capacitors and batteries. Their main advantage is that they can store up to 100 times more energy per unit mass than conventional capacitors and can accept and deliver charge much faster and with much more number of cycles than standard batteries. There are two main types of supercapacitors based on the mechanism of energy storage: electrostatic double-layer capacitors and electrochemical pseudocapacitors. The first one uses carbon electrodes or derivatives, which have much higher electrostatic double-layer capacitance and large surface area, which achieve the separation of charge at the interface between the surface of the electrode and the electrolyte. The second one uses metal oxide or conducting polymer electrodes with a high electrochemical pseudocapacitance, which is achieved by reversible Faradaic electron charge-transfer with redox reactions in the solid phase.

1.2 Objectives

This Ph.D. project aimed at developing MMO electrodes to be used as cathodes for hydrogen production by water electrolysis and as electrochemical supercapacitors electrode materials. The main objective of the work was to investigate the influence of electrode chemical composition of selected Ni-oxide based materials on the resulting electrocatalytic activity in the HER and on amount of electrical charge that selected compositions can store/deliver. The goals were to achieve high electrocatalytic activity and long-term performance stability in the HER, and high energy (charge) storage capacity, under various operating conditions (metal oxide composition, electrolyte type, different pH, and temperature). The combinations of MMOs based on nickel oxide (Ni-

Co-oxide, Ni-Mo-oxide, and Ni-Mo-Ir-oxide) were chosen due to their availability, low cost, and promising results obtained in other research studies as pure metals (non-oxides) [16, 27-30]. Specific objectives of the project were:

- Optimization of experimental conditions for fabrication of the MMO coatings employing a thermal-salt decomposition method on a two-dimensional titanium substrate.
    - Evaluation of MMOs' electrochemical activity and fouling resistance in the HER under various experimental conditions, and their physicochemical properties (chemical composition, surface topography, crystalline structure).
- Evaluation of the charge storage/delivery performance of Ni-Mo-Ir-electrodes.

1.3 Thesis organization

This manuscript-based thesis contains eight chapters and follows the guidelines outlined by the Faculty of Graduate and Postdoctoral Studies (GPS) at McGill University.

Chapter 1 is the introduction section of the thesis, where a brief description of the importance of the use of new and renewable energy production and storage techniques is explained. Additionally, the objectives of this thesis are presented. Chapter 2, the literature review, introduces concepts about the way that electrochemistry can be applied for the development of novel energy (vector) generation and storage technologies. This chapter explains in detail the concepts related to the hydrogen evolution reaction and the use of supercapacitors as energy storage devices.

Chapters 3–6 present scientific papers published (or submitted for publication) in peer-reviewed scientific journals in which main results related to this Ph.D. project are presented and discussed. Chapter 3 discusses the development of Ni-Co-oxides cathodes for hydrogen generation by electrochemical water splitting in acidic and alkaline medium and the influence of the temperature on the kinetics of the hydrogen evolution. Chapter 4 addresses the use of Ni-Mo-oxides cathodes for hydrogen production by water electrolysis in the acidic, alkaline, and neutral electrolytes and the long-term performance stability of the electrodes. Chapter 5 presents results on the fabrication of Ni-Mo-Ir-oxide cathodes for hydrogen production in acidic media and the effect of deactivation/reactivation of these cathodes in the presence of the most common impurities in the acidic and alkaline electrolytes (Cu, Fe, and Cu + Fe). Chapter 6 investigates the employment of the same Ni-Mo-Ir-oxides electrodes as supercapacitors in acidic and alkaline electrolytes and their charge-discharge cycle capacity.

Chapter 7 summarizes the content of this thesis unifying the main conclusions, while Chapter 8 reports original contributions to scientific knowledge and proposed future work and research about the use of these tailor-made cathodes in energy storage applications.

Chapter 2

2 Literature review

The following chapter presents background information related to the use of mixed metal oxides for energy storage applications. In addition, an explanation of the current state-of-the-art research on the technologies, techniques, methods, and materials are included to understand the importance of hydrogen generation by water electrolysis and the use of electrochemical supercapacitors.

2.1 Hydrogen as an energy vector

Most of currently-used energy comes from fossil fuels, which are harmful to the environment considering that their use generates greenhouse emission gases, such as CO, CO_2, NO, etc. [31]. There is an alternative “source” of energy that can be employed to avoid these problems: hydrogen, the most abundant element in the universe [32]. In fact, hydrogen is not an energy source, but rather an energy vector (energy storage media); however, through the thesis, the two terms will be used interchangeably, although bearing in mind the actual definition of hydrogen as a vector.

Despite its abundance, hydrogen is hard to find as an isolated element since it is primarily found in combination with hydrocarbon compounds, and oxygen in water [33]. Nonetheless, once it is extracted, this colorless, odorless, and tasteless element becomes a fuel for a variety of industrial uses. Compared alongside other fuels, hydrogen has the highest energy content (120 MJ/kg for hydrogen versus 44 MJ/kg for gasoline) [33]. When it is consumed to produce energy, the combustion of hydrogen generates water; it does not produce any toxic side products and is not, therefore, an environmental threat. The primary benefits of hydrogen as a renewable energy resource are two-fold: it is a virtually inexhaustible element, and it is an environmentally friendly energy source that could meet most of our future energy needs.

Even more, hydrogen's chemical energy can be converted into electrical energy without any need of an intermediate step of operating a heat engine. This direct conversion is performed in fuel cells. The elimination of an intermediate step overcomes Carnot efficiency limitations, thereby achieving high-energy yields. Unlike electrical energy, hydrogen can be accumulated and stored in large quantities [34]. It is for this reason that hydrogen is increasingly seen as "the cleanest future fuel (energy) vector" [35, 36]. As for its applications, hydrogen is versatile: it can provide energy for factories, electric utilities, vehicles, and airplanes, to name a few [33]. Nowadays, Honda and Toyota have already started selling hydrogen-fuel-cell-powered cars, and an increasing number of hydrogen refueling stations are being built in Japan, Europe, and the USA to meet these needs. In the meantime, hydrogen-fuel-cell–powered battery chargers for portable devices (e.g., cell phones and drones) are already being sold. In the not-too-distant future, it would not be unreasonable to say that hydrogen could be used to a much larger extent to fuel vehicles and aircraft and provide power for our homes and offices.

2.2 The current state of hydrogen production and its routes

The annual global production of hydrogen in 2015 reached about 60 million tons. Hydrogen consumption is on the increase: there has been a steady rise of about 4% per year over the past decade [1]. There are several products and industries for which hydrogen is employed: metallurgical applications, electronics industry, food industry (hydrogenation of fats and oils), glass manufacture, cooling of power generators, organic-synthesis industries, and space applications (as a fuel).

Hydrogen can be produced from different sources. Figure 2.1 displays the main production sources from where it can be obtained. As it can be seen, currently, 96% of hydrogen that is generated comes from fossil fuels (natural gas, petroleum, and coal). Meanwhile, only 4% comes from water, which is a renewable source.

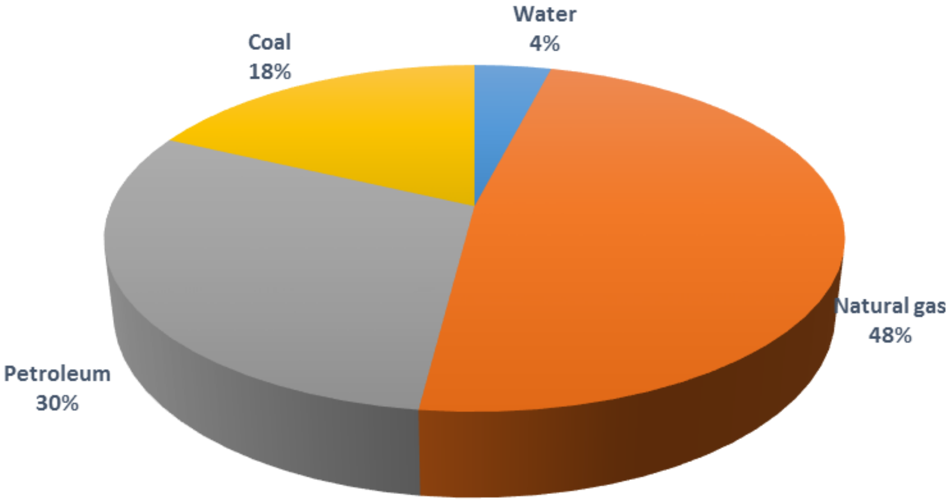

Figure 2.1: Feedstock used in the current global production of hydrogen (adapted from [37]).

On the other hand, hydrogen can be produced employing different technologies depending on the source where it is obtained from. Figure 2.2 shows the main production routes from which hydrogen can be obtained. The primary industrial processes to produce hydrogen will be explained briefly in the following sections.

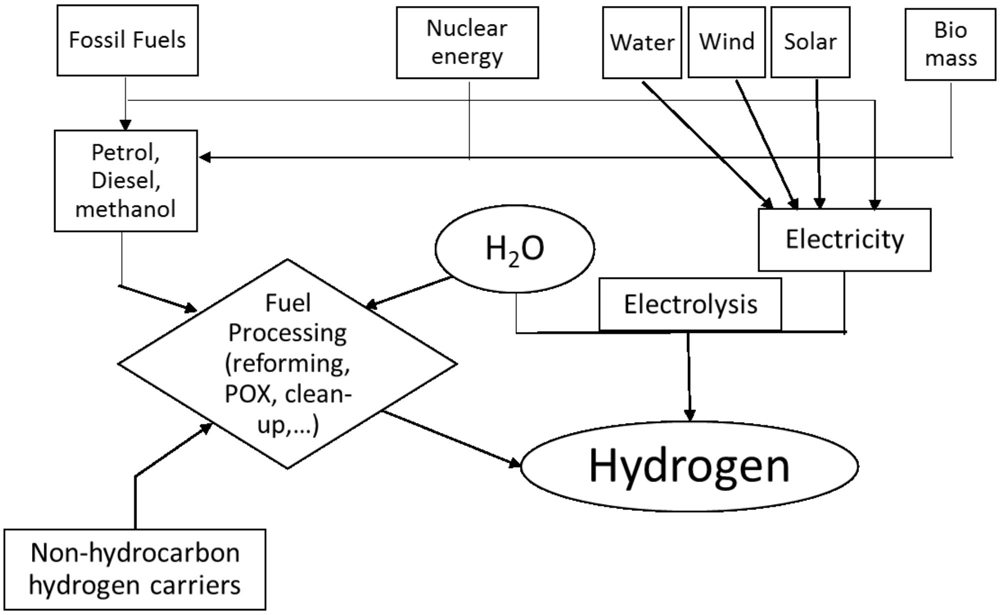

Figure 2.2: Current hydrogen production routes, adapted from [38].

2.2.1 Steam reforming

Steam reforming has been the dominant industrial method of hydrogen production since its introduction in 1930 [39]. At present, it is the most-widely used method to produce hydrogen in the industry. Steam reforming consists of using hydrocarbons as raw materials such as natural gas (as a primary source), liquid hydrocarbons, and alcohols at a high temperature to form hydrogen (H_2), carbon monoxide (CO), and carbon dioxide (CO_2). When natural gas is used, the chemical reactions are as follow:

$$CH_4 + H_2O \rightarrow CO + 3H_2 \tag{2.1}$$

$$CO + H_2O \rightarrow CO_2 + H_2 \tag{2.2}$$

The process involves three stages. In the first step, as shown in equation 2.1, steam reacts with methane using a nickel-based catalyst via an endothermic reaction (at temperatures around 800–1000^{o}C) to yield CO and H_2. The produced gas is directed to the CO-shift unit in which the second reaction (2.2) occurs over copper catalysts, generating additional H_2 through an exothermic, water gas shift reaction at a temperature of around 300-400°C. After this, the gas goes through a condenser in which the water vapor is dropped. This leads to the third stage of the purification process: a separation system using membranes or an adsorption unit, where hydrogen is obtained with a purity of 99%. The efficiency of this process is approximately 80% [39].

2.2.2 Partial oxidation of hydrocarbons

This process entails an exothermic reaction whereby a fuel reacts with a low quantity of oxygen to produce an incomplete oxidation, yielding hydrogen. For methane (CH_4), the reaction (2.3) is as follows:

$$CH_4 + \frac{1}{2}O_2 \rightarrow CO + 2H_2 \tag{2.3}$$

The reaction is carried out with pure oxygen or air in the presence of catalysts and at a temperature of around 800°C. The presence of CO is undesirable since it can cause catalyst poisoning, although the formed CO can be removed by oxidizing to CO_2 or by treating it with steam to generate more hydrogen. A disadvantage of this process is that partial oxidation presents a higher investment cost, and has a lower degree of conversion, around 70% [40].

2.2.3 Gasification

The gasification process consists of a combustion with an oxygen deficit in which CO, CO_2, H_2, and CH_4 are obtained in different ratios depending on the composition of the feedstock and operating conditions. Oxygen is limited between 10% and 50% of the stoichiometric ratio, and the operating temperature ranges between 700°C and 1500°C. Consequently, it is a process with high energy consumption. Biomass or coal can be used as a feedstock in gasification. In the case of coal, it is treated with steam to generate CO_2 and H_2 [40]. On the other hand, if biomass is used (i.e., cellulose), the gasification process consists of several depolymerization stages as well as the conversion of methane.

In this process, large amounts of CO_2 are released when coal is used, which causes environmental concerns. If biomass is employed as feedstock, the process is more environmentally ‘neutral’ since the amount of CO_2 produced can be the same amount that the biomass captured from the atmosphere. On balance, it is a null contribution to the emission of greenhouse gases. Moreover, the yields obtained with this procedure are relatively low.

2.2.4 Water electrolysis

The complete environmental neutrality of hydrogen production is achieved using renewable energy sources for water splitting. Nonetheless, the high-energy cost of the process and the electrode materials constitute the main disadvantage of this technology. Subsequently, cost reduction will be a significant challenge in R&D. Because of the importance of this topic in this thesis, this concept will be explained in detail in the following section.

Water electrolysis is the most environmentally friendly option of producing hydrogen. Nevertheless, it has the disadvantage of high operating cost. This Ph.D. thesis presents a contribution to improving the energy efficiency of the process which could lead to lowering the costs of this technology. This could eventually lead to a competitive hydrogen production process that is consistent with the model of the hydrogen economy (a concept that will be explained in the following paragraphs).

Hydrogen economy, a term coined by John Bockris in 1970, refers to the vision of using hydrogen as an energy source, which is indeed needed to solve the global warming issues related to the use of fossil fuels [41]. Notwithstanding, it is relevant to note that, regarding water electrolysis as an environmentally friendly option via hydrogen production, the extraction of H_2 is only considered green when it is produced by renewable electricity-generation sources, such as solar and wind. After this is achieved, the obtained hydrogen can then be stored or used in fuel cells in domestic, commercial, and industrial applications (i.e., heating systems and power generation), in places where it is difficult to have access to electricity, and in transportation (i.e., hydrogen fuel-cell cars), as it is illustrated in Figure 2.3. When hydrogen is consumed, the end product is water, which can be then reused. Hence, this becomes the hydrogen economy cycle.

Before entering a discussion on the use of hydrogen and its economy, it is important to state again the following: hydrogen gas is not a direct fuel but is instead an energy carrier (vector). That is, in order to produce hydrogen, an additional primary energy source is required (hydrocarbon reformation, electrolysis from nuclear heating, wind, solar, to name but a few).

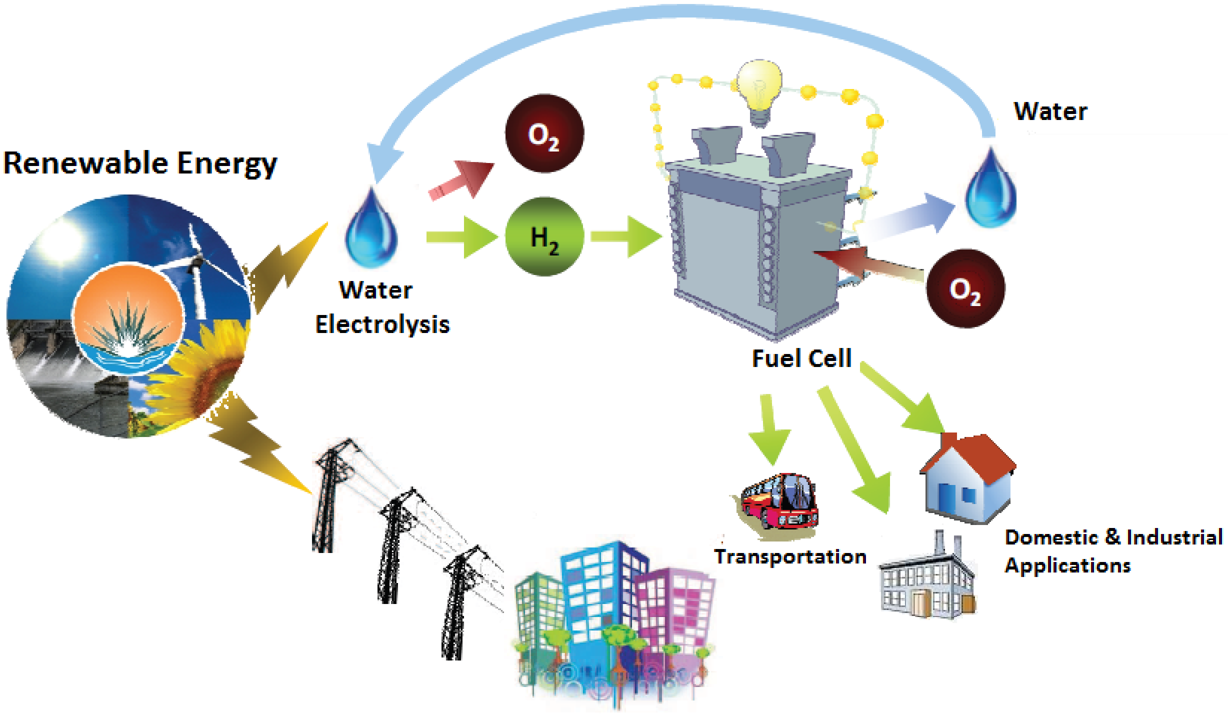

Figure 2.3: Scheme describing the concept of the hydrogen economy (adapted from [2]).

There are still many challenges to overcome in making hydrogen an economical energy pathway. Hydrogen is currently more expensive than traditional energy sources due to the high initial investment and operation costs. Further, hydrogen produced by water electrolysis costs more than that one produced using hydrocarbons. High costs of electrochemical hydrogen production are primarily associated with the poor efficiency of current electrocatalyst materials on which the hydrogen evolution reaction (HER) and oxygen evolution reaction (OER) is conducted. For this reason, much research is focused on developing inexpensive, more electroactive and stable-performance electrode materials for electrochemical water splitting. As a result, reducing costs, improving yields, and opening markets for new hydrogen-based technologies are among top priorities in the field of R&D. If adverse effects on the environment and their economic impact (such as carbon and environmental taxes) are added to the traditional hydrocarbon-based system, the hydrogen economy would be more competitive.

2.3 Water Electrolysis and Hydrogen Evolution Reaction (HER)

As the name suggests, electrocatalysis is an amalgamation of two fields of physical chemistry: electrochemistry and catalysis. Nicholson and Carlisle were the first to observe the electrolysis of water in 1800 [42] and in doing so created the entire field of electrochemistry. In an electrochemical cell with an aqueous electrolyte, water molecules were observed to “split” into their base constituents, H_2 and O_2:

$$H_20 \rightarrow H_2 + \frac{1}{2} O_2 \tag{2.4}$$

When a current was passed through the cell in the presence of a metal catalyst, M, the hydrogen cation (H^+) can be adsorbed on the catalyst surface at adequate potentials, increasing the rate of reaction and evolving hydrogen gas. The amount of hydrogen produced, V (m^3), can be calculated using the Faraday’s law:

$$m = \frac{MIt}{nF} \tag{2.5}$$

where M is the molar mass of hydrogen (kg mol^{-1}), n is the number of electrons passed in the reaction (-), F is Faraday's constant (96485 C mol^{-1}), I is current (A), and t is the applied current time (s). Electrochemical water splitting is not a thermodynamically-spontaneous process (the Gibbs free energy of reaction (2.4) is positive), which requires electrical energy to be supplied to this reaction in order to proceed (the amount of electrical energy has to be larger than the Gibbs free energy of the reaction at given conditions).

The electrolytic water-splitting reaction does not proceed in one step. Given that the focus of this Ph.D. work is on the development of new materials for cathodes, focus will be directed to only the hydrogen evolution reaction, while electrocatalysis of the oxygen evolution reaction is a completely different area and is outside the focus of this thesis. The widely-accepted mechanism for hydrogen evolution on most electrocatalysts is a step involving the formation of adsorbed atomic hydrogen followed by either electrochemical or chemical desorption [12, 23]:

$$M + H^+ + e^- \leftrightarrow M - H_{ads} \quad \text{(Volmer reaction)} \tag{2.6}$$

$$M - H_{ads} + H^+ + e^- \rightarrow H_2 + M \quad \text{(Heyrovsky reaction)} \tag{2.7}$$

$$M - H_{ads} + M - H_{ads} \rightarrow H_2 + 2M \text{ (Tafel reaction)} \tag{2.8}$$

where M represents a metal (cathode) surface.

First, hydrogen cations reach the surface of the catalyst material and are discharged by the formation of adsorbed hydrogen atoms on the electrode surface on empty metal atom sites through the Volmer reaction (2.6). The creation and strength of the M-H$_{ads}$ bond significantly affect the mechanism and kinetics of the HER by changing its thermodynamics and kinetics.

Following the Volmer step, one of two reactions occurs: (a) the Heyrovsky step (2.7) or (b) the Tafel step (2.8). Both steps require cleavage of the adsorbed hydrogen atom and a recombination to molecular hydrogen. Thus, the M-H$_{ads}$ bond strength ultimately controls the kinetics of the HER. The maximum rate of hydrogen generation is achieved for intermediate M–H_{ads} bond strengths such that the adsorption and desorption (release) steps are balanced. In addition to the M–H_{ads} bond, the reaction mechanism is also influenced by other properties of the system such as the electrode properties, type, and concentration of the electrolyte, as well as the operating temperature, pressure, and pH [23].

At this point, the central question remains: what are the properties of a cathode material that define it as a good electrocatalyst for the HER? It has been well established that Pt metal is the best electrocatalyst available for the HER. The answer is rather complicated owing to many physical properties of the material, including electronegativity, work function, and electronic configuration [43, 44]. These properties contribute to the intrinsic electrocatalytic nature of the material and its preferential adsorption of hydrogen. A correlation between activity and electrode material expressed by the bond strength of intermediates to the electrode surface has been proposed. The outcome is the volcano-shaped curve (Figure 2.4). In the following sections, the concept of electrocatalysis and the volcano curve will be explained in detail to answer this critical question in a better way.

2.4 Electrocatalysis and the Volcano Curve

An electrocatalyst is a material that modifies and increases the rate of electrochemical reactions without being consumed in the process [45, 46]. The electrocatalytic activity of an electrode material depends on two different factors: electronic and geometric. The former affects the surface-intermediate bond strength and electron-transfer rate, and it depends on the chemical composition and physicochemical properties of the material. The latter is related to the extension of the surface area and has nothing to do directly with real electrocatalysis since the energy of activation of the reaction is not affected [20].

In 1972, Trasatti presented a very detailed analysis of the exchange current density (current at zero overpotential), the work function (the energy required to remove an electron from the metal surface), electronegativity (the tendency of an atom to attract electrons toward itself), and their link to the HER, on various metals [44]. Trasatti was able to correlate the heat of hydrogen adsorption onto the metal catalyst to the (logarithm of the) exchange current density for HER, j_0. In this case, the heat of hydrogen adsorption represents the strength of the M–H_{ads} bond formed.

Figure 2.4 shows the volcano curve as described by Trasatti [44]. The volcano curve explains the intrinsic electrocatalytic nature of materials in terms of the strength of the M-H_{ads} bond. This volcano dependence of exchange current density for HER, j_0, on the M-H_{ads} bond strength is a clear demonstration of electrocatalysis of metals for this particular reaction. The exchange current density, j_0, is often used as a comparison parameter, where a higher value of j_0 indicates better electrocatalytic activity due to little resistance [12]. Thus, the volcano curve is often used as the primary predictive basis to understand the electrocatalytic phenomenon in the HER.

As it can be seen in the volcano curve, the exchange current density increases with the strength of M–H_{ads} to a maximum near 60 kcal mol^{-1} (Pt) and then drops off, resulting in a graph with an inverted "V" shaped curve. For metals that form weak M-H_{ads} bonds, the kinetics of the first HER step (Volmer reaction, reaction (2.6)) is slow, while the kinetics of the second step (Heyrovsky or Tafel reactions, reactions (2.7 and 2.8, respectively)) is fast. Subsequently, the kinetics of the overall HER is slow. On the other side of the abscissa (higher binding energies), the kinetics of the first HER step is fast since hydrogen adsorbs strongly to these metals due to the empty d-orbitals of these metals and the fact hydrogen is an electron donor. However, due to the high strength of the M-H_{ads} bond, the kinetics of the second HER step is slow, thus rendering the overall HER kinetics slow. A suitable catalyst should offer a balance between the rates of the two steps and, unfortunately, it is evident from the volcano curve (see Figure 2.4) that expensive noble metals (e.g., Pt, Re, Rh, and Ir) lie at the peak and express much higher electrocatalytic activity than non-noble metals [12].

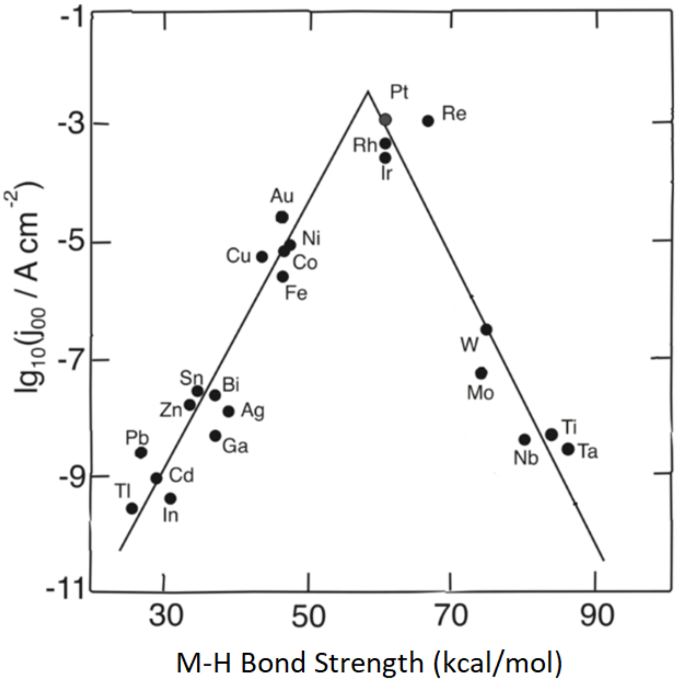

Figure 2.4: The volcano curve correlating the exchange current density and the metal adsorbed hydrogen bond strength [44].

As it is seen in Figure 2.4, the volcano curve is based on the behavior of pure metals. The catalytic activity of a metal depends on the group of the periodic table of the elements to which it belongs. The characteristic *d* orbitals of the transition metals are essential for chemisorption. In transition metal catalysts, the unpaired electrons of the *d* orbitals are coupled with the unpaired adsorbate *s* or *p* orbitals; for the HER, the hydrogen is strongly adsorbed when the electron pairs are formed. The elements of group VII possess a large percentage of paired electrons of *d* orbital and average adsorption heats, with the highest electrochemical activities, particularly the group of platinum metals (Pt, Rh Ir), and the transition metals (Ni, Co, Fe, Mo).

The improvement of cathode activity (otherwise known as the activation process) has two objectives: to replace the active but expensive materials (such as Rh, Ir, Pt) by cheaper materials, and to increase the activity of more economical materials in order to resemble the electrocatalytic properties of more expensive metals.

2.5 Hydrogen generators

Electrolysis is a very efficient method to generate high-purity hydrogen. To produce molecular hydrogen by electrolysis of water, three main types of electrolyzers based on the electrolyte-type are used: alkaline, seawater (still in development), and acidic (also known as a polymer-electrolyte membrane (PEM)) electrolyzers [12].

Alkaline electrolyzers are cheaper in terms of investment (usually using nickel catalysts) but less efficient. In contrast, PEM electrolyzers are more expensive (they use platinum group metal catalysts and expensive polymer-electrolyte membranes, such as Nafion®) but are more efficient and can operate at higher current densities and, therefore, may be cheaper if the production of hydrogen is sufficient.

In the following subsections, the main characteristics of the different types of electrolyzers will be described in detail.

2.5.1 Alkaline electrolyzer

The alkaline hydrogen generator is an electrochemical cell and consists of four main elements: a container (vessel), an electrolyte, an anode (the electrode on which oxygen evolution occurs), a cathode (the electrode on which hydrogen evolution occurs), and a separator. Figure 2.5 shows a very simple schematic of an alkaline hydrogen generator. Industrial electrolyzers contain multiple cathode/separator/anode arrays pressed together to form a multi-cell stack. The stack is connected in series of upwards of several hundred elementary arrays (unit cells). Each cell shares a common metallic plate current-collectors with its neighboring cells, forming what is known as a bipolar plate. A current is supplied by a direct current

(DC) power supply, and it passes through the electrodes and electrolyte. At cell potentials that are larger than the reversible water electrolysis potential, water is split into its base constituents, H_2 and O_2.

At the cathode, the water reduction reaction occurs:

$$4e^- + 4H_2O\ (l) \rightarrow 2H_2(g) + 4\ OH^-(aq) \tag{2.9}$$

At the anode, the water oxidation happens:

$$6H_2O\ (l) \rightarrow O_2(g) + 4\ H_3O^+(aq) + 4e^- \tag{2.10}$$

The electrodes are chosen as such to maximize the kinetics of both the hydrogen and oxygen evolution reactions at a given cell voltage (potential difference between the two electrodes). For the hydrogen-producing electrode (the cathode), Ni is typically used as a cathode material because of its relatively high intrinsic electrocatalytic activity in the HER (see the volcano curve in Figure 2.4), its relatively good stability in the alkaline medium, its availability, and relatively low cost. Nickel can also be used as an anode, and during the cell operation, its surface will be oxidized to form a Ni-oxide layer.

The electrolyte is usually aqueous 30 wt.% KOH, due to its excellent ionic conductivity [15]. The separator, also called a membrane or a diaphragm, is placed between the anode and cathode to keep the hydrogen and oxygen from combining and to prevent short-circuiting (anode/cathode contact). The separator allows ions to be transferred in the liquid electrolyte and it must have a pore size smaller than the diameter of the smallest gas bubbles (10 µm in the case of hydrogen bubbles). The commonly used separators are polymeric materials such as polytetrafluoroethylene (PTFE), ceramic oxides such as NiO and cement like Ni-$BaTiO_3$.

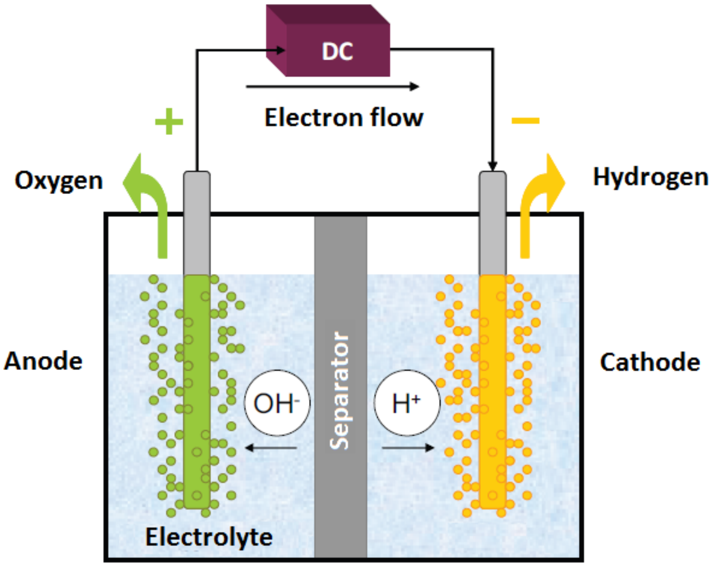

Figure 2.5: Schematic of a hydrogen generator. As the direct current (dc) power supply is applied, the HER reaction occurs on the cathode whereas the oxygen evolution reaction (OER) takes place on the anode [15].

Alkaline electrolyzers constitute the majority of water electrolyzers currently used in industry [12, 18, 47]. Currently, only alkaline-based electrolysis is well proven and easily scalable. Alkaline electrolyzers offer other advantages over other electrolyzer types, including: (i) relatively low capital expenses (all materials are inexpensive and easy to obtain), (ii) proven technology with well-established operating costs, (iii) demonstration of large capacity units, and (iv) raw water can be used in the electrolyte directly without further purification.

The main drawback of the alkaline electrolyzer is the purity of the evolved H_2. Because of the high concentration of electrolytes and the potential use of raw water, impurities, including oxygen and dissolved salts within water vapor, may be present (along with additional metal impurities that would foul/deactivate the electrodes). These impurities result in a ca. 99.0–99.9% pure H_2 (vs. $\geq$ 99.99% in a PEM electrolyzer) [11]. Alkaline water electrolysis is a mature technology that presents itself as the current standard for large-scale water electrolysis. The typical working temperature of the commercial alkaline electrolyzers is 80-90°C. Conventional cells operate at 1.8-2.2 V voltages, with current densities below 0.4 A cm^{-2}, having power 60-80% efficiency [42].

2.5.2 Proton exchange membrane electrolyzers

The development of PEM-type electrolyzers is linked to the invention of polymer exchange membrane fuel cells. In the 1950s, scientists at General Electric (GE) developed fuel cells using a sulfonated polystyrene electrolyte. In 1966, fuel cells were prepared using very superior membranes, the Nafion developed by DuPont, for special NASA projects. In 1973 GE developed polymer (also known as proton) exchange membranes (PEM)-type electrolyzers, with technology initially utilized for the generation of oxygen in nuclear submarines. PEM-type electrolyzers have become a well-accepted and industrially viable technology.

Compared to alkaline, PEM type water electrolyzers can operate at lower cell voltages and higher current densities as well as higher temperatures and pressures. The efficiencies of these systems can reach almost 100%, but they generally work in a range of 90–95% [48]. One of the central sales of PEM technology is that it can generate extremely pure hydrogen (99.999%). Figure 2.6 illustrates the configuration of a PEM electrolyzer which is very similar to the alkaline electrolyzer, since the elements are the same, with the exception of the inclusion of the polymer exchange membrane. This specific element will be described in the following paragraph.

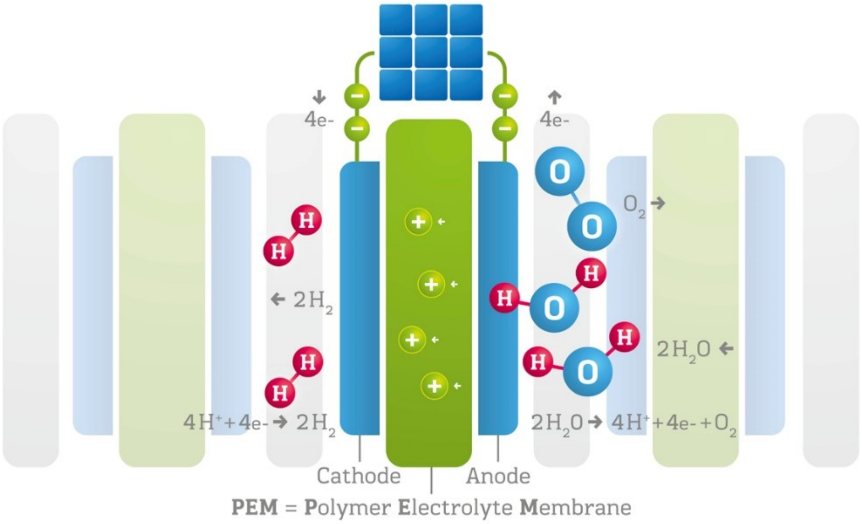

Figure 2.6: Schematic of a polymer electrolyte membrane (PEM) electrolyzer.

In PEM electrolyzers, the Nafion membrane, which has chains terminated in sulfonated ion exchange groups, simultaneously serves as an electrolyte and a separator. The water circulating through the cell dissociates into oxygen and hydrogen, thanks to the help of electrocatalysts located on the surface of the membrane. The membrane has a thickness usually from 150 to 300 µm, and it is permeable to water and gases. Furthermore, it has a low ionic conductivity but a high proton conductivity when saturated with water. The sulfonic acid groups (HSO_3^-) incorporated in the membrane are hydrated when in contact with water and then dissociated $(SO_3^{-2} + H^+)_{aq}$ facilitating the proton conduction [49]. Thus, the membrane is very acidic, so electrocatalysts resistant to this medium are required, particularly noble metals such as platinum, iridium, ruthenium, rhodium, or their alloys. The use of these metals significantly increases the cost of this type of electrolyzer in comparison to the alkaline electrolyzer. Contrary to the alkaline electrolyzer non-noble metals, such as Ni, can be used since they would corrode [11].

2.5.3 Seawater electrolyzer

Seawater, an abundant and available resource on earth, is one of the most promising sources to produce hydrogen from. A number of studies have suggested the direct electrolysis of seawater as a source of hydrogen on a large scale [50-53]. Seawater is a natural electrolyte with a salinity of about 3.5 wt.% consisting of mostly the ions of sodium and chloride, where their conductivity enables the electrolysis process to be effective [51].

Seawater electrolysis has a high capital investment cost mainly due to the use of electrocatalysts based on noble metals. Hence, it is essential to develop highly active and stable electrocatalysts for seawater electrolysis without using noble metals. Seawater electrolysis has been commercialized for reducing organic fouling in process cooling water, for disinfecting sewage streams, and for sterilizing water used in pressure injection in oil and gas formations [53].

Hydrogen production by seawater electrolysis occurs by the cathodic release of hydrogen gas in the same way it is produced in alkaline electrolyzer, and its efficiency is dependent on the physicochemical properties of electrocatalysts. Unfortunately, seawater electrolysis has severe problems of electrode fouling and low electrolyte conductivity [53]. During the seawater electrolysis process, the electrode surface can have a gradual build-up of insoluble precipitates on the surface (e.g., electrodeposited metals) which significantly reduces the efficiency of the hydrogen evolution reaction. As a result, the electrode fouling causes increased operational costs and reduced hydrogen production. In case of direct use of untreated seawater, electrode fouling becomes an even more significant problem because of more impurities present at higher concentrations. Periodic cleaning and high electrolyte flow rates can be used to scour the electrode surfaces and reduce the fouling. Nonetheless, these methods are not practical since they also increase the operating costs [53]. In addition, there are problems related to the performance of the anode (oxygen and/or chlorine evolution electrode), but these are outside the scope of this thesis.

Another problem of seawater electrolysis is the low conductivity of the seawater electrolyte and subsequent high power requirements [50]. This problem can be solved by adding acid to adjust the pH and to improve conductivity by reducing the Ohmic resistance [54]. Besides, electrolyte recirculation can be utilized to attain a more concentrated product solution for seawater electrolysis, which increases the electrolyte conductivity and thereby reducing power requirements [53]. Still, these improvements may be offset by increased maintenance costs resulting from electrode fouling.

Most of the scientific contributions on seawater electrolysis research have been focused on the development of electrode materials with high selectivity for the oxygen evolution reaction over chlorine evolution. On the other hand, very few past studies can be found to address the cathodic fouling and precipitation issues. In conclusion, hydrogen production by seawater electrolysis is a promising technology, but it requires further investigation.

Table 2.1 summarizes the different operating conditions of the three types of electrolyzers describe above.

Table 2.1: Conditions of different electrolyzers [55-57].

Technology	**Alkaline electrolysis**	**Seawater electrolysis**	**PEM electrolysis**
Development stage	Commercial large-scale units	Small laboratory scale	Commercial small-scale units
Cell voltage (V)	1.84–2.25	>2.1	1.75–2.2
Decomposition voltage (V)	1.47	2.1	1.23
Current density (mA cm^{-2})	130–250	25–130	250
Temperature ℃	70–90	23–25	50–80
Cathode	Ni, Steel, Stainless steel	Pt	Pt
Anode	Ni	Pt	Ir
Cell type	H_2/O_2	$H_2/(Cl_2/O_2)$	H_2/O_2
Electrolyte	25–35wt.% KOH	Seawater + drops of HCl	PEM membrane
Salinity level	200–400 ppm	3.4wt.%	-
Main product(s)	H_2	H_2	H_2
By-product	O_2	$Cl_2, NaOCl$	O_2
Advantages	Proven technology, Large-scale H_2 production, low production cost.	The electrolyte is already partially salted.	Higher H_2 purity Lower energy costs It can work at high total and differential pressures
Disadvantages	Low efficiency, low current density, corrosive electrolyte Cannot operate at high pressures High energy costs	Within-laboratory scale	The high cost of the noble catalyst and membrane Technology under development, only used on a small scale

Although Pt is considered to be the best HER electrocatalyst [12], due to its very high cost, it is not employed in commercial alkaline electrolyzers, while it is used as cathode material in PEM electrolyzers. Nickel is the alternative material that is used in the alkaline environment. Nevertheless, the intrinsic HER activity of the Ni cathode and its long-term stability/activity is significantly inferior to that of Pt. To address the former, many research groups have attempted to increase Ni's electrocatalytic activity by alloying Ni with other elements or by nanostructuring the Ni electrode surface [12, 14, 29, 47]. Despite some good outcomes, these cathodes are still susceptible to cathodic fouling by electrodeposition of trace metals present in the electrolyte. Likewise, they are not suitable for use in the very acidic environment that is present in PEM water electrolyzers due to the poor corrosion resistance of Ni at low pH (during the operation Ni cathode is cathodically protected from corrosion, but it corrodes at open circuit). For these reasons, new materials, such as metal oxide electrodes, could potentially be promising electrode materials for cathodes in water electrolyzers (both alkaline and PEM) because of their good stability and their ability to be used in any medium.

2.6 State of the art design of cathodes for HER

An electrode for the electrochemical hydrogen evolution reaction (HER) should have characteristics such as low overpotential, a large active surface area, physical and electrochemical stability, low cost, ease of use, and good electrical conductivity [17].

There are two approaches commonly employed to improve electrocatalyst efficiency, cost, and effectiveness: (i) the development of intrinsically better electrocatalysts based on the materials' physicochemical properties and (ii) modification of the materials' extrinsic properties. The former typically involves the combination of various metals and oxides to form metallic mixtures or alloys; while the latter includes the modification of an electrocatalyst, usually by an increase of its active surface area to allow additional active sites on which the HER can take place.

2.6.1 Intrinsic electrocatalytic activity

Many theories give a substantial basis for the design of intrinsically active HER electrocatalysts, but none of them offer definite answers that could be used for direct design. Researchers agree with the fact that the improvement in the HER electrocatalytic activity is related to the electron density distribution [12, 13, 44, 58]. Hence, the starting point for designing HER electrocatalysts is usually in the electronic structure. A general conclusion for this effect is that the intrinsic catalytic activity for the HER is related to the electronic structure of metals [13]. Miles and Thomason have shown that the intrinsic catalytic activity increases with the number of *d*-orbital electrons, then sharply decreases when the *d*-orbitals are filled [58]. Their results reported that high catalytic activities were obtained for Ni, Pd, and Pt, which have d^8s^2, $d^{10}s^0$, and d^9s^1 electronic configurations, respectively [58]. On the other hand, a decrease in catalytic activity was observed for Zn, Cd, and Hg, which have $d^{10}s^2$ electronic configurations [58]. Their results suggest that an ideal electrocatalyst for the HER should require two electrons for filling its outermost *s* and *d* orbitals and form a M-H_{ads} bond of 60 kcal/mol [58].

The alloying effect of transition metal-based alloys on both the hydrogen evolution activity and catalyst stability has been discussed by Jaksic et al. [13, 59]. This research group postulates that the combination of metals on the left-hand side of the transition metal series that have empty or half-filled *d*-orbital (hypo-*d*-electronic elements), with metals of the right half of the transition metal series, having internally paired *d*-electrons (hyper-*d*-electronic elements) results in a significant change of their bonding strength [13]. In such hypo-hyper-*d*-electronic interactions, paired *d*-electrons of the hyper-*d*-electronic element undergo partial or total transfer to the half-filled or empty semi-*d*-shells of the hypo-*d*-electronic element [13]. This results in the optimal d^8-electrons configuration, and the synergism of the bimetallic catalysts led to improved electrocatalytic activity in the HER.

2.6.2 Extrinsic electrocatalytic activity

Several research groups have proposed novel methods to increase the active surface area of materials [10, 29, 60-62]. Recall that an increase in the electrocatalytic activity of the catalyst allows for a larger production rate of molecular hydrogen and hence a lower operating overpotential for the electrolyzers. Omanovic's group has done work on enhancing the 3D surface structure of Ni electrocatalysts, including supporting nanoparticles (NPs) on polymer templates and layers [63, 64].

Currently, Raney-type Ni is a popular choice for cathode design in industrial alkaline hydrogen generation [15, 61]. Raney-type Ni is an alloy formed between Ni and a more electroactive metal (typically Al or Zn). The resulting material is porous and offer a high specific surface area (extrinsic effect). It is observed that using this alloy, the energy input required to produce hydrogen is lower, which considerably reduces the cost of hydrogen production. Unfortunately, under typical alkaline electrolyzer operating conditions (30 wt.% KOH electrolyte at ca. 70 °C), these Raney-type alloys will disintegrate in solution unless a sufficiently large Ni content is present. More recently, high-specific-area carbon nanowalls (CNWs) have been used as a support for Pt particles in PEM fuel cell research (in an acidic medium) [65]. Due to the high conductivity and low activity in electrochemical reactions, nanostructured carbons, including all forms of carbon nanotubes (CNTs), make an ideal support.

2.6.3 Nickel-based electrocatalysts

Although platinum-based catalysts show the highest activity for the hydrogen evolution reaction (see the volcano curve in Figure 2.4), the scarcity and high cost of platinum, unfortunately, limits the large-scale applications of this material. Furthermore, Pt is very sensitive to poisoning due to the underpotential deposition (UPD) phenomenon (deposition of trace metals from the electrolyte on the Pt surface)

[66]. To overcome these significant barriers without sacrificing catalytic performance, numerous research efforts have been devoted to reducing the Pt consumption or the replacement of Pt with other materials [23].

There have been many studies investigating materials that lower the overpotential of both the hydrogen and oxygen evolution reactions [12, 17, 41, 67-71]. Among the studied transition metals, nickel, in particular, is a good candidate for lowering the overpotential of hydrogen production *via* water electrolysis [72]. Nickel is a very attractive metal for hydrogen production by water electrolysis as it has a relatively high catalytic activity, is inexpensive (13.20 CAD kg^{-1} [67]), and is widely abundant [73]. On the volcano curve (Figure 2.4), Ni appears to be the closest to the best catalysts, i.e., the expensive noble metals.

For these reasons, Ni is an acceptable and interesting alternative for use as a cathode material [15]. Ni has already been accepted as a suitable electrode material in alkaline water electrolysis for both the cathode and anode [15]. Nevertheless, the intrinsic electrocatalytic activity of bare Ni is unable to compete with noble metal catalysts, such as Pt, Ir, and Rh (see Figure 2.4) and it experiences extensive deactivation as a cathode during PEM water electrolysis.

Nickel can be modified to increase its activity in HER. Several attempts have been made to alloy Ni with left transition metals to increase the alloy's intrinsic electrocatalytic activity. The rationale for doing this is based on the modification of the electronic structure of the material to match that of the noble metals [59, 74], as the electronic configuration of the metal electrocatalyst strongly influences its affinity towards the HER, as already stated previously in the thesis [75, 76]. However, there is no universally accepted explanation for the observed improvements to transition metal-based alloy catalysts. It has been proposed that the increased activity towards the HER and the increased catalytic stability of transition metal-based alloys relative to pure metal catalysts can be explained by the Engel-Brewer valance-bond theory (beyond the scope of this thesis) [77, 78].

These improvements were also proposed to be a result of the change in the electronic structure of the alloys. This applies especially to the electron transfer direction between alloy atoms and its effect on the respective metal's Fermi levels [12, 63]. It was proposed that the electronic configuration of the metal catalyst strongly influences its affinity towards the HER [29]. When alloyed with other less active transition metals, the electrocatalytic activity of Ni was shown to increase for specific compositions [24]. It was thought that after an alloy is formed, its electronic configuration would resemble that of a noble metal catalyst such as Pt.

Navarro-Flores et al. showed that Ni alloyed with the left-transition metals Mo, W, and Fe yields an increased intrinsic catalytic activity towards the HER relative to pure Ni in an acidic electrolyte [12]. Of the three alloys tested, $Ni_{7.3}Mo$ showed the largest overall activity towards HER, mostly due to the high surface roughness (extrinsic effect). However, $Ni_{3.4}W$ showed the largest intrinsic catalytic activity towards HER. In their study, they claim that the enhancement of electrocatalytic activity was due to the increased active surface area and a favorable change in electron density in the d-orbital of the material [24]. Another significant result of this study came from the X-ray Diffraction (XRD) measurements. It was found that these catalysts were mostly amorphous. Since amorphous materials lack any structural order, high corrosion resistance can be achieved. Hence, an amorphous transition-metal based electrocatalyst should have a high level of stability [14].

Kirk et al. tested the electrocatalytic activity of an amorphous Ni-Co catalyst in an alkaline media [14]. It was found that the stability of these alloys was excellent under potential cycling conditions, but the electrocatalytic activity of these Ni-Co amorphous alloys was found to be lower in the HER than that of pure crystalline Ni. Thus, it was concluded that crystalline materials are more electrocatalytically active than amorphous materials. Nonetheless, crystalline materials have a lower corrosion resistance than amorphous materials. In this way, a balance must be found between these two factors when synthesizing cathode materials for HER.

Besides pure metal and alloy electrocatalysts, metal oxides have also been examined as potentially suitable cathode materials in the HER. Among others, transition metal oxides have shown an excellent resistance to deactivation and a good stability under acidic and basic conditions. In the next section, more information about the possibilities of using transition metal oxides as cathodes for hydrogen evolution will be presented.

2.6.4 Transition metal oxides as cathodes for HER

In the continuous search for new materials and new applications of technologically established materials, recent patents have claimed good performances for oxide electrodes in the cathodic evolution of hydrogen [79-81]. Transition metal oxides are among the most versatile electrocatalysts ever known. These materials have been used in many electrochemistry-based applications, such as in the chloro-alkali industry, mainly, to produce different valuable chemicals and gases (e.g., chlorine, sodium hydroxide, oxygen, etc.). Metal oxides have been employed for other uses such as corrosion protection of metals, production of electrodes for organic synthesis and wastewater treatment.

Furthermore, they have shown activity for electrocatalytic reactions such as O_2 evolution, O_2 reduction, and even H_2 evolution [20]. However, only a few papers in the open literature deal with the study of HER at oxide electrodes [10, 16-26]. The primary reason for the lack of investigations of oxides as a cathode material is the following: oxides, in general, are insulating or semiconducting materials, which makes them less attractive as electrode materials [26]. Nonetheless, depending on their type of semiconductivity (*p* or *n*) and on the corresponding flat-band potential, they can also be good conductors in particular potential regions and can, thus, be used as good electrocatalysts.

Several aspects make oxides suitable as a cathode material. Metal-oxides significantly enhance the electrochemical and surface properties of the electrode system by providing (i) surface stability, (ii) prolonged service life, (iii) improved electrocatalytic activities, and (iv) optimum operating voltages for specific applications [82]. These characteristics make metal-oxide coatings an attractive electrode material for research. In addition, as a consequence of the different surface chemistry of oxides, compared to the respective pure metals, oxides are more resistant to deactivation caused by the deposit of metal ions (electrolyte impurities) present in the electrolyte [16]. Furthermore, a number of metal-oxide electrodes are known to be very stable across the whole pH scale, even when used as anodes. Due to this fact, they could potentially be promising electrodes materials for both cathodes and anodes in water electrolyzers that operate in the whole pH range (PEM, seawater, alkaline). In fact, the literature has reported a good performance of some metal oxide electrodes for HER: TiO_2 [83], RuO_2 [18], and Co_3O_4 [19], which have been investigated in alkaline media.

Among the class of oxide electrode materials, ruthenium dioxide (RuO_2) and iridium dioxide (IrO_2) are the most promising candidates [84]. RuO_2 has attracted considerable attention as an excellent candidate for electrode material, due to its low resistivity, high chemical, and thermodynamic stability under electrochemical environment. Moreover, It has excellent HER activity, and a higher tolerance toward metal deposition, making it a promising Pt-alternative catalyst for the HER [10]. RuO_2 has also been used as an electrode material for Cl_2 and O_2 evolution. For O_2 evolution in acid media, RuO_2 is the best material with respect to catalytic activity, but it suffers degradation. Early research about the use of RuO_2 as HER cathode by Trasatti and co-workers [26] showed interesting electrocatalytic properties both in acid [6] and in alkaline solutions [2]. Furthermore, long-term experiments have demonstrated the stability of RuO_2 cathodes for more than 4,000 hours at a current density of 1 A cm^{-2} and a temperature of 80°C, demonstrating its catalytic activity for the HER between that of platinum and nickel [26].

Blouin and Guay examined the hydrogen evolution activity of RuO_2, IrO_2, and mixed RuO_2 and IrO_2 electrodes in acidic and basic solutions. They found that the prepared electrodes exhibited large electrocatalytic activity due to the increased number of active sites for the production of H_2 gas [84]. Additionally, cyclic voltammetric measurements revealed no changes in the redox reactions and surface chemistry of the prepared electrodes following HER. This result shows that these oxide electrodes have high stability under electrochemical environment and are suitable for long-term use [84]. However, Ru and Ir are still expensive metals, making them less attractive for industrial purposes when used as major electrode electroactive components [21].

Leonard et al. [23] developed coatings consisting of SiO_2, AlOOH, TiO_2, and ZrO_2 synthesized by the sol-gel technique. These coatings inhibited stainless steel corrosion allowing oxygen evolution and reduced the HER overpotential without precious metal catalysts. This was attributed to the ability of the oxide coatings to adsorb hydrogen on the surface of the electrode. In addition, they measured the electrocatalytic efficiency of the electrodes and compared their results to the values displayed by commercial electrolyzers. The obtained values were very similar in all cases[23].

In another study, Shibli et al. [17] found that the introduction of mixed oxide composite Fe_2O_3–TiO_2, synthesized via thermal decomposition method, increased the catalytic efficiency for the HER of Ni–P electrodes in alkaline solution. The lower overpotential noted during the cathodic polarization revealed the enhanced electrocatalytic activity of the composite towards HER. The improved electrocatalytic activity was obtained due to the mixed hypo-hyper *d*-electronic inter-oxide interaction, in accordance with the Brewer-Engel valence bond theory previously discussed by Jaksic [13, 59].

2.7 Electrochemical supercapacitors

Electrochemical supercapacitors (ES), also known as ultracapacitors or simply supercapacitors (SCs), are electrochemical cells that store electrostatic/chemical energy and liberate electrical energy in a process similar to a battery. ES and batteries are both electrochemical energy storage devices, but they differ in the way they store/liberate the energy. In batteries, the charge is stored by electrochemical reactions with relatively slow kinetics [85]. This mechanism leads to a substantial energy density with a low power density which prevents batteries from being used in applications requiring rapid charging and discharging. Additionally, the electrode materials suffer irreversible phase changes during charge/discharge cycles.

On the other hand, in electrochemical capacitors, energy is stored by charging of the double-layer (electrostatic interactions) or by reversible Faradaic surface/sub-surface reactions (oxidation/reduction) [86]. Moreover, their charge storage mechanism makes them have a longer cycle life than batteries. In Figure 2.7 the electrical energy storage/conversion devices are represented in the so-called "Ragone diagram" in terms of their specific energies and powers [87]. As seen, ES (ultracapacitors in the Figure 2.7) cover the gap between conventional capacitors and batteries.

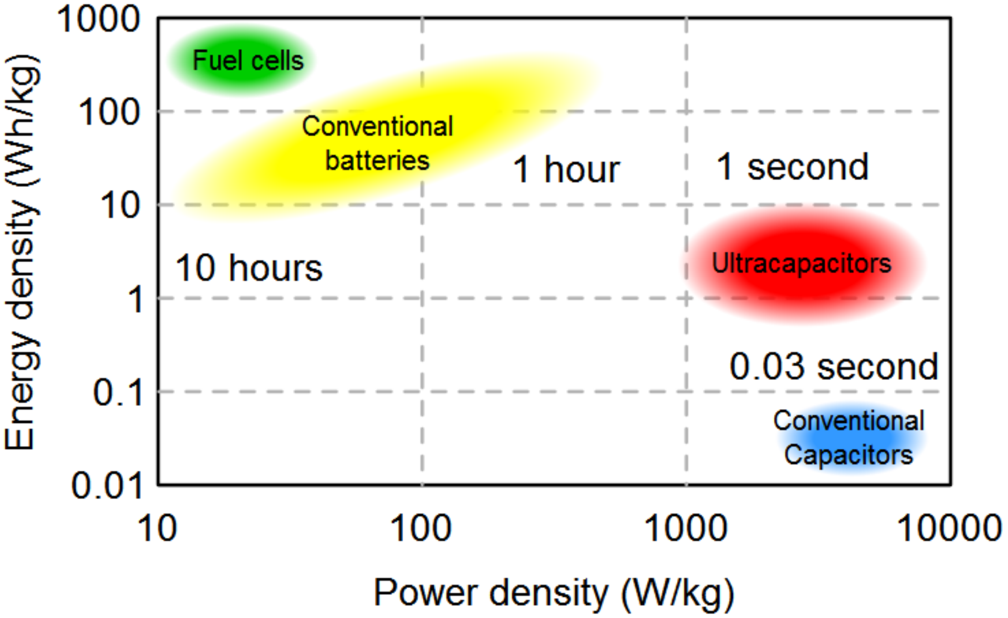

Figure 2.7: Ragone-style plot comparing the power density, energy density, and the time of discharge of several charge storage/conversion devices [88].

Compared with conventional capacitors, the specific energy of the SCs is several orders of magnitude higher, being able to store between 10 and 1000 times more energy than the former, while, at the same time providing only slightly lower power density [85, 89]. Compared to batteries and fuel cells, SCs have higher power density, but their energy density is lower. Therefore, electrochemical capacitors can improve the behavior of a battery in terms of power density or enhance the behavior of a conventional capacitor in terms of energy density [86]. These characteristics make them extremely versatile both for working as power supply devices and in combination with batteries or other electric power generation or storage systems. Table 2.2 shows a comparison between the properties of a battery, a conventional capacitor, and a supercapacitor.

Table 2.2: Comparison between the properties of batteries, conventional capacitors, and supercapacitors.

	Conventional Capacitor	**Supercapacitor**	**Battery**
Charge time	10^{-3} - 10^{-6} s	0.3 - 30 s	1 – 5 h
Discharge time	10^{-3} - 10^{-6} s	0.3 - 30 s	0.3 – 3 h
Energy density (Wh kg^{-1})	< 0.1	1 – 10	10 -150
Power density (Wh kg^{-1})	> 10,000	~10,000	50 -200
Efficiency (%)	> 98	85 – 98	70 – 85
Cycle life (no.)	> 500,000	>100,000	500 – 2000

Electrochemical supercapacitors are energy storage systems of relatively recent appearance, considering that the first practical capacitor of this type was patented by General Electric in 1957 [90]. A schematic representation of one of these devices is shown in Figure 2.8. In general, an ES is composed of two electrodes in contact with an electrolyte and a current collector. Moreover, a sheet of porous material called a separator, which is an electrical insulator and an ion conductor, is interposed between the electrodes. In this way, the separator prevents electrical contact between the two electrodes and, consequently, a possible short circuit of the system, while at the same time allowing the free circulation of the electrolyte through its pores.

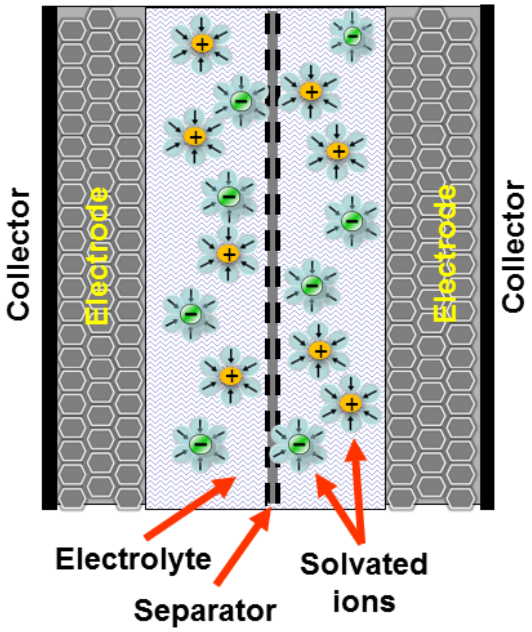

Figure 2.8: Schematic representation of a supercapacitor [91].

There are three types of electrolytes used in an ES: aqueous electrolyte, organic electrolyte, and ionic liquids. Ideally, the electrolyte should have a high ionic conductivity, as well as low viscosity and high thermal and electrical conductivity [85]. Aqueous electrolytes, usually H_2SO_4 or KOH, have a higher ionic concentration and lower resistance, but the useful voltage window is typically small and is limited by the decomposition of water (1.23 V at standard conditions). Organic electrolytes, which are formed commonly by tetraalkylammonium salts dissolved in acetonitrile or polypropylene carbonate, have a wider voltage window. However, the water content in them must be below 3-5 ppm. Otherwise the ES's voltage will be reduced. In general, organic electrolytes are used in commercial applications that require high energy densities, while the selection of an aqueous electrolyte is related to high power requirements. Finally, ionic liquids have a low vapor pressure (meaning that it is less likely to evaporate), high thermal and chemical stability and low flammability. The problem with ionic liquids is that they cannot provide a wide potential range and high conductivity in a wide temperature range [89].

The nature of the separator used in the construction of the supercapacitor is determined by the type of electrolyte used. If an aqueous solution is used, the separators will be of a ceramic material or fiberglass. If the electrolyte is organic, the separators will be polymeric or paper [92]. Furthermore, to optimize the behavior of the capacitor, the separator must have high electrical resistance, high ionic conductivity and small thickness [93].

There are two types of electrochemical supercapacitors. The first one is called the electrical double-layer supercapacitor (EDLS). EDLS has a limited specific capacitance and low energy density. The second one is the faradaic supercapacitor (FS), and it is superior to the EDLS in terms of capacitance and energy density. FSs are also known as pseudocapacitors. In the following sections, these types of ESs will be explained in more detail.

2.7.1 Electrical Double-Layer Supercapacitors (EDLS)

In capacitors based on the electric double layer mechanism, energy is stored by electrostatic forces at the electrode/electrolyte interface as a consequence of the charge separation that is established by applying a potential difference. The formation of the electric double layer occurs at all charged interfaces, and has typical values between 15-50 µF cm^{-2} for flat electrodes (based on the active surface area) in aqueous electrolytes, decreasing this value in organic solvents and in the presence of surfactants [94].

Several charge storage models for SCs have been developed in the past few decades with increasing accuracy in modeling the behavior of ES [94]. Von Helmholtz first introduced an over-simplified concept of the electric double layer that is responsible for the capacitive charge. The model suggested that, when a potential is applied, the ions from the solution will accumulate on the surface of the electrode that is oppositely charged. A counter-layer would develop from within the solid to achieve charge neutrality. Helmholtz model was modified by the Guoy-Chapman model that introduced the diffusive layer. However, the model only gives correct values when the voltage is nearly zero. Models later developed by Parsons; Stern; and Grahame solved this problem by adding the compact layers called inner and outer Helmholtz layers[89].

The double layer mechanism is represented in Figure 2.9. For EDLS, when a voltage is applied to the electrodes, the electrodes would be polarized. Ions in the electrolyte will form electric double layers of opposite polarity to that of the electrode. One layer is within the solid electrode while the second one forms from solvated ions distributed in the electrolyte. These two layers are separated by a monolayer of solvent molecules, which forms the inner Helmholtz plane (IHP). This plane adheres by physical adsorption on the electrode surface and separates the oppositely polarized ions from the charged solid surface (negative electrode in the figure below), creating a molecular dielectric. There is also another area close to the IHP, in which the polarized electrolyte ions are collected. This area is known as the outer Helmholtz plane (OHP).

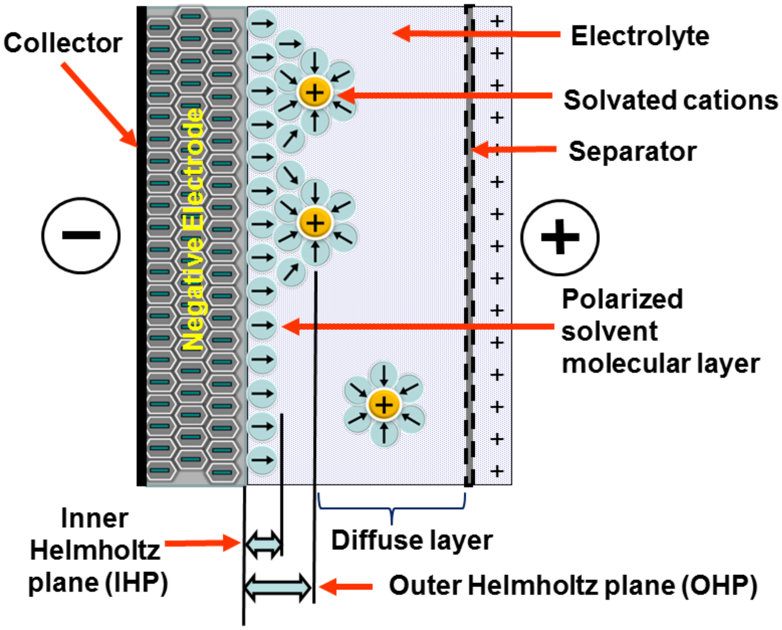

Figure 2.9: Schematic representation of an electrical double-layer supercapacitor [95].

The mechanism of storage of the EDLCs consist purely of electrostatic forces, and that does not involve chemical phase changes, which determines its main associated operation advantages: a high capacity of response (typically, < 30 s) and, therefore, better performance in terms of power than batteries (with values higher than 10 kW kg^{-1}), excellent efficiency (90-95% or higher), and a high number of cycles (see Table 2.3). Nonetheless, the electrostatic nature of the charge storage mechanism governs the most notable disadvantage - a limited energy density, lower than 10 Wh kg $^{-1}$ for most commercial capacitors [96].

The capacitance of a two-place capacitor can be calculated by the formula:

$$C = \varepsilon\varepsilon_0 \frac{A}{d} \tag{2.11}$$

where A is the surface area of the plates (m^2), ε is the permittivity of the dielectric material (-), ε_0 is the electric constant ($\varepsilon_0 \approx 8.854\times10^{-12}$ F·m^{-1}) and d is the distance between the plates (m). When comparing with conventional capacitors, EDLS have a much higher capacitance (see Table 2.2) due to their small thickness of the double layer (ca. two-molecular layers) at the electrode/electrolyte interface and their larger electrode area (due to the use of porous electrodes). Activated carbon is currently the most commonly used electrode material for EDLS due to its low cost and availability and high specific surface area, and large specific capacitance ca 295 F g^{-1} at a current density of 0.1 A g^{-1}.

2.7.2 Faradaic supercapacitors (FS) or pseudocapacitors

Three types of electrochemical processes can be used in the development of pseudocapacitive phenomena: [94] reversible adsorption, redox reactions of electroactive materials (e.g., RuO_2, IrO_2, etc.), and reversible electrochemical doping processes that take place in electrically conductive polymers. The first two processes occur through mechanisms that take place on the surface of the solid electrode. The third process involves the entire volume of the polymeric material and, although it is much less dependent on the surface characteristics of the electrode.

This research will focus more on the pseudocapacitance originated via reversible faradic redox reactions occurring on the surface and sub-surface of the electrodes. The redox reactions are electrode potential dependent. Consequently, when a potential is applied to a pseudocapacitor, reduction and oxidation take place on the electrode material, which involves the passage of charge across the double layer and solid phase, resulting in faradic current passing through the supercapacitor [85, 94]. These electron transfer reactions occur very quickly (contrary to the redox reactions in batteries, which are considerably slower. Additionally, the faradic process involved in pseudocapacitors allows them to achieve larger specific capacitance (by 10–100 times) and energy densities compared to EDLCs.

The ability of electrodes to accomplish pseudocapacitance effects by redox reactions strongly depends on the chemical affinity of the ions exchanged on the electrode surface and the structure and size of the electrode pores. Transition metal oxide such as ruthenium (RuO_2), iridium (IrO_2), iron (Fe_3O_4), manganese (MnO_2) or their combinations can generate faradaic electron–transferring reactions with low conducting resistance.

In this Ph.D. thesis, the addition of iridium oxide into the Ni-Mo-oxide coating is investigated for supercapacitor applications. IrO_2 is one of the most studied materials due to its high capacitance, long cycle life, high conductivity, and reversibility of its redox reactions [114]. IrO_2 is considered a good pseudocapacitor due to its multiple oxidation states. Pseudocapacitance originates from a coupled, fast and reversible redox reaction with several oxidation steps with overlapping potential. For iridium oxides, the electron transfer reaction [97] takes place according to:

$$IrO_a(OH)_b \longleftrightarrow IrO_{(a+\delta)}\,(OH)_{(b-\delta)} + \delta H^+ + \delta e \tag{2.12}$$

During the redox reactions, H^+ (protons) are combined into or removed from the IrO_2 crystal lattice, which generates storage of electrical energy.

Table 2.3 summarizes some general differences between the double-layer and the faradaic capacitors.

Table 2.3: Main characteristics of an ideal double-layer capacitor and a faradaic capacitor.

	EDLC	**FS**
Energy Density	low	High
Mechanism	double-layer	redox reactions
Power Density	high	Medium
Cycle life (no.)	10^6	10^6

In general, both energy storage mechanisms, electrostatic and faradaic, coexist in a supercapacitor, although it is always one of the two that determines their overall behavior [98]. In the case of supercapacitors built with carbon materials, the electric double layer mechanism is the predominant one, while in the case of supercapacitors with transition metals or polymeric electrodes, the faradaic reactions prevailed.

2.7.3 Electrode Materials for Electrochemical Supercapacitors

The selection of the electrode material strongly determines the electrochemical properties of a SC, since it is generally the one that defines the energy storage mechanism of the overall device. The ideal properties that an electrode for electrochemical supercapacitor applications must have are large surface area, excellent electric conductivity, electrochemical stability, and short diffusion paths for ions transfer. The most commonly used materials in electrodes for SCs can be divided into three main categories: capacitors built with carbon material electrodes, those made with transition metal oxides, and those that contain conductive polymers. This thesis only will focus on the transition metal oxides.

Metal oxides are considered the best candidates as electrode materials for faradaic electrochemical capacitors because they combine a high specific capacity and a low resistance, which gives them a high specific power, being very interesting in specific commercial applications. The energy storage mechanism of this type of material is based on a pseudo-capacitive faradaic reaction. Among them, the most commonly used transition metals can be divided into two types: noble (RuO_2 and IrO_2) and cheap transition metal oxides (MnO_2, Co_3O_4, NiO).

Nowadays RuO_2 is been considered the most promising material because it has a high theoretical specific capacity of 2000 F g^{-1} [99], a highly reversible redox reaction, excellent cyclability, long cycle life, and high electric conductivity, [100]. The capacitive behavior of this oxide has been the object of study during the last 30 years, describing itself as a fast and reversible electron transfer. However, the supercapacitive behavior of RuO_2 depends on the type of the electrolyte, the amount of water that contains, the degree of crystallinity, and particle size.

Some research groups have worked in on improving these characteristics of Ru to achieve a better capacitance performance [85, 92, 101-103]. In this regard, Hu et al. [104] performed experiments combining $RuOx{\cdot}nH_2O$ and $IrOx{\cdot}nH_2O$ and they found that the resulted coating is enhanced by the presence of $IrOx \cdot nH_2O$ due to an increase in nonstoichiometric sites within the $RuOx \cdot nH_2O$ matrix, yielding a ca. 3-fold increase (ca. 125 to 350 F g^{-1}) in specific capacitance over $RuOx \cdot nH_2O$ alone.

Nonetheless, the scarcity of these materials and, therefore, the high price of them (Ru and Ir), have restricted their use only to military applications [105]. To this must be added the fact that these materials are only suitable for working with aqueous electrolytes, which limits their window of potential work to 1 V and that they, in addition, generate environmental problems [106].

These drawbacks have made it necessary to open new research channels aimed at: (i) the reduction of the amount of noble metal oxides by mixing them with other metal components, which has the advantage of increasing the working electrochemical window and improving the capacity of the electrode materials [107, 108], (ii) the replacement of the oxides of Ru and Ir by other oxides such as MnO_2, Fe_3O_4, NiO, Co_3O_4 [103] more abundant and less harmful to the environment, and (iii) the study of hybrid electrodes formed by the combination of metal oxides with polymeric or carbon materials [85, 94, 103].

2.7.4 Electrochemical supercapacitors applications

ESs are widely used to supply energy in a very short time period owing to their high pulse power. Applications that utilize this characteristic of ES include computers, cameras, and cell phones [86, 106, 109]. ESs can protect the circuit when there are power disturbances, or they could offer low energy for an extended period. Another benefit of SCs is that they have faster charge times than batteries and significantly longer cycle life. The reliability of ES is demonstrated by the fact that ES technology is used in the emergency doors of Airbus A380. ESs are also being used to address the power supply problems in hybrid electric cars since HEVs need a high energy power source. The main challenges of this developing technology are their low energy density and high costs [85, 94]. The issues are being tackled by researching ionic liquid electrolytes and by employing new materials for the electrode.

.

Chapter 3

3 Nickel-Cobalt-Oxide Cathodes for Hydrogen Production by Water Electrolysis in Acidic and Alkaline Media

3.1 Preface

This chapter presents an article that has been published in the *International Journal of Hydrogen Energy*. The citation of the published article is the following:

> A. Gomez Vidales, K. Choi, S. Omanovic, *Nickel-cobalt-oxide cathodes for hydrogen production by water electrolysis in acidic and alkaline media.* International Journal of Hydrogen Energy, 43 (2018), 12917-12928.

The work was planned, performed, analyzed, and written by Abraham Gomez Vidales (the Ph.D. candidate). The Ni-Co-oxide electrodes were synthesized by Kanhoong Choi (a McGill University undergraduate student at that time), who also made the electrochemical characterization of them. Prof. Sasha Omanovic was responsible for supervision of the work, helped in the interpretation and discussion of results, and reviewed the manuscript. In the results and discussion section, each data point and the corresponding deviation presented in figures represent an average of 9-15 measurements: between 3 to 5 separate samples, each tested 3 times.

The following chapter presents an initial study of the nickel-oxide based electrodes for energy storage applications. In this particular case presents results about the electrochemical properties of the Ni-Co-oxides coatings of different compositions for the hydrogen evolution reaction (HER) prepared using a thermal-salt decomposition method. The experimental work is focused on the composition, morphology, and structure of the coatings, their electrochemical activity, and their long-term stability. Furthermore, the electrochemically-active surface area and the activation energy were determined.

This academic article is dedicated to the LORDS: Jorge Alberto Acosta, Juan Bautista Martinez, Alejandro Renteria, and Octavio Salinas, thanks for your friendship.

Nickel-Cobalt-Oxide Cathodes for Hydrogen Production by Water Electrolysis in Acidic and Alkaline Media

Abraham Gomez Vidales*, Kanghoon Choi, Sasha Omanovic

Department of Chemical Engineering, McGill University, 3610 University St., Montreal, Quebec, H3A 0C5, Canada

* Corresponding author: abraham.gomezvidales@mail.mcgill.ca

Keywords: Hydrogen; Water electrolysis; Cobalt, Nickel; Metal oxides; Cathodes.

Highlights

- Ni-Co-oxide cathodes were used for hydrogen production by water electrolysis in acidic and alkaline media.
- The oxide electrodes were found to be of a semi-crystalline structure, yielding the surface morphology characterized by relatively high surface roughness.
- $Ni_{0.2}Co_{0.8}$-oxide yielded the highest apparent electrocatalytic activity in both electrolytes.
- Nickel electrode showed the highest intrinsic electrocatalytic activity.
- Ni-Co-oxides were found to be significantly more fouling/deactivation-resistant than Ni during long-term testing.

Abstract

Mixed Ni-Co-oxide cathodes of various compositions were fabricated by a thermal-decomposition method and used as electrocatalysts for hydrogen production by water electrolysis in acidic and alkaline media. The oxide electrodes were found to be of a semi-crystalline structure, yielding the surface morphology characterized by relatively high surface roughness factor (up to 25). Linear potentiodynamic and potentiostatic electrochemical measurements revealed that the Volmer reaction step controlled the kinetics of the hydrogen evolution on all the Ni-Co-oxide cathodes, and also on the pure metal Ni electrode (control). The $Ni_{0.2}Co_{0.8}$-oxide was identified as the best electrode material candidate among the investigated metal oxides, which was linked to the surface-area effect. However, its intrinsic activity was found to be lower than that of pure metallic Ni. Nevertheless, the $Ni_{0.2}Co_{0.8}$-oxide electrode showed a significantly higher electrocatalytic stability (fouling/deactivation tolerance) in comparison to metallic Ni.

3.2 Introduction

The demand on novel renewable energy have been increasing over the past few years due to the rapid depletion of the traditional energy sources, such as fossil fuels. Many research efforts have sought ways to reduce the dependency on fossil fuels by trying to find an alternative power source. Hydrogen, the most abundant element in the universe, is considered to be an excellent green energy source due to its minimal impact on the environment [4]. Despite its abundance, hydrogen is hardly found as a separate element. Instead, it is primarily found in combination with carbon in hydrocarbon compounds, and with oxygen in water [33].

Hydrogen (H_2) can be obtained by water electrolysis, where electrical current is applied to split water into its components (oxygen and hydrogen). Hydrogen obtained by water electrolysis is a clean energy carrier since it can produce energy in fuel cells (or by burning) without emitting carbon dioxide [8]. Unfortunately, water electrolysis is not yet cost-competitive to hydrocarbon reforming due to its high operational costs (electricity cost, electrodes degradation). In the case of production of hydrogen by polymer-electrolyte-membrane (PEM) electrolyzers, the operational costs per amount of produced hydrogen are lower in terms of the electricity used, but the cost of the PEM technology is higher in comparison to the conventional alkaline electrolyzers. This is mainly a consequence of the use of expensive noble metals (platinum, ruthenium, and iridium) as electrocatalyst (electrode) materials, which is required due to the high acidity of the electrolyte environment [12]. In addition, despite the use of noble metals, the long-term stability and activity of electrodes are still not satisfactory. On the other hand, in alkaline electrolyzers, nickel electrodes could be used because of a much milder electrolyte environment (high pH). However, neither currently-used nickel electrodes offer satisfactory performance, especially regarding the fouling susceptibility (deactivation of Ni cathodes by electrochemically deposited trace metals) and mechanical stability. Also, further decrease in the hydrogen evolution reaction (HER) overpotential is required to make this process feasible.

An ideal electrode for the HER should have characteristics such as low overpotential, large active surface area, physical and electrochemical stability, high fouling resistance, low-cost, ease of use, and excellent electrical conductivity [17]. In this context, extensive research has been performed on the development of new electrode materials for hydrogen production [12-15, 17, 24, 61, 63, 64, 70, 77, 110, 111]. Ni-based alloys have been identified as suitable candidates for electrodes in the alkaline water electrolysis, and in particular, Ni-Co has been found to offer electrocatalytic activity comparable to that of noble metals [20, 69, 111-114].

Unfortunately, pure metallic Ni-based alloys suffer two significant drawbacks. First, they cannot operate in PEM water electrolyzers due to their poor corrosion stability in the acidic medium. Second, they are susceptible to deactivation by electrodeposition of metallic impurities presented in the electrolyte, and thus their long-term stability and activity are not satisfactory even in alkaline water electrolyzers. [16]. In the search for new materials, certain metal oxide electrodes have demonstrated excellent performance in the hydrogen evolution reaction, but they have not been widely studied [16-18]. The most intriguing aspect of metal oxides is that they have the ability to remain active for HER even in the presence of metallic impurities [16]. Furthermore, oxide electrodes have been claimed to be stable in both acidic and alkaline environments [84]. Due to the unique features of the metal oxides, they have been recognized as promising cathode materials for the electrocatalysis of HER.

The purpose of this research was to develop and study mixed Ni-Co-oxide cathodes for the hydrogen production by water electrolysis in both the acidic and alkaline media. The rationale for choosing Ni-Co-oxides was due to their availability, low-cost, and promising results obtained in previous research studies as pure (non-oxide) alloy cathodes for hydrogen evolution [12, 16]. Moreover, this study reports the effects of electrode composition and electrolyte temperature on the electrocatalytic performance for the HER.

3.3 Experimental procedure

3.3.1 Electrode preparation

$Ni_xCo_{(1-x)}$-oxide coatings (x = 0, 0.2, 0.4, 0.6, 0.8, 1; where x is the molar fraction and refers to the content of Ni and Co in the precursor solution) were formed on a flat titanium substrate by employing a thermal-decomposition method. A titanium button-shaped plate of 1.27 cm in diameter (purity 99.2%, Alfa Aesar, USA), with a thickness of 0.2 cm was used as a substrate. A first step of the electrode preparation process was to wet-polish the titanium substrate using 600-grit SiC sandpaper. Next, the polished plate was rinsed thoroughly and sonicated for 30 minutes in deionized water (resistivity 18.2 MΩ cm) to remove polishing residues. Then, the plate was etched in a boiling solution of hydrochloric acid (37wt.%, Fisher Scientific, Canada) and deionized water (1:1 by volume) for 30 minutes. After etching, the plate was again thoroughly rinsed with deionized water, and dried in argon gas (MEGS Specialty Gases Inc., 99.998wt% pure, Canada).

To coat the titanium plate, a 0.2 M precursor solution was prepared by dissolving the metal precursor salts in an equivolume mixture of 37wt.% hydrochloric acid and deionized water. $NiCl_2 \times 6H_2O$ (purity 99.9%, Sigma-Aldrich, Canada), and $Co(NO_3)_2 \times 6H_2O$ (purity 99.7%, Acros Organics, Canada) were used as a source of nickel and cobalt, respectively. The coating solution was applied uniformly to the titanium substrate with a paintbrush (only one side of the titanium plate was coated with the precursor solution). After applying the first layer, the sample was placed in an oven at 383 K for five minutes to vaporize the solvent, followed by annealing the sample at 773 K in an air-natural-convection furnace for fifteen minutes. Next, the sample was removed from the furnace and allowed to cool for ten minutes, before another coating was applied. This same procedure was repeated six times to form a six-layered coating on the titanium substrate. Lastly, the sample was annealed in the furnace at 773 K for one hour to complete the oxidation of the coating to produce the $Ni_xCo_{(1-x)}$-oxides.

3.3.2 Electrochemical and surface/chemical composition characterization

The electrochemical characterization of electrodes towards hydrogen evolution reaction was investigated using a three-electrode cell, at 293±2 K and atmospheric pressure. The working electrode (WE) was at the bottom of the cell, fitted between a steel plate (to provide electrical contact) and the Teflon base of the cell containing an opening to the electrolyte. The geometrical area of the electrode exposed to the electrolyte solution was 0.68 cm^2. The counter electrode (CE), a graphite rod, was placed inside a glass tube plugged with a glass frit (Ace Glass Inc., USA) which prevented O_2 gas produced at the CE to migrate towards the WE and get reduced, thus interfering with the HER. A saturated calomel electrode (SCE) (Accumet electrode, Fisher

Scientific, USA) was used as the reference electrode (RE). To maintain an oxygen-free electrolyte solution, argon gas was purged through the electrolyte before electrochemical measurements for 30 minutes and continued to be purged during the measurements. In order to characterize the electrochemical behavior of the coatings, linear Tafel polarization (LTP), chronoamperometry (CA), chronopotentiometry (CP) measurements were performed using an Autolab PGSTAT30 potentiostat/galvanostat with NOVA software (v. 2.1; Metrohm, the Netherlands). Electrochemical measurements were done using two different electrolytes: 0.5 M H_2SO_4 (pH = 0.25) for the acidic electrolysis (prepared using 96wt.% H_2SO_4, Fisher Scientific, Canada), and 1 M NaOH (pH = 14) for the alkaline electrolysis (prepared using 95wt.% purity NaOH crystals; Sigma-Aldrich, Canada).

The surface topography and chemical composition of the metal-oxide coatings were investigated using the scanning-electron-microscopy (SEM) and energy-dispersive X-ray spectroscopy (EDS) analysis (instrument: Hitachi SU-3500 Variable Pressure SEM/EDS detectors). The coatings' structural characterization was done employing the X-ray diffraction (XRD) analysis (instrument: Bruker D8 Discovery X-Ray Diffractometer).

3.3.3 Electrochemical surface area determination

The electroactive surface area of the metal-oxide cathodes was determined by performing cyclic voltammetry (CV) and chronoamperometry (CA), using a solution of 1 mM HexRu(III) chloride (purity 98wt.%, Sigma-Aldrich, USA) in 0.1 M KNO_3 (purity 99wt.%, Fisher Scientific, Canada) as a redox probe [115-118]. For CV, a detailed description of this procedure can be found in our previous paper [119]. For CA, a current response at selected electrode potentials was recorded during the time of 15 seconds. Since the reduction of Ru(III) ion is a mass-transport controlled process, the recorded chronoamperogram follows the Cottrell equation $i = nFACD^{1/2}/(\pi t)^{1/2}$, where n is the number of electrons appearing in half-reaction for the redox couple (one, in the current case), F is the Faraday constant (96485 C mol^{-1}), A is the electrochemically-active surface area (cm^2), *C* is the concentration of the analyte in the bulk solution, HexRu(III) chloride (mol cm^{-3}), *D* is the diffusion coefficient (8.70×10^{-6} cm^2s^{-1} in the case of HexRu(III) in the used electrolyte), and *t* is the time (s). The electrochemically-active area of the metal-oxide electrode was determined from the *i* vs. $t^{-1/2}$ linear plot, and the values are combined with those obtained from CV measurements.

3.4 Results and discussion

3.4.1 Composition and structural characterization

Energy-dispersive spectroscopy verified the actual chemical composition of the coatings, and the results are presented in Table 3.1. From the results, it is seen that the actual Ni/Co ratio in the coating is very close to the nominal Ni/Co ratio (the ratio of Ni and Co in the precursor solutions). Furthermore, the EDS mapping of the coatings at several selected areas on the sample surface confirmed that the composition was uniform over the entire coating surface.

Table 3.1: Relative atomic percentage of Ni and Co in $Ni_xCo_{(1-x)}$-oxide coatings (excluding the contribution of oxygen in the coatings) obtained by EDS. These values refer to the measured concentration of Ni and Co on the surface of the coatings.

Element content, at. %	
Nominal	**Experimental**
NiOx	NiOx
$Ni_{0.8}Co_{0.2}Ox$	$Ni_{0.74}Co_{0.26}Ox$
$Ni_{0.6}Co_{0.4}Ox$	$Ni_{0.56}Co_{0.44}Ox$
$Ni_{0.4}Co_{0.6}Ox$	$Ni_{0.42}Co_{0.58}Ox$
$Ni_{0.2}Co_{0.8}Ox$	$Ni_{0.12}Co_{0.88}Ox$
CoOx	CoOx

Another significant result emerged from the X-ray diffraction measurements. Figure 3.1 shows the XRD patterns of all the samples. The spectra show that the coatings are mostly semi-crystalline. Distinct peaks characterized the diffraction pattern recorded on the pure Ni substrate: the peaks correspond, in increasing order of 2θ, to the

(1 1 1), (2 0 0), and (2 2 0) reflections of the f.c.c. the structure of nickel (JCPDS card no. 4-0835) [120]; NiO peaks also appeared, and these were due to the oxidation of Ni in the air. For the NiO coating, the diffraction pattern obtained was identical to pure Ni but with higher intensity of peaks recorded at reflection planes of NiO (1 1 1) and (2 0 0) (JCPDS card no. 47-1049) [121]. Moreover, XRD detected the presence of Ni_2O_3 in the coating. Figure 1 also reveals that Co-oxides present in each coating are characterized by some degree of amorphousness since they have relatively broader peaks than the Ni-oxides characteristic diffraction patterns. Two crystalline forms of Co-oxide are present in the coatings: CoO and Co_3O_4. Concerning the XRD pattern of Co-oxide coating, this matched well with the standard (JCPDS card no. 9-402). Based on the results of synthesis and characterization, it can be concluded that the stable phases of $Ni_xCo_{(1-x)}$-oxide using the proposed chemical route can be synthesized and that the degree of amorphousness augmented with the increase in cobalt content in the coatings.

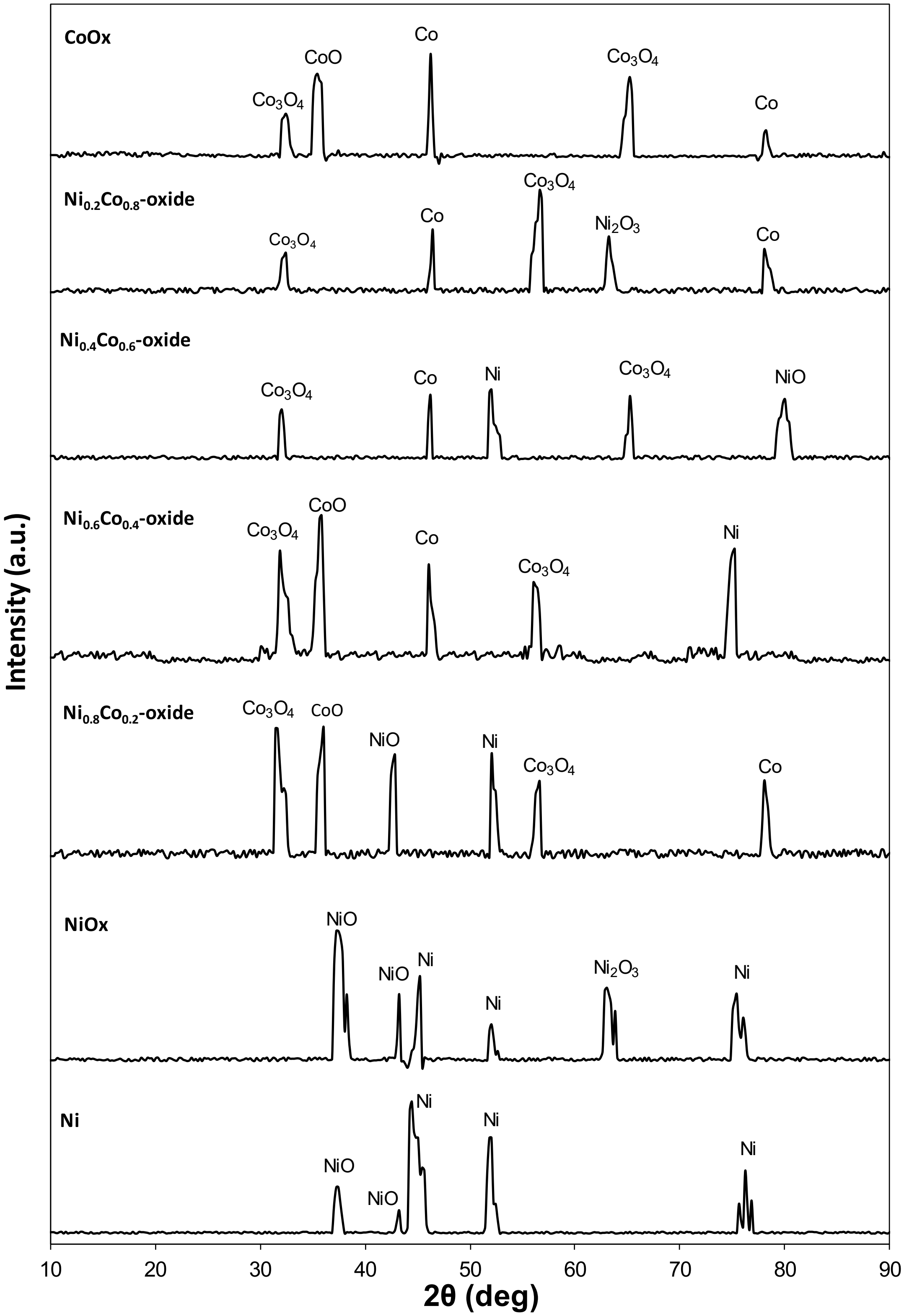

Figure 3.1 X-ray diffraction spectra of $Ni_xCo_{(1-x)}$-oxide coatings deposited on a titanium substrate. Results for Ni-control sample are also presented for comparison.

3.4.2 Morphology and electrochemical-active surface area of the electrodes

To examine the morphology of the coatings, a scanning electron microscopy technique was employed. The SEM images in Figure 3.2 show differences in morphology of the investigated coatings. The corresponding particle size distribution was analyzed employing ImageJ software (v. 1.51, NIH, USA). The 600-grit polished Ni control sample (Figure 3.2a) shows a surface of a certain degree of roughness. Instead, the Ni-oxide surface, Figure 3.2b, shows a sponge-like structure. This structure displays a higher degree of roughness and a porous structure, relative to the nickel control sample.

The addition of Co into the coating significantly influences the morphology of the surface, as presented in Figure 3.2c-f. Unlike the sponge-like structure of Ni-oxide, Co-containing $Ni_xCo_{(1-x)}$-oxide coatings display a granular structure. The $Ni_{0.8}Co_{0.2}$-oxide coating displays a lower degree of surface roughness and porosity than the pure Ni-oxide coating. Nevertheless, by increasing the Co content from 20% to 40%, the coating's porosity increases while the diameter of polygonal particles slightly increases from size ca. 0.8 ± 0.6 μm for the $Ni_{0.8}Co_{0.2}$-oxide coating to ca. 2.5 ± 0.9 μm for the $Ni_{0.6}Co_{0.4}$-oxide. By further increasing the Co content to 60%, the diameter (2.9 ± 1.1 μm) and the distribution of the particles remains similar to the 40% Co sample. For the $Ni_{0.2}Co_{0.8}$-oxide surface (Figure 3.2f) and Co-oxide, the granular particle diameter slightly increased to 3.4 ± 1.5 μm and 3.1 ± 1.6 μm. Surprisingly, the pure Co-oxide coating (Figure 2g) shows the morphology resembling that of the $Ni_xCo_{(1-x)}$-oxide coatings. This indicates that the Co-oxide present in of these mixed metal oxide coatings most-likely governs their morphology rather than the Ni-oxide.

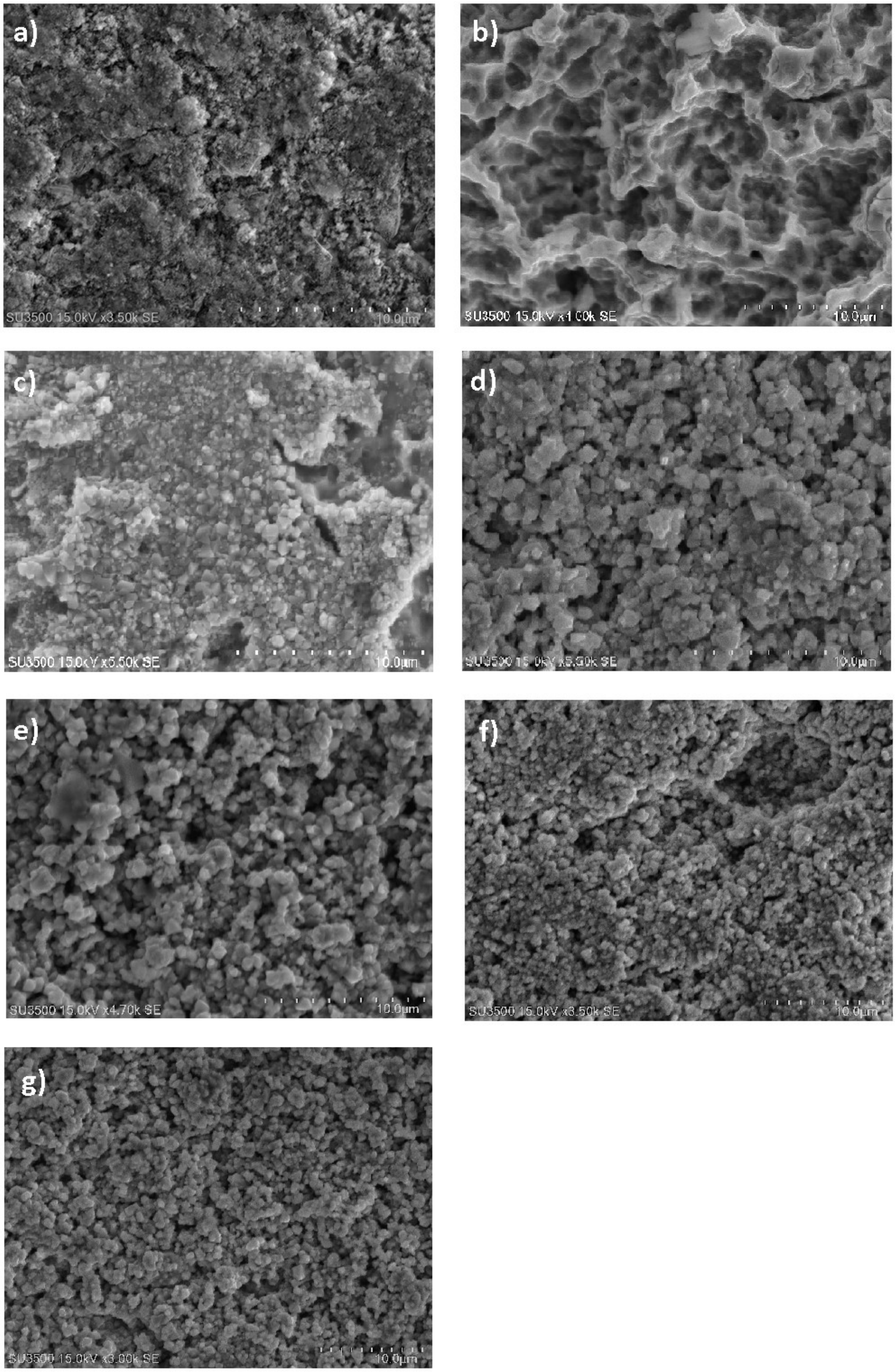

Figure 3.2 SEM images showing a surface morphology of a) Ni metal plate (control sample), b) Ni-oxide, c) $Ni_{0.8}Co_{0.2}$-oxide, d) $Ni_{0.6}Co_{0.4}$-oxide, e) $Ni_{0.4}Co_{0.6}$-oxide, f) $Ni_{0.2}Co_{0.8}$-oxide, and g) Co-oxide coating. The overall scale length on the images is 10 μm.

Figure 3.2 shows that the produced coatings display a varying degree of surface roughness and morphology, which implies differences in size of the area of the coating exposed to the electrolyte, i.e., the electrochemically-active surface area size. To determine the electrochemically-active area of the surfaces, cyclic voltammetry and chronoamperometry in a ruthenium-complex solution was performed, as explained in the experimental section of the paper. The obtained values combining both techniques are presented in Table 3.2, together with the corresponding surface roughness factor.

Table 3.2: True electrochemically-active surface area of Ni and $Ni_xCo_{(1-x)}$-oxide cathodes shown in Figure 2 obtained by cyclic voltammetry and chronoamperometry. The geometric area is 0.68 cm^2.

Material	**Electrochemically-active surface area (cm^2)**	**Surface roughness factor**
Ni	3.9 ± 0.6	5.7
NiOx	9.8 ± 2.6	14.4
$Ni_{0.8}Co_{0.2}Ox$	6.2 ± 1.7	9.1
$Ni_{0.6}Co_{0.4}Ox$	10.7 ± 2.7	15.7
$Ni_{0.4}Co_{0.6}Ox$	8.5 ± 2.3	12.5
$Ni_{0.2}Co_{0.8}Ox$	10.8 ± 3.1	15.9
CoOx	17.2 ± 3.5	25.3

Overall, in all the cases, the electrochemically-active surface areas were determined to be considerably larger than the geometrical surface area of the electrocatalysts, i.e., 0.68 cm^2. Co-oxide electrode displayed the highest electrochemically active surface area, whereas the nickel control sample displayed the lowest active area. Additionally, $Ni_{0.6}Co_{0.4}$-oxide, $Ni_{0.4}Co_{0.6}$-oxide, and $Ni_{0.2}Co_{0.8}$-oxide have surface areas which are very similar between them; this could be due to the similar diameter of the particles in these coatings. These results are consistent with the observations made based on the surface characterization of the coatings by SEM presented in Figure 3.2.

3.4.3 Electrocatalytic activity in the HER

The electrocatalytic activity of the cathodes towards hydrogen evolution was investigated using linear Tafel polarization (LTP) and chronoamperometry (CA). Tafel polarization measurements were performed using two different electrolytes: 0.5 M H_2SO_4 and 1 M NaOH. Before electrochemical measurements, the electrode was pretreated for one hour at a potential of -1.60 V in 1M NaOH and at -1.4 V in 0.5 H_2SO_4, to ensure that all scans start with a conditioned surface. The polarization curves were corrected for the ohmic drop, where the electrolyte resistance value was obtained from EIS data (not shown here). CA measurements were done at selected potentials within the HER region for 300 seconds. From the CA measurements, the average current in the last 100 seconds was taken for further analysis.

Figures 3.3 and 3.4 show sets of HER polarization curves recorded in 0.5 M H_2SO_4, and 1 M NaOH on all the investigated coatings, respectively. In these curves, the abscissa represents the overpotential, η (V), which is the input driving force for the HER, while the current density, j (A cm-2), presented on the ordinate, represents the HER kinetics which is related to the amount of hydrogen produced, through the Faraday law.

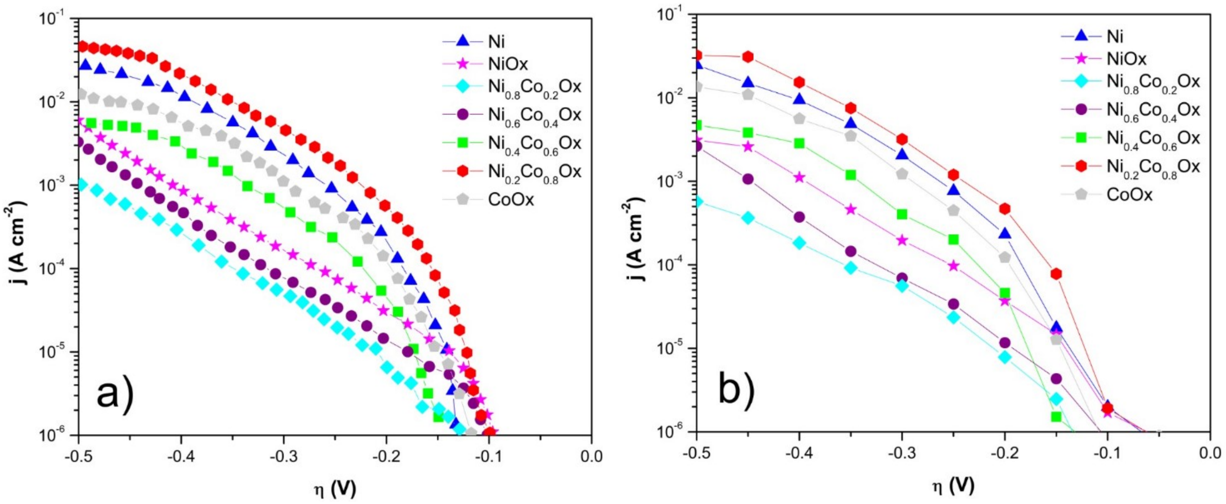

Figure 3.3: Polarization curves recorded in 0.5 M H_2SO_4 on a Ni control sample and on $Ni_xCo_{(1-x)}$-oxide coatings by (a) LPT and b) CA. Temperature = 293±2 K. Scan rate in LPT was 1 mV$s^{-1,}$ and in both cases, the polarization was done from high to low overpotentials.

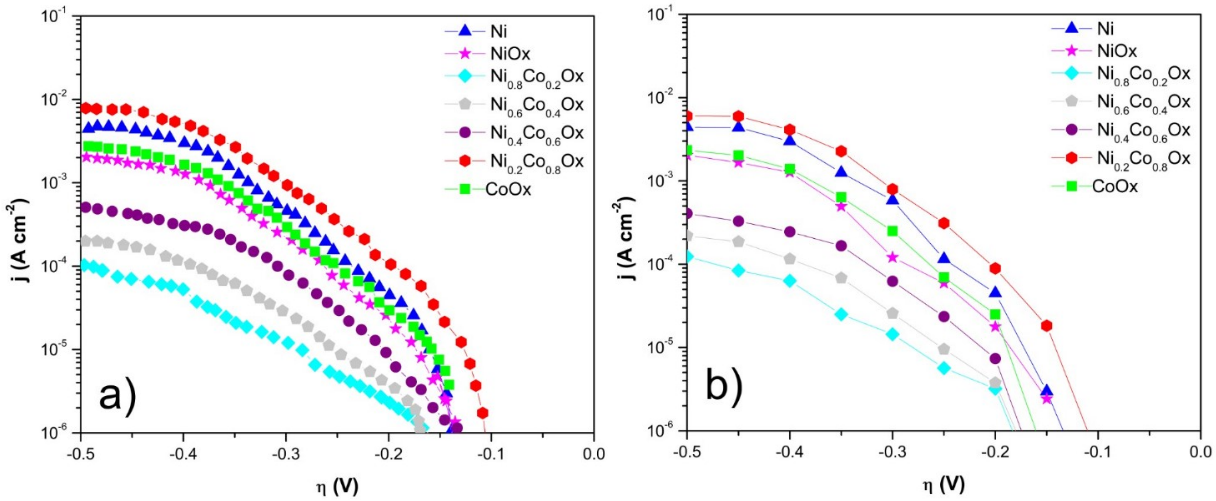

Figure 3.4: Polarization curves recorded in 1 M NaOH on a Ni control sample and on $Ni_xCo_{(1-x)}$*-oxide coatings by (a) LPT and b) CA. Temperature = 293±2 K. Scan rate in LPT was 1 mV s*$^{-1,}$ *and in both cases, the polarization was done from high to low overpotentials.*

The curves in Figures 3.3 and 3.4 display the classical Tafelian behavior, with a linear region in the mid-potential range. The figures also evidence that there is a good agreement between the Tafel (semi-steady-state) and chronoamperometry (steady-state) curves. At high overpotentials, the curves start leveling into a plateau, possibly due to (i) a decrease in surface area of the electrode in contact with the electrolyte because of the attachment of produced H_2 bubbles to the surface, (ii) the formation of hydrides, and (iii) the local pH changes (increase) at the solid/liquid interface [112]. As it can be seen, this effect is more prominent in the alkaline medium. As expected, when comparing the curves in the two electrolytes, the current densities obtained are, on average, higher in the acid medium than in the alkaline medium, since the acidic electrolyte has a higher concentration of hydrogen ions and therefore higher conductivity. From the curves in Figures 3.3 and 3.4, the cathodic Tafel slope, b (mV dec^{-1}), the transfer coefficient, α (-), and the exchange current density, j_0 (μA cm^{-2}) were obtained, and the corresponding values are reported in Tables 3.3 and 3.4 for acidic and alkaline media, respectively. In general, a very good agreement between the Tafel and chronoamperometry sets of data was obtained, validating the values presented in both tables.

The HER is a two-step reaction, in which the first step is the formation of an adsorbed hydrogen atom intermediate, M-H_{ads} (Volmer reaction). The second step is the generation of H_2 gas either through the reaction of an adsorbed hydrogen atom with the hydrogen ion (Heyrovsky reaction) or the chemical desorption by reaction of two hydrogen atoms adsorbed at neighbouring electrode sites (Tafel reaction). The corresponding Tafel slope values at 293 K for the previously mentioned reactions are 116, 40, and 30 mV dec^{-1}, respectively. These values govern the rate determining step of the HER mechanism [12]. The experimentally observed Tafel slope in Tables 3.3 and 3.4 range from 126 mV dec^{-1} to 234 mV dec^{-1} in the acidic medium and from 144 mV dec^{-1} to 264 mV dec^{-1} in the alkaline medium, indicating that the Volmer reaction is the rate-determining step for the HER on all the electrodes investigated in both electrolyte media. Lower values of Tafel slope are preferred since a smaller change in electrode overpotential results in a more significant increase in HER current, and thus higher hydrogen production rate [12]. In both acidic and alkaline media, only the $Ni_{0.2}Co_{0.8}$-oxide coating yielded average Tafel slope values lower than those on Ni (control sample), but the difference is not statistically significant. All other electrocatalysts have larger Tafel slopes, which could be due to the weaker electronic conductivity of the oxide coatings in comparison to pure Ni. Nonetheless, the Tafel slopes obtained for the $Ni_xCo_{(1-x)}$-oxide cathodes produced here are considerably lower than what has been reported on other bimetallic-oxides [60].

Another comparison parameter used to investigate the electrocatalytic activity of the prepared catalysts is the transfer coefficient α, derived from the Tafel slope: $b = 2.303\, RT/(\alpha F)$ where R is the gas constant (8.314 J K^{-1} mol^{-1}), T is temperature (K), and F is the Faraday constant 96485 C mol^{-1}. A higher transfer coefficient value indicates better electrocatalytic activity. Similarly, to the Tafel slope values, only the $Ni_{0.2}Co_{0.8}$-oxide catalyst yielded an average transfer coefficient value that is higher than that of the Ni control sample, but again, the difference is not statistically significant (Tables 3.3 and 3.4). The same occurs when the exchange current density values are compared. With respect to the latter, the exchange current density value obtained for Ni agrees with the value presented on the HER volcano plot [44]. The value recorded on $Ni_{0.2}Co_{0.8}$-oxide is a higher, but it is still ca. 1.5-2 orders of magnitude lower than the value obtained on noble metals (Pt, Ir, Ru).

Table 3.3: Kinetic parameters (Tafel slope, transfer coefficient, and exchange current density) for the $Ni_xCo_{(1-x)}$-oxide coatings obtained in 0.5 M H_2SO_4 solution. Results for the Ni-control sample are also presented for comparison. Presented errors are standard deviations of the mean. Temperature = 293±2.

Sample	***Tafel polarization data***			***Chronoamperometry data***		
	b **(mV dec^{-1})**	**α**	***j_0*** **(μA cm^{-2})**	***b*** **(mV dec^{-1})**	**α**	***j_0*** **(μA cm^{-2})**
Ni	134 ± 9	0.44 ± 0.03	15.2 ± 3.21	142 ± 12	0.42 ± 0.06	10.2 ± 4.62
NiOx	173 ± 16	0.34 ± 0.05	1.82 ± 0.24	170 ± 19	0.32 ± 0.08	1.21 ± 0.44
$Ni_{0.8}Co_{0.2}Ox$	223 ± 21	0.26 ± 0.02	0.21 ± 0.02	234 ± 26	0.24 ± 0.04	0.16 ± 0.05
$Ni_{0.6}Co_{0.4}Ox$	214 ± 18	0.27 ± 0.04	0.47 ± 0.09	223 ± 22	0.25 ± 0.07	0.35 ± 0.08
$Ni_{0.4}Co_{0.6}Ox$	162 ± 12	0.36 ± 0.08	1.53 ± 0.83	179 ± 14	0.34 ± 0.04	1.34 ± 0.71
$Ni_{0.2}Co_{0.8}Ox$	126 ± 8	0.47 ± 0.07	25.3 ± 2.42	133 ± 13	0.45 ± 0.09	20.2 ± 3.82
CoOx	154 ± 11	0.38 ± 0.06	3.12 ± 0.91	165 ± 15	0.36 ± 0.05	2.71 ± 0.72

Table 3.4: HER kinetic parameters (Tafel slope, transfer coefficient, and exchange current density) for the $Ni_xCo_{(1-x)}$-oxide coatings obtained in 1 M NaOH solution. Results for the Ni-control sample are also presented for comparison. Presented errors are standard deviations of the mean. Temperature = 293±2.

Sample	***Tafel polarization data***			***Chronoamperometry data***		
	b **(mV dec^{-1})**	**α**	***j_0*** **(μA cm^{-2})**	***b*** **(mV dec^{-1})**	**α**	***j_0*** **(μA cm^{-2})**
Ni	156 ± 10	0.38 ± 0.04	0.96 ± 0.17	163 ± 18	0.36 ± 0.04	0.73 ± 0.24
NiOx	176 ± 12	0.33 ± 0.08	0.64 ± 0.13	186 ± 21	0.31 ± 0.08	0.42 ± 0.19
$Ni_{0.8}Co_{0.2}Ox$	234 ± 14	0.25 ± 0.03	0.07 ± 0.03	264 ± 22	0.23 ± 0.03	0.02 ± 0.02
$Ni_{0.6}Co_{0.4}Ox$	224 ± 18	0.26 ± 0.05	0.08 ± 0.02	241 ± 24	0.24 ± 0.05	0.06 ± 0.01
$Ni_{0.4}Co_{0.6}Ox$	203 ± 13	0.29 ± 0.02	0.11 ± 0.06	212 ± 18	0.27 ± 0.02	0.14 ± 0.06
$Ni_{0.2}Co_{0.8}Ox$	144 ± 9	0.41 ± 0.09	3.63 ± 1.12	153 ± 12	0.39 ± 0.09	2.91 ± 1.12
CoOx	182 ± 12	0.32 ± 0.06	0.35 ±0.08	202 ± 19	0.30 ± 0.06	0.21 ±0.08

Although the kinetic parameters in Tables 3.3 and 3.4 offer information on the relative performance of the coatings in the HER, a more practical way of evaluating them is by comparing the HER current (amount of H_2 evolved) at a fixed overpotential

[12]. Figure 3.5 displays the current density values for HER recorded in both the acidic and alkaline media at an overpotential of -300 mV, normalized to the geometrical area of the electrode (the values were obtained from the curves in Figure 3.3 and 3.4). It is evident that the highest apparent electrocatalytic activity is obtained for the $Ni_{0.2}Co_{0.8}$-oxide electrode in both electrolyte media, which is in accordance with the kinetic parameters in Tables 3.3 and 3.4. The other $Ni_xCo_{(1-x)}$-oxide coatings are significantly inferior to the control electrode in the acidic medium, while in the alkaline electrolyte pure Ni-oxide and Co-oxide coatings show the HER electrocatalytic activity slightly lower than that of the control surface.

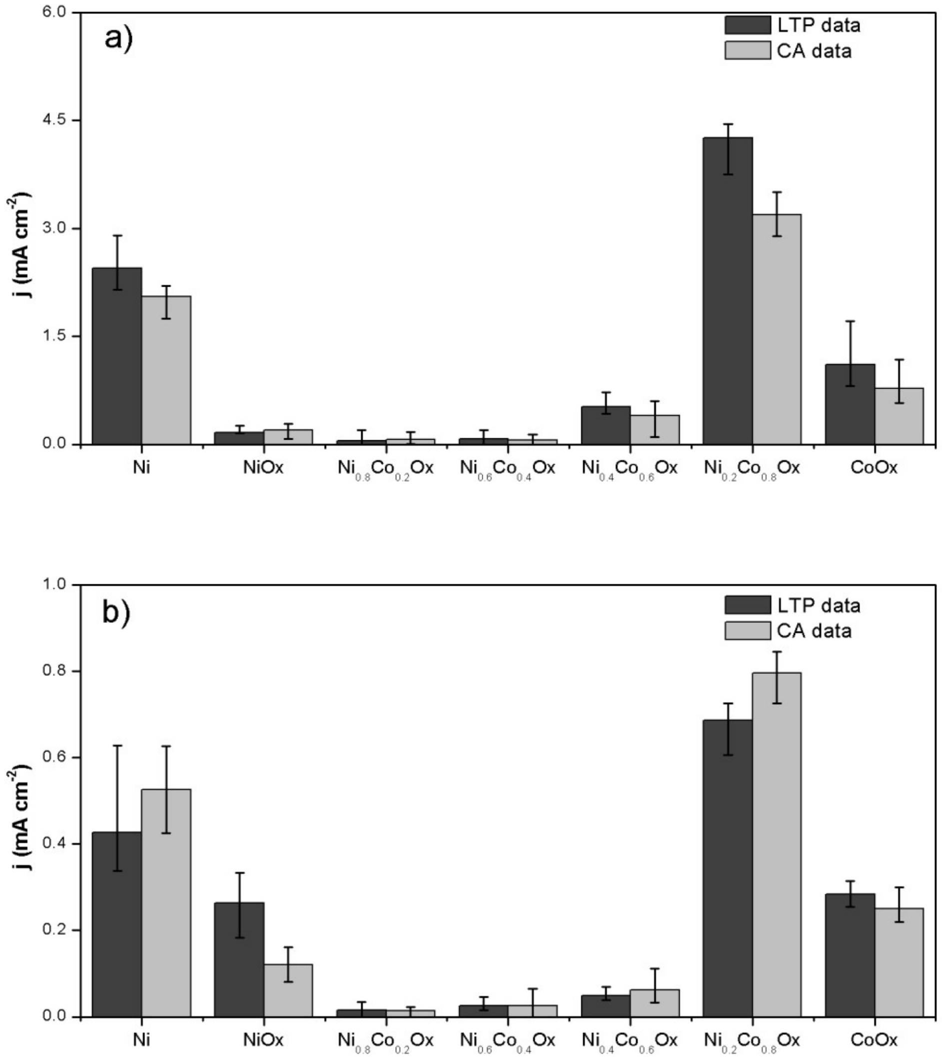

Figure 3.5: Comparison of the electrocatalytic activity of the investigated electrode materials in the HER in terms of current density expressed per geometric area of the electrode and measured at an overpotential of −300 mV in a) 0.5 M H_2SO_4 and b) 1 M NaOH. Temperature = 293±2 K.

The information obtained from the polarization data demonstrates that the $Ni_{0.2}Co_{0.8}$-oxide catalyst shows superior apparent electrocatalytic activity over pure Ni in both acidic and alkaline media. However, the data in Figure 3.5 are normalized with respect to the geometrical area of the electrode, which does not enable us to evaluate the intrinsic electrocatalytic activity of the metal-oxide electrodes in the HER. Consequently, to assess which of the electrocatalysts is intrinsically the best material for the HER, the results presented in Figure 3.5 were normalized with respect to the true electrochemically-active surface area of the electrocatalyst (Figure 3.6), the latter obtained from average of the CV and CA measurements in the HexRu(III) chloride-containing solution.

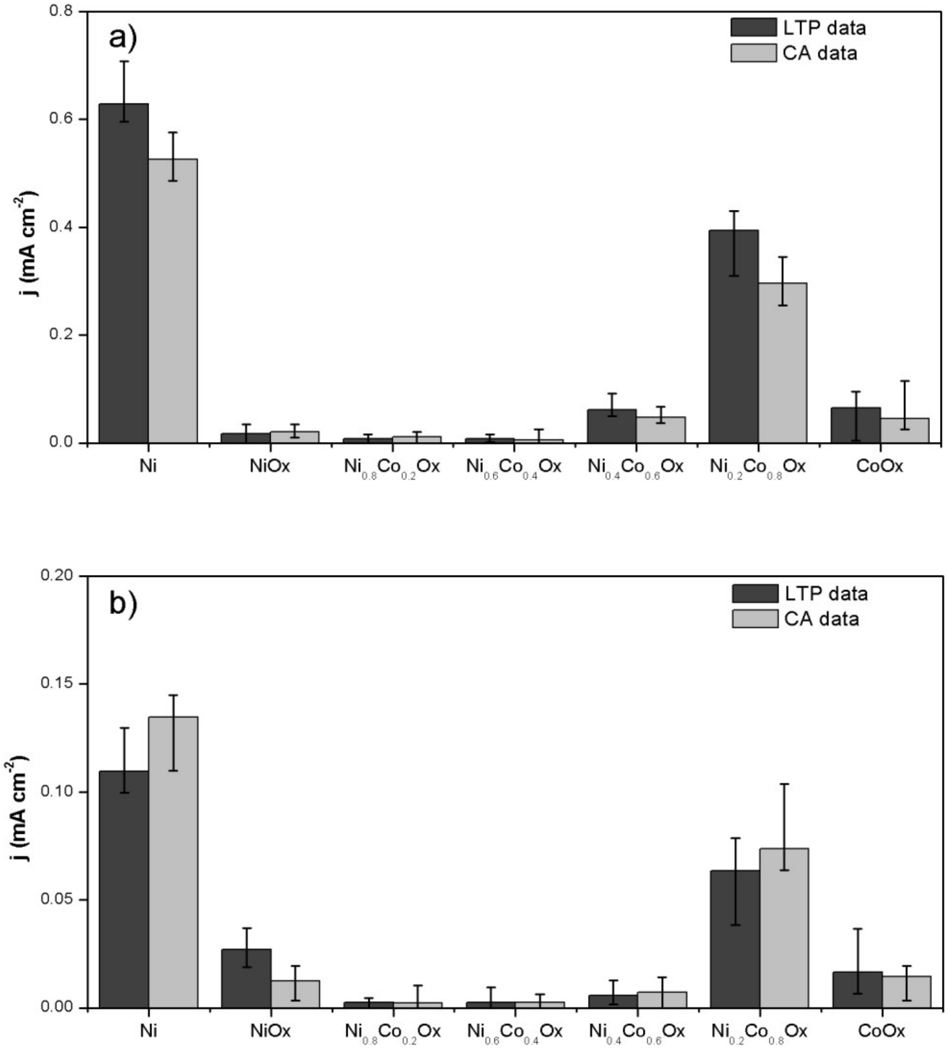

Figure 3.6: Comparison of the electrocatalytic activity of the investigated electrode materials in the HER in terms of current density expressed per true electrochemically-active area of the electrode and measured at an overpotential of -300 mV in a) 0.5 M H_2SO_4 and b) 1 M NaOH. Temperature = 293±2 K.

As shown in Figure 3.6, the control Ni sample has the highest intrinsic catalytic activity in both media, followed by $Ni_{0.2}Co_{0.8}$-oxide. This observation demonstrates that the higher electrocatalytic activity of the $Ni_{0.2}Co_{0.8}$-oxide coating seen in Figure 3.5 is due to the surface-area effect. Nevertheless, one should note that the control Ni surface cannot be used in PEM-type electrolyzers due to poor corrosion stability of Ni in the acidic medium. In addition, metal-oxide electrodes are significantly less susceptible to fouling (deactivation) than pure metal electrodes. Hence, among the investigated electrodes (including the control Ni surface), the $Ni_{0.2}Co_{0.8}$-oxide electrode seems, from the practical point of view, to be the best surface for the HER in the acidic medium, but also in alkaline media that contain traces of heavy metals.

3.4.4 Long-term stability of the electrodes

The electrocatalytic stability of selected electrodes used in this work was tested in aggressive 0.5 H_2SO_4 by running linear Tafel polarization (LTP) and chronopotentiometry (CP) measurements consecutively in the following order: LTP on freshly-prepared electrodes, CP at -0.5 A cm^2 for 72 hours (note that this current is higher by an order of magnitude than the maximum current in Figure 3.3), and LTP again on the previously used electrodes. Then, the current at -300 mV was determined from the LTP curves before and after 72 hours; the corresponding percentage of electrode activity is presented in Figure 3.7.

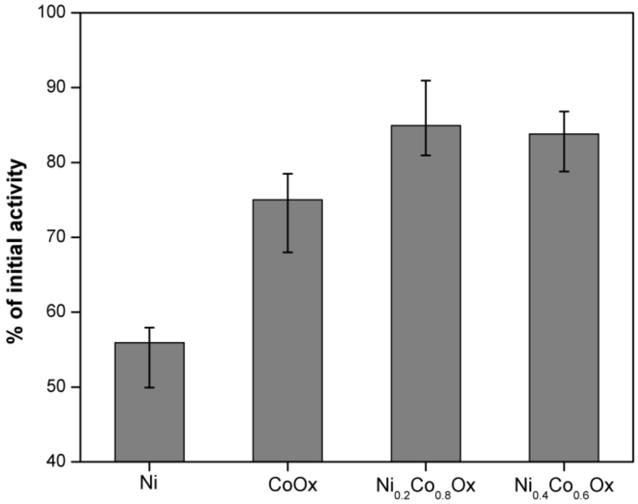

Figure 3.7: Percentage of electrode deactivation of selected electrodes in the HER measured at an overpotential of -300 mV in 0.5 M H_2SO_4 after 72 hours of electrolysis at 0.5 A cm^{-2}.

Figure 3.7 exhibits a significant decrease in electrocatalytic activity recorded for the Ni control sample (ca. by 45%). Given that the *bulk* Ni metal was used as the cathode in these measurements (thus, the anodic leveling of the surface, i.e., a decrease in surface roughness, can be excluded), this indicates that the decline in electrocatalytic activity with time could be due to the fouling of the Ni electrode surface by metal impurities present in traces in the electrolyte (the source of these impurities is the 96 wt.% stock H_2SO_4 used to prepare the electrolyte). On the other hand, the oxide electrodes showed a much smaller decrease in electrocatalytic activity, indicating that they are significantly more fouling/deactivation tolerant in comparison to metallic Ni. Thus, the HER current recorded on the most (apparently) active $Ni_{0.2}Co_{0.8}$-oxide electrode decreased by ca. 15%, while for the other two oxide electrodes the decrease is not statistically significant. Nonetheless, a more detailed analysis of the coatings, over a more extended period is recommended to evaluate both the kinetics and mechanism of deactivation, which is outside of the scope of current work.

3.4.5 Temperature effect and activation energy

To evaluate the effect of temperature on the kinetics of the HER on the $Ni_{0.2}Co_{0.8}$-oxide electrode, steady-state polarization curves for the HER in 0.5 M H_2SO_4 were recorded in the temperature range from 293 K to 323 K (see Figure 3.8). As it was expected, with an increase in temperature, the HER activity is enhanced.

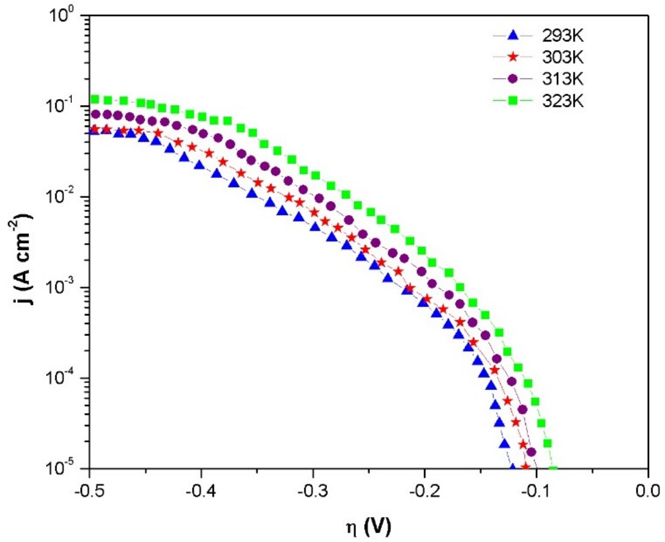

Figure 3.8: Polarization curves recorded in 0.5 M H_2SO_4 on a $Ni_{0.2}Co_{0.8}$-oxide electrode at different temperatures.

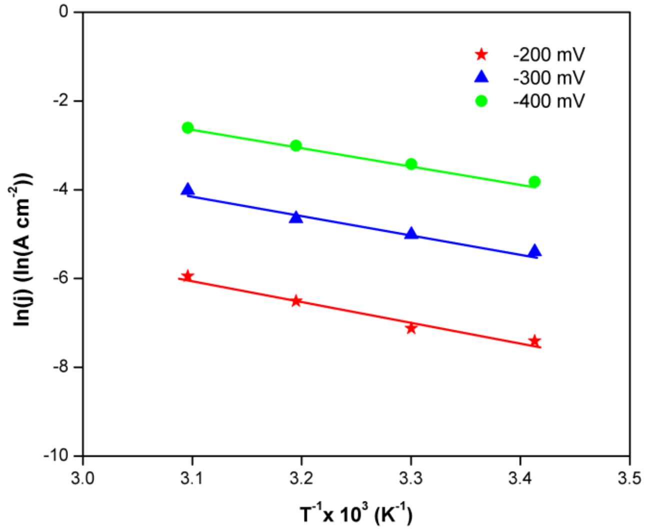

Figure 3.9: Arrhenius-type semi-logarithmic dependence of current density on inverse temperature obtained at several selected overpotentials from the polarization curves presented in Figure 3.8.

In order to test whether the HER kinetics on $Ni_{0.2}Co_{0.8}$-oxide follows the Arrhenius type of behavior, the data from Figure 8 were used to estimate the linearity w.r. to the Arrhenius equation: $ln(j_{\eta=const}) = -E_a/RT + ln(A)$, where E_a (J mol^{-1}) represents the apparent activation energy for the HER, and A (A cm^{-2}) is the pre-exponential factor. Figure 3.9 shows the corresponding behavior at three selected HER overpotentials. Evidently, the HER kinetics on $Ni_{0.2}Co_{0.8}$-oxide indeed follows the Arrhenius law. From the slope of the lines, the corresponding apparent activation energy was calculated at each potential, and the following values were obtained: 39.2, 35.3, 31.9 kJ mol^{-1} at -200, -300 and -400 mV, respectively. As it can be seen, the activation energy is a potential-dependent value [122], and if the HER mechanism remains constant within a given potential range, with an increase in overpotential a linear decrease in activation energy can be expected from the theory of electrochemical kinetics [109]. Therefore, in order to make a proper comparison, the corresponding activation energy at zero overpotential, $E_{a,rev}$, was calculated from the E_a *vs.* η dependence (plot not shown here; $R_2 = 0.998$). The value obtained is $E_{a,rev} = 46.4$ kJ mol^{-1}, which is in the range of values reported for nickel and nickel metal (non-oxide) alloys [12,15]. Savadogo et al. [123] obtained values ranging from 36 to 56 kJ mol^{-1} on Pt-Co supported on carbon, while Damian et al. [63] reported values of 44 to 73 kJ mol^{-1} on Ni-Mo cathodes electrodeposited in a three-dimensional polyaniline matrix.

3.5 Conclusion

The use of $Ni_xCo_{(1-x)}$-oxide electrode coatings of various composition produced by a thermal-decomposition method was investigated in the hydrogen evolution reaction in acidic and alkaline media. The oxide electrodes were found to be of a semi-crystalline structure, yielding the surface morphology characterized by relatively high surface roughness factor (up to 25). The potentiodynamic and potentiostatic measurements were used to determine the mechanism and kinetics of the HER. From this, it was shown that the kinetics of the HER on Ni_xCo_{1-x}-oxide cathodes was controlled by the Volmer reaction step as the rate-determining step, i.e., by the electrochemical adsorption of hydrogen. $Ni_{0.2}Co_{0.8}$-oxide was identified as the most apparently-active coating among the investigated materials, as it yielded the highest apparent electrocatalytic activity (normalized with respect to the geometric surface area) in both the acidic and alkaline media. However, when the activity was evaluated taking into account the electrochemically-active area, the control Ni sample showed the highest intrinsic electrocatalytic activity. Nevertheless, we still suggest $Ni_{0.2}Co_{0.8}$-oxide be used as the cathode since (*i*) pure Ni cannot be used in PEM-type electrolyzers due to poor corrosion stability of Ni in the acidic medium, (*ii*) pure Ni is prone to fouling even in alkaline electrolyzers due to electrodeposition of impurities present in the electrolyte in traces, and since (*iii*) metal-oxide electrodes are significantly less susceptible to fouling (deactivation) by impurities (e.g., heavy metals) present in electrolytes used in alkaline hydrogen electrolyzers. Nonetheless, for PEM-type electrolyzers, it is recommended to produce $Ni_{0.2}Co_{0.8}$-oxide in the form of nanoparticles, which could potentially increase the electrode electrical conductivity and also their intrinsic activity due to the increase in surface energy.

Acknowledgements

Financial support from the McGill University through the McGill Engineering Doctoral Award (MEDA) program, the National Council of Science and Technology of Mexico (CONACYT), and the Natural Sciences and Engineering Council (NSERC) of Canada is gratefully acknowledged.

Chapter 4

4 Evaluation of Nickel-Molybdenum-Oxides as Cathodes for Hydrogen Evolution by Water Electrolysis in Acidic, Alkaline, and Neutral Media

4.1 Preface

This chapter presents an article that has been published in *Electrochimica Acta*. The citation of the published article is:

> A. Gomez Vidales, S. Omanovic, *Evaluation of nickel-molybdenum-oxides as cathodes for hydrogen evolution by water electrolysis in acidic, alkaline, and neutral media.* Electrochimica Acta, 262 (2018), 115-123.

Abraham Gomez Vidales (the Ph.D. candidate) designed and conducted the experiments, performed analysis of the results, and wrote the manuscript. Prof. Sasha Omanovic was responsible for supervision of the work, helped in the interpretation and discussion of results, and reviewed the manuscript. In the results and discussion section, each data point and the corresponding deviation presented in figures represent an average of 9-15 measurements: between 3 to 5 separate samples, each tested 3 times.

Based on the previous work on pure Ni-Mo alloys, the addition of Mo-oxide to Ni-oxide was hypothesized to result in better performance than Ni-Co-oxides. Considering this information, the aim of this research was the development of Ni-Mo-oxides coatings of different compositions for the hydrogen evolution reaction in acidic, alkaline, and neutral media using a thermal-salt decomposition method. It was found that these oxides have a better performance than the control sample (nickel) and that they are stable at the whole pH scale even during long-term electrolysis in acidic medium. Their better performance of some samples was attributed to the increase of the electrochemically active surface area and the enhancement of the electrochemical activity of the alloys.

This article is dedicated to my friend Michael Patrick Dougan. Thank you for everything!

Evaluation of Nickel-Molybdenum-Oxides as Cathodes for Hydrogen Evolution by Water Electrolysis in Acidic, Alkaline, and Neutral Media

Abraham Gomez Vidales*, Sasha Omanovic

Department of Chemical Engineering, McGill University, 3610 University St., Montreal, Quebec, H3A 0C5, Canada

* Corresponding author: abraham.gomezvidales@mail.mcgill.ca

Keywords: Hydrogen; Water electrolysis; Cathode; Molybdenum; Nickel; Metal oxides.

Abstract

Hydrogen produced by electrolysis employing wind/hydro/solar electricity has been identified as a promising renewable and environmentally-friendly energy carrier. The current paper is a study on the investigation of electrocatalytic properties of Ni-Mo-oxides in the hydrogen evolution reaction (HER) by water electrolysis in the acidic, alkaline, and neutral electrolytes. The Ni-Mo-oxides of several compositions were formed on a titanium substrate employing a thermal-decomposition method. The morphology of the obtained coatings was investigated by scanning electron microscopy, and their crystallinity by X-ray diffraction. Linear Tafel polarization and chronoamperometry were used to determine the extrinsic and intrinsic electrocatalytic activity of the coatings (cathodes) in the HER. The most extrinsically active coating was found to be $Ni_{0.6}Mo_{0.8}$-oxide (in all three electrolytes), while this coating showed the highest intrinsic activity only in the neutral electrolyte. In the acidic and alkaline electrolyte, the $Ni_{0.8}Mo_{0.2}$-oxide coating was found to be most

intrinsically active. In the alkaline electrolyte, the $Ni_{0.8}Mo_{0.2}$-oxide cathode had twice the intrinsic electrocatalytic activity of the current state-of-the-art, pure nickel.

4.2 Introduction

Renewable alternative energy sources are needed as a replacement for environmentally unfriendly fossil fuels. In recent years, there has been a growing interest in viewing hydrogen as an alternative source of energy storage. Hydrogen has already been introduced into the consumer sector: Toyota and Honda are introducing hydrogen fuel cell powered cars, hydrogen refueling stations have rapidly been built in the USA, Europe, and Japan, and mobile phone off-grid hydrogen fuel cell chargers have been commercialized. Currently, most of the hydrogen (approximately 95%) is produced *via* a relatively cost-effective technology that consists of reforming hydrocarbons, but this does not address the adverse effects of fossil fuel use. However, there is another, environmentally-friendly way to produce hydrogen: water electrolysis coupled with solar/wind/hydroelectricity. What is even more important here, the source of this hydrogen is practically endless - water. However, current water electrolysis technologies are still not cost-competitive to hydrocarbon reforming, and further improvement of these technologies is needed. One of the directions in this task is the development of more electroactive, durable, and cheaper electrode materials.

Platinum and some other noble metals have shown to be the most active cathodes in the hydrogen evolution reaction (HER) [64, 124]. However, due to its cost, Pt is not used in commercial alkaline electrolyzers, and its use in polymer electrolyte membrane (PEM) electrolyzers has made it a primary obstacle for large-scale commercialization of the technology. Alkaline electrolyzers constitute the majority of water electrolyzers currently used in industry, and nickel has long been regarded as the cathode material-of-choice because of its optimum electronic structure that enables relatively good HER kinetics [12, 63]. Nevertheless, the intrinsic activity of Ni in the HER and its long-term stability/activity are significantly inferior to those of Pt. To address this, many research groups have attempted to increase Ni's intrinsic and extrinsic electrocatalytic activity by alloying it with other elements or by nanostructuring the Ni electrode surface, respectively [12, 24, 29, 63, 64, 69, 70, 77, 125-127]. Despite some promising outcomes, these cathodes still remain susceptible to cathodic fouling by the electrodeposition of trace metals present in the electrolyte (even under open-circuit conditions), and they do not offer satisfactory structural and long-term stability [128]. Furthermore, due to the poor corrosion resistance of Ni at low pH, metallic Ni and its alloys are not suitable for the acidic environment present in PEM water electrolyzers. On the other hand, certain metal-oxide electrodes are known to be quite stable across the entire pH scale, even when they are used as anodes [113, 129, 130]. This means that they could potentially be promising electrode materials for both cathodes and anodes in water electrolyzers that operate in the entire pH range (PEM, seawater, and alkaline). In fact, the literature has claimed good performance for some metal oxide electrodes in the HER [10, 17, 69, 126, 127].

Considering the previously discussed, this paper presents results on the development of mixed-metal-oxide (MMO) based electrodes to be used for hydrogen production by water electrolysis across the whole pH range. Namely, based on previous research studies of our and other laboratories that worked on pure metallic (non-oxide) Ni-based cathodes [12, 29, 77, 126, 127, 131], Ni and Mo have been chosen in the current research as the MMO materials to produce Ni-Mo-oxide cathodes. Ni-Mo alloys have shown activity enhancement for HER due to a synergetic effect explained on the basis of the ‘spillover effect.' The rationale for using the oxide form of Ni-Mo combinations instead of pure metals is to achieve higher stability (both electrochemical and structural) and to increase the cathode resistance to fouling by underpotential disposition (UPD) or cathodic deposition of metals, and hence to extend the service life of the cathodes. Besides aiming at developing cathodes that could be used across the whole pH scale and be less prone to fouling, the additional aim was to develop cathodes that could conveniently and rapidly be reactivated by anodic ‘cleaning' (dissolution of UPD/electrodeposited metals).

4.3 Experimental

4.3.1 Sample preparation

$Ni_xMo_{(1-x)}$-oxide coatings (x = 0.2, 0.4, 0.6, 0.8, 1; x is the molar ratio, and it refers to the relative content of Ni and Mo in the precursor solution) were formed on a 2 mm thick titanium coin-type substrate (purity 99.2%, Alfa Aesar, USA) of 1.21 cm in diameter, employing the thermal salt-decomposition method. To coat the titanium coins, a 0.2 M precursor solution was prepared by dissolving the corresponding metal precursor salts in a mixture of 50vol.% HCl (37wt.%, Fisher Scientific, Canada) and 50vol.% H_2O. $NiCl_2 \times 6H_2O$ (purity 99.9wt.%, Sigma-Aldrich, Canada) and $Na_2MoO_4 \times 2H_2O$ (purity 99.5wt.%, Sigma-Aldrich, Canada) were used as precursor salts to form the metal-oxide coatings. All solutions were prepared using nanopure deionized water (resistivity: 18.2 MΩ cm).

The titanium substrate was first wet-polished using 600-grit SiC sandpaper. Afterwards, the plate was rinsed with nanopure water and then sonicated for 30 minutes in nanopure water to remove residues. Next, the substrate was etched in a boiling solution of HCl and nanopure water (1:1 by volume) for 30 min [132]. Then, the substrate was again rinsed with nanopure water and then dried in argon. The prepared $Ni_xMo_{(1-x)}$ solution was applied uniformly on the titanium substrate using a paintbrush. After the first coat was applied, the sample was placed in an oven at 383 K for five minutes to vaporize the solvent, and the sample was annealed in a furnace at 773 K for fifteen minutes. The sample was subsequently removed from the furnace and cooled for ten minutes before another coating was applied. This procedure was repeated for six times to form a six-layered metal-oxide coating on the substrate (the number of coatings had previously been optimized to yield the best coating stability). Finally, the sample was annealed in the furnace for one hour to yield $Ni_xMo_{(1-x)}$-oxide coatings [132, 133].

4.3.2 Characterization techniques

The electrocatalytic activity of the tailor-made metal oxides toward hydrogen evolution was investigated using the following electrochemical techniques: linear Tafel polarization (LTP) and chronoamperometry (CA). These measurements were performed in a standard three-electrode electrochemical cell in 0.5 M H_2SO_4 (prepared using 96wt.% H_2SO_4, Fisher Scientific, Canada), in 0.6 NaCl (prepared using 99wt.% purity NaCl crystals, Fisher Scientific, Canada), and in 1 M NaOH (prepared using 95wt.% purity NaOH crystals; Sigma-Aldrich, Canada) at 295 ± 2 K and atmospheric pressure. Metal-oxide samples served as the working electrode (WE); the oxide-coated coins were mounted in a special electrode holder, and only the coated side of the coins was exposed to the solution, yielding a geometric surface area of 0.68 cm^2. Cyclic voltammetry (CV) was used to determine the true electrochemically-active surface area of the metal-oxide cathodes employing a well-established procedure based on the reduction of a ruthenium complex. Briefly, the hexaammineruthenium III/II (HexRu(III)|HexRu(II)) chloride redox couple reaction ($[Ru(NH_3)_6]^{3+} + e^- \leftrightarrow [Ru(NH_3)_6]^{2+}$) was used [115-118]. CVs were recorded at a range of scan rates (300, 200, 150, 100, 70, 50, 30, 20, and 10 mV s^{-1}) in 1 mM HexRu(III) chloride (purity 98wt.%, Sigma-Aldrich, USA) in deoxygenated and quiescent 0.1 M KNO_3 electrolyte (purity 99wt.%, Fisher Scientific, Canada). Then, the Randles-Sevcik equation $i_p = (2.69 \times 10^5) n^{3/2} A D^{1/2} C v^{1/2}$ was applied to the cathodic peak and from the slope of the i_p vs. $v^{1/2}$ trend, the true electrochemically-active area of the metal-oxide electrode was determined [134]. In the Randles-Sevcik equation, n is the number of electrons appearing in half-reaction for the redox couple (-), A is the electroactive surface area (cm^2), D is the diffusion coefficient of the species being oxidized/reduced (for HexRu(III)) in 0.1M KNO_3 it is 8.70×10^{-6} $cm^2\ s^{-1}$), C is the concentration of the analyte (i.e., HexRu(III)) i n the bulk solution (mol cm^{-3}) and v is the scan rate (V s^{-1}).

In all electrochemical experiments, a graphite rod was used as the counter electrode (CE). Before each measurement, the graphite rod was sonicated for 30 minutes in ethanol, followed by a thorough rinsing with nanopure water. During measurements, the counter electrode was separated from the main cell compartment by a glass frit (Ace Glass, Inc., USA) to prevent oxygen formed on the CE to reach the WE and interfere with the HER. A saturated calomel electrode (SCE) (Accumet electrode, Fisher Scientific, USA) was used as the reference electrode. To maintain an oxygen-free electrolyte, argon (MEGS Specialty Gases Inc., 99.998wt.% pure, Canada) was purged through the electrolyte prior electrochemical measurements for 30 minutes, and the purging was continued during the measurements. The electrochemical measurements were performed employing a computer-controlled potentiostat/galvanostat/frequency response analyzer (Autolab PGSTAT30, Metrohm, the Netherlands) using Autolab GPES and FRA software packages (v. 4.9; Metrohm, the Netherlands).

Additional characterization techniques were employed to learn about the morphology, composition, and crystalline structure of the coatings: scanning electron microscopy (SEM) analysis and energy dispersive spectrometry (EDS) analysis (Hitachi SU-3500 Variable Pressure—SEM with EDS detector); and X-ray diffraction (XRD) analysis (Bruker D8 Discovery X-Ray Diffractometer (VANTEC detector, Cu-source).

4.4 Results and discussion

4.4.1 Composition and electrocatalyst morphology characterization

To investigate the chemical composition of the electrocatalytic coatings and map the distribution of the elements on the electrode surface, energy dispersive spectroscopy (EDS) was carried out. Table 4.1 shows the nominal and experimental relative values of Ni and Mo in the precursor solution and in the coating, respectively. The agreement between the two sets of data is good. EDS has also detected Ti in the coating, which is due to the dissolution from the Ti substrate during the coating preparation method. Some Na and Cl have also been detected, which is due to the presence of these elements present in the precursors solutions used to prepare the coatings, $Na_2MoO_4 \times 2H_2O$ and $NiCl_2 \times 6H_2$, respectively. However, the content of these impurities is lower than 8% in all the cases. In addition, the surface mapping of Ni and Mo confirmed a uniform distribution of the elements on the surfaces of all the coatings.

Table 4.1: Relative atomic percentage of Ni and Mo in $Ni_xMo_{(1-x)}$-oxide coatings (excluding the contribution of oxygen and other impurities in the oxide film). The nominal values refer to the relative Ni and Mo content in the precursor solution, while the experiential values refer to the relative content in the coating measured by energy dispersive spectroscopy (EDS).

Element content, at.%	
Nominal	**Experimental**
NiOx	NiOx
$Ni_{0.8}Mo_{0.2}Ox$	$Ni_{0.83}Mo_{0.17}Ox$
$Ni_{0.6}Mo_{0.4}Ox$	$Ni_{0.63}Mo_{0.37}Ox$
$Ni_{0.4}Mo_{0.6}Ox$	$Ni_{0.37}Mo_{0.63}Ox$
$Ni_{0.2}Mo_{0.8}Ox$	$Ni_{0.14}Mo_{0.86}Ox$
MoOx	MoOx

To examine the morphology of the metal oxide coatings, a scanning electron microscopy (SEM) technique was used. Figure 4.1 shows the SEM surfaces displaying the microstructure of surfaces of the $Ni_xMo_{(1-x)}$-oxide coatings of different compositions. As it can be seen, the images show significant differences in morphology of the investigated coatings. Furthermore, the SEM images indicate that the total surface area of the coatings is considerably larger than the corresponding geometric area.

The pure Ni sample (Figure 4.1a), which was used as a control, shows a relatively homogeneous surface of a relatively small roughness. On the other hand, the NiOx surface, Figure 4.1b, shows a sufficiently more rough/porous structure. Images in Figure 4.1c-f indicate that the four binary Ni-Mo-oxide coatings have a spherical (globular) pattern with a surface that is considerably rougher than pure nickel (Figure 4.1a). Surprisingly for thermally-prepared metal-oxide coatings, the coatings in Figure 4.1c-f do not show a 'cracked-mud' morphology, but rather a compact/continuous layer of an amorphous-like structure. Additionally, the morphology of the binary compositions is quite different from that of the two single metal oxides (Figure 4.1b and 1g) which show a sponge-like structure.

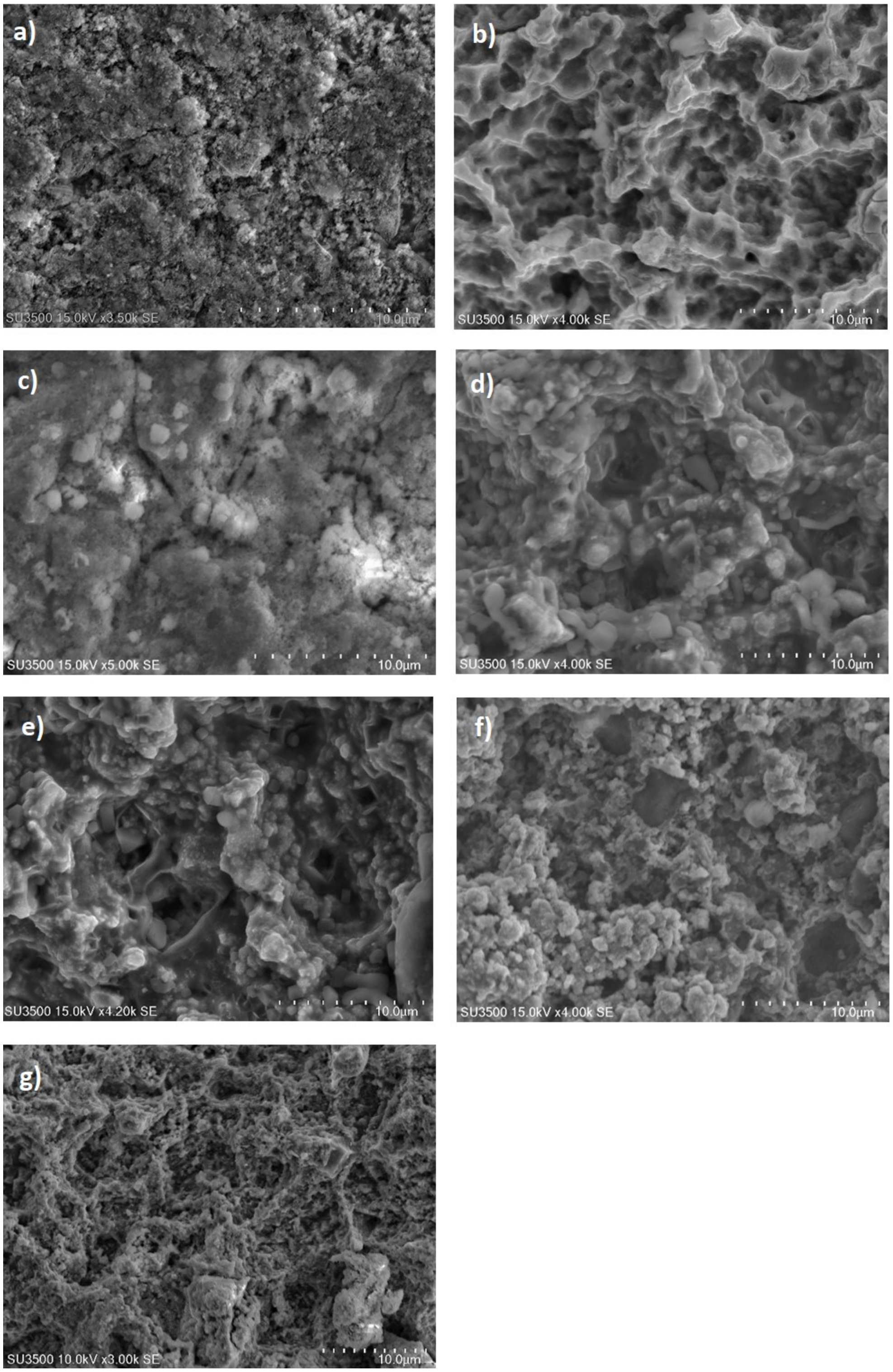

Figure 4.1: SEM images showing a surface morphology of a) Ni metal plate (control sample), b) Ni-oxide, c) $Ni_{0.8}Mo_{0.2}$-oxide, d) $Ni_{0.6}Mo_{0.4}$-oxide, e) $Ni_{0.4}Mo_{0.6}$-oxide, f) $Ni_{0.2}Mo_{0.8}$-oxide, and g) Mo-oxide coating.

Overall, all the surfaces presented in Figure 4.1 show some degree of surface roughness, the value of which is highly dependent on the material composition. It is important to estimate the surface roughness of the coatings to determine the intrinsic activity of each coating composition. The increased surface roughness is beneficial for the HER as it can enable higher specific (per geometric area) hydrogen production at a fixed potential. Nevertheless, one should note that an increased surface roughness might not result in a proportional increase in electrochemically active surface area, which is of actual relevance in electrocatalytic applications. Consequently, to determine a true electrochemically-active area of the surfaces in Figure 4.1, cyclic voltammetry (CV) in a ruthenium-complex solution was performed, as explained in the experimental section of the paper, and the values are presented in Table 4.2, together with the corresponding surface roughness factor.

Table 4.2: True electrochemically-active surface area of Ni and $Ni_xMo_{(1-x)}$-oxide cathodes presented in Figure 1. The geometric area is 0.68 cm^2.

Coating	**Electrochemically active surface area (cm^2)**	**Surface roughness factor**
Ni	3.5 ± 1.2	5.2
NiOx	10.7 ± 3.4	15.7
$Ni_{0.8}Mo_{0.2}Ox$	6.7 ± 2.8	9.8
$Ni_{0.6}Mo_{0.4}Ox$	19.2 ± 6.1	28.2
$Ni_{0.4}Mo_{0.6}Ox$	17.4 ± 7.3	25.6
$Ni_{0.2}Mo_{0.8}Ox$	35.4 ± 8.3	52.0
MoOx	31.1 ± 9.1	45.8

The results displayed in Table 4.2 are consistent with the observations made based on the surface characterization of the coatings by SEM, presented in Figure 4.1. The $Ni_{0.2}Mo_{0.8}$-oxide coating yielded the largest electrochemical surface area, characterized by the surface roughness factor of 52. The values in Table 4.2 indicate that the kinetics of the hydrogen evolution reaction should, in the first approximation, follow the same trend; nonetheless, as it will be seen later, the actual

HER activity of the oxides is more dependent on the cathode composition (intrinsic effect) rather than on the surface area (extrinsic effect).

To analyze the crystalline structure of the $Ni_xMo_{(1-x)}$-oxide coatings, X-ray diffraction (XRD) measurements were employed. The resulting diffraction patterns of the electrode coatings with different composition are shown in Figure 4.2 together with the labeled main diffraction peaks. The spectrum recorded on pure Ni reveals that the coating is crystalline. The peaks recorded correspond in increasing order of 2θ to the (1 1 1), (2 0 0), (2 2 0), reflections of the f.c.c structure of nickel at 44.5^o, 51.8^o, and 76.4^o (JCPDS no. 4-0835) [121] (the presence of the NiO peaks is due to the naturally-formed surface nickel-oxide film). The NiOx coating shows the presence of metallic Ni and two oxide forms: NiO and Ni_2O_3. The binary $Ni_xMo_{(1-x)}$-oxide coatings also present the metallic form of nickel and the same nickel oxides (NiO and Ni_2O_3). Molybdenum and its oxides (MoO_2 and MoO_3) are recorded on the binary and pure Mo-oxide coatings. Unlike with EDS, no titanium peaks were detected, indicating that its amount in the coating is below the XRD detection limit.

Figure 4.2 shows that a crystalline structure characterizes the Ni plate and NiOx coating, but the addition of Mo in the oxide coating (binary compositions) introduces some level of amorphousness, while the pure Mo-oxide coating again shows a higher degree of crystallinity. This is in agreement with the surface morphologies presented in Figure 1. It should be noted that, from the electrocatalytic point of view, it would be desirable for all the coatings to be crystalline, rather than amorphous; this could potentially be achieved by optimizing the Ni-Mo-oxide formation method or employing a different oxide formation method.

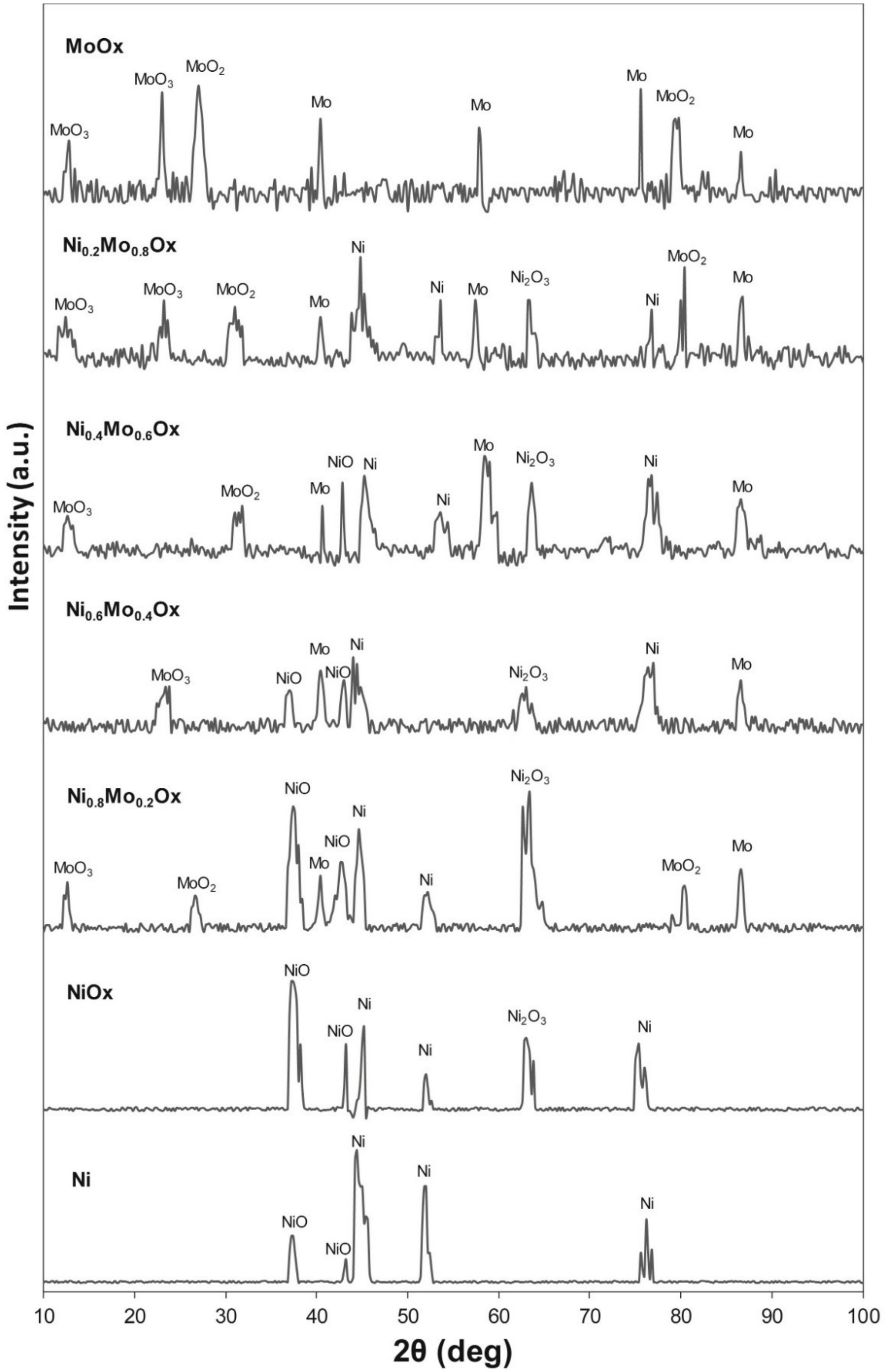

Figure 4.2: X-ray diffraction patterns of the $Ni_xMo_{(1-x)}$-oxide coatings deposited on a titanium substrate. Results for the Ni-control sample are also presented for comparison.

4.4.2 Electrochemical characterization

To investigate the electrocatalytic activity of the $Ni_xMo_{(1-x)}$-oxide coatings in the HER, linear Tafel polarization (LTP) and chronoamperometry (CA) measurements were performed. Figure 4.3 shows a set of LTP Tafel curves (corrected for the *jR-drop*) recorded in 0.5 M H_2SO_4 on all the investigated metal oxide coatings (a Ni plate was used as a control sample); a very similar response was also recorded in 0.6 M NaCl and in 1 M NaOH (not shown here). In these curves, the applied overpotential presented on the abscissa represents the driving force for the electron transfer in the HER (the input energy), while the current density on the ordinate represents the HER kinetics (the amount of H_2 produced)[64].

Moreover, chronoamperometry (CA) measurements were performed to validate the data obtained from the LTP measurements. CA measurements were done in the same overpotential range, with a step potential of 50 mV and for 300 seconds at each potential. To obtain the Tafel plot, the average of the current recorded in the last 100 seconds was determined at each potential. Figure 4.4 displays the Tafel curves obtained from CA (corrected for the *jR-drop*) recorded in 0.5 M H_2SO_4.

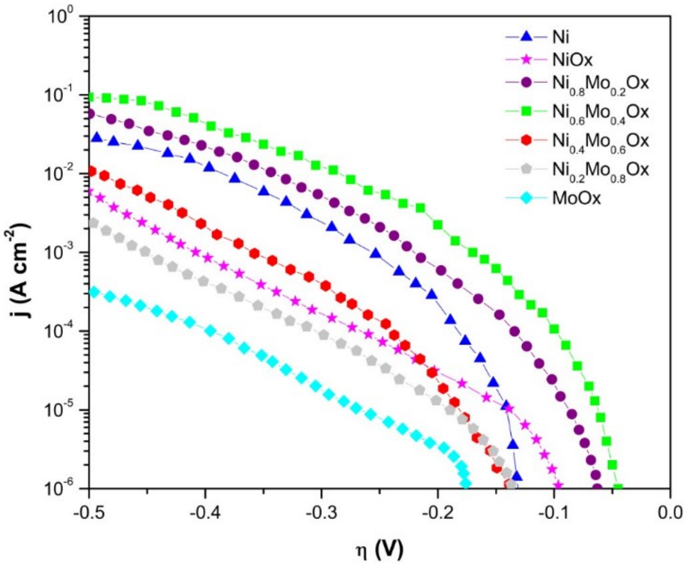

Figure 4.3: Tafel polarization curves recorded on Ni-control sample and $Ni_xMo_{(1-x)}$-oxide coatings in 0.5 M H_2SO_4 employing LTP. Scan rate = 1 mVs^{-1}.

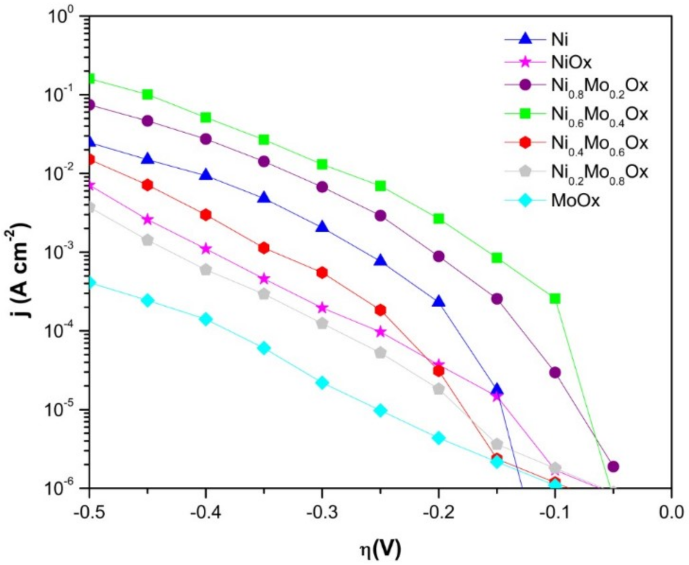

Figure 4.4: Tafel polarization curves recorded on Ni-control sample and $Ni_xMo_{(1-x)}$-oxide coatings in 0.5 M H_2SO_4 employing CA measurements.

The trends in Figures 4.3 and 4.4 look very similar. The curves show a relatively well defined linear (Tafelian) behavior over a wider overpotential range. A slight deviation from linearity at high overpotentials for some of the cathodes is visible; this effect has also been reported in the literature [12, 29, 61, 62, 125, 135], and has been explained on the basis of formation of hydrides and/or surface blockage by hydrogen bubbles.

From the linear part of the Tafel curves, one can extract information related to the electrocatalytic activity of the metal-oxide cathodes tested: the Tafel slope, b_C (mV dec^{-1}), which is the inverse of the linear-line slope; the electron transfer coefficient α using equation $b_C = (2.3RT)/(\alpha nF)$, where R (= 8.314 J mol^{-1} K^{-1}) is the gas constant, and T is the temperature (K), n represents the number of electrons exchanged, F (= 96485 C mol^{-1}) is the Faraday constant; and j_0 is the exchange current density (A cm^{-2}), which is the value extrapolated from the linear part of the Tafel curves to zero overpotential. These parameters are displayed in Table 4.3 and 4.4 for the three electrolytes used (the values were determined from the corresponding LTP and CA plots). In general, the data in Table 4.3 agree well with the corresponding data in Table 4.4, which validates their reliability.

Table 4.3: Tafel slope, transfer coefficient, and exchange current density for the $Ni_xMo_{(1-x)}$-oxide coatings obtained from LPT measurements in 0.5 M H_2SO_4, 1M NaOH and 0.6 NaCl. Results for the Ni-control sample are also presented for comparison.

Sample	**0.5M H_2SO_4**			**1M NaOH**			**0.6M NaCl**		
	b_c (mV dec^{-1})	**A**	**j_0 (μA cm^{-2})**	**b_c (mV dec^{-1})**	**α**	**j_0 (μA cm^{-2})**	**b_c (mV dec^{-1})**	**α**	**j_0 (μA cm^{-2})**
Ni	133 ± 9	0.44 ± 0.03	15 ± 3	156 ± 10	0.38 ± 0.04	0.96 ± 0.17	148 ± 12	0.39 ± 0.04	6.8 ± 2.7
NiOx	172 ± 16	0.34 ± 0.05	1.8 ± 1.2	176 ± 12	0.33 ± 0.06	0.64 ± 0.13	173 ± 15	0.34 ± 0.03	1.1 ± 0.5
$Ni_{0.8}Mo_{0.2}Ox$	127 ± 6	0.46 ± 0.09	42 ± 7	144 ± 9	0.41 ± 0.05	9.6 ± 2.8	152 ± 9	0.38 ± 0.06	2.6 ± 1.3
$Ni_{0.6}Mo_{0.4}Ox$	120 ± 8	0.49 ± 0.12	122 ± 10	130 ± 6	0.45 ± 0.11	23.9 ± 7.7	137 ± 7	0.43 ± 0.06	14.3 ± 3.3
$Ni_{0.4}Mo_{0.6}Ox$	151 ± 12	0.39 ± 0.07	3.1 ± 1.1	145 ± 10	0.41 ± 0.09	2.08 ± 1.6	169 ± 11	0.35 ± 0.02	0.6 ± 0.2
$Ni_{0.2}Mo_{0.8}Ox$	185 ± 13	0.32 ± 0.05	0.7 ± 0.3	198 ± 15	0.29 ± 0.06	0.41 ± 0.03	173 ± 12	0.34 ± 0.03	0.24 ± 0.1
MoOx	194 ± 18	0.30 ± 0.04	0.3 ± 0.1	209 ± 17	0.28 ± 0.04	0.16 ± 0.01	209 ± 18	0.28 ± 0.05	0.008 ± 0.004

Table 4.4: Tafel slope, transfer coefficient, and exchange current density for the $Ni_xMo_{(1-x)}$-oxide coatings obtained from CA measurements in 0.5 M H_2SO_4, 1M NaOH and 0.6 NaCl. Results for the Ni-control sample are also presented for comparison.

Sample	**0.5M H_2SO_4**			**1M NaOH**			**0.6M NaCl**		
	b_c (mV dec^{-1})	**A**	**j_0 (μA cm^{-2})**	**b_c (mV dec^{-1})**	**α**	**j_0 (μA cm^{-2})**	**b_c (mV dec^{-1})**	**α**	**j_0 (μA cm^{-2})**
Ni	140 ± 14	0.41 ± 0.04	9 ± 5	145 ± 16	0.40 ± 0.06	1.3 ± 0.34	142 ± 18	0.41 ± 0.08	8.7 ± 3.4
NiOx	174 ± 21	0.33 ± 0.07	1.4 ± 0.8	186 ± 20	0.31 ± 0.08	0.54 ± 0.29	164 ± 25	0.35 ± 0.06	3.1 ± 0.8
$Ni_{0.8}Mo_{0.2}Ox$	123 ± 9	0.47 ± 0.08	58 ± 12	137 ± 16	0.42 ± 0.11	14.6 ± 5.3	149 ± 16	0.39 ± 0.12	7.5 ± 2.4
$Ni_{0.6}Mo_{0.4}Ox$	112 ± 14	0.52 ± 0.09	160 ± 17	135 ± 10	0.43 ± 0.013	18.7 ± 9.1	138 ± 12	0.42 ± 0.14	11.6 ± 6.2
$Ni_{0.4}Mo_{0.6}Ox$	146 ± 18	0.40 ± 0.08	2.5 ± 1.1	156 ± 17	0.37 ± 0.06	1.9 ± 1.3	176 ± 19	0.33 ± 0.06	0.5 ± 0.3
$Ni_{0.2}Mo_{0.8}Ox$	192 ± 22	0.30 ± 0.06	0.9 ± 0.4	189 ± 26	0.31 ± 0.09	0.52 ± 0.08	186 ± 23	0.31 ± 0.07	0.13 ± 0.09
MoOx	202 ± 26	0.29 ± 0.07	0.6 ± 0.3	200 ± 28	0.29 ± 0.05	0.34 ± 0.07	220 ± 31	0.26 ± 0.09	0.004 ± 0.002

The HER is a two-step reaction [12], and the Tafel slope indicates the rate determining step. If the Volmer reaction step, i.e., adsorption of hydrogen to the electrode surface, is rate determining, the resulting Tafel slope at 298 K is 116 mV dec^{-1}; if the Heyrovsky step, i.e., electrochemical hydrogen desorption, is rate determining, the Tafel slope is 40 mV dec^{-1}; if the Tafel step, i.e., chemical hydrogen desorption, is rate determining, the Tafel slope is 30 mV dec^{-1}. From the data in Tables 4.3 and 4.4 it can be seen that the values of the Tafel slope are in the range from ca. 112 to 220 V dec^{-1}, indicating that the determining step for all the cases (all electrodes / all electrolytes) is the Volmer reaction step. The deviation of the Tafel slope to higher values (above 116 mV dec^{-1}) seen in the tables indicate poorer electrocatalytic activity of those surfaces in the HER. From the point of analyzing only the Tafel slope values, it appears that the $Ni_{0.6}Mo_{0.4}$-oxide electrode could potentially yield the highest electrocatalytic activity in the HER among the investigates materials. Namely, a lower Tafel slope value is desired as a smaller change in overpotential (energy input) results in a larger increase in HER current density (hydrogen production).

The other useful parameter to consider is the electron transfer coefficient, α (which ranges from 0 to 1), and it is desirable to have a large electron transfer coefficient value since this value is related to the amount of input energy (overpotential) that is used to lower the activation barrier for the cathodic process [64]. The data in Tables 4.3 and 4.4 show that the $Ni_{0.6}Mo_{0.4}$-oxide electrode also yields the highest transfer coefficient value among the investigated surfaces, and the same is true when the exchange current density value, j_o, is considered. The latter value is frequently used as the basis for comparison of HER catalysts, as it represents the activity of electrocatalyst at equilibrium conditions (zero overpotential).

In general, the transfer coefficient and exchange current density trends in Tables 4.3 and 4.4 show a volcano-type behavior, with a maximum for the $Ni_{0.6}Mo_{0.4}$-oxide electrode, while the Tafel slope trend shows an inverted volcano trend (a valley trend) with a minimum also for the $Ni_{0.6}Mo_{0.4}$-oxide electrode, indicating that the electrocatalytic behavior of the Ni-Mo-oxide electrodes depend on their composition, with the optimum at $Ni_{0.6}Mo_{0.4}$-oxide.

Another, more practical way of evaluating the electrochemical activity of the produced metal oxide coatings in the HER, is to compare current density values (H_2 production rate) measured at a specific overpotential (input energy). This procedure is used in the literature for comparison of HER catalysts more frequently than the exchange current density since hydrogen is produced at a certain overpotential, rather than at zero overpotential. In the current case, the selected overpotential in Figures 3 and 4 is chosen at -300 mV, since at this overpotential the curves display mostly a linear (Tafelian) behavior and at this potential, it is possible to relatively compare all the surfaces. The resulting values are presented in Figure 4.5 for all three electrolytes employed. These data were obtained from both the LTP and CA measurements. In all the cases, the $Ni_{0.6}Mo_{0.4}$-oxide shows the best performance, which is consistent with the observations made by analyzing the values in Tables 4.3 and 4.4. Taking into account the data from LTP, in the acidic medium (Figure 4.5a), the $Ni_{0.6}Mo_{0.4}$-oxide yields ca. 4 times higher H_2 production rate than that on the control Ni electrode, while the improvement from CA measurements is even larger (6 times). In the alkaline electrolyte, in which Ni is currently used as state-of-the-art cathode (Figure 4.5b), the improvement increases further to ca. 6.5 times for LTP data (4 times for CA data), but in the neutral electrolyte (Figure 4.5c) the $Ni_{0.6}Mo_{0.4}$-oxide produces only ca. 1.5-2 times the amount of hydrogen than the control Ni cathode. This shows that the relative performance of the electrodes in the HER is highly dependent on the electrolyte used. Though, in all the cases, the HER activity of the oxide electrodes displays a volcano-type trend.

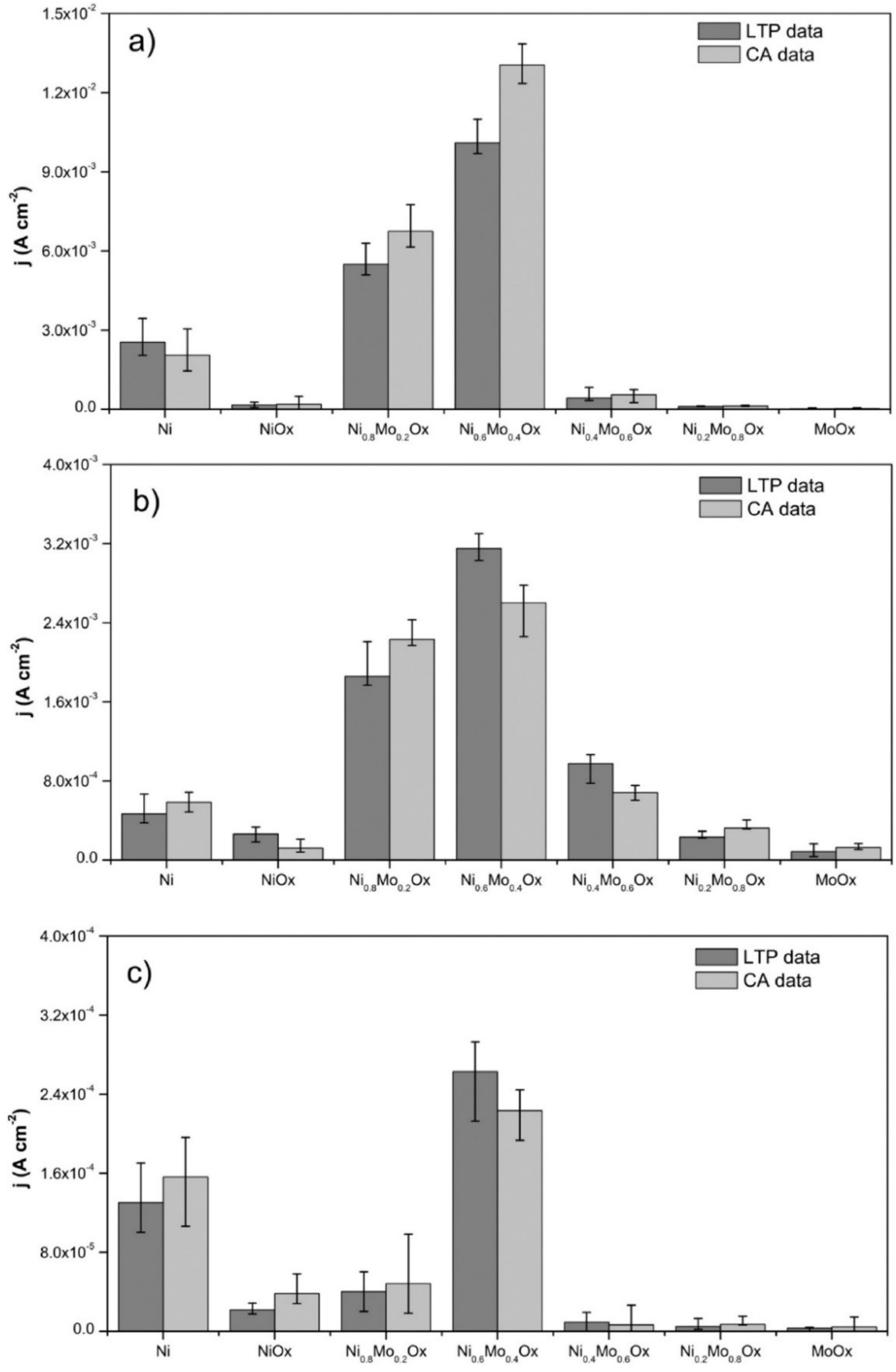

Figure 4.5: Comparison of the electrocatalytic activity of the investigated electrode materials in the HER in terms of current density expressed per geometric area of the electrode and measured at overpotential of −300 mV in a) 0.5 M H_2SO_4, b) 1 M NaOH, and c) 0.6 M NaCl.

In all three media, the activity of the $Ni_{0.6}Mo_{0.4}$-oxide is improved over the Ni control sample. Although further experimental and theoretical studies will be required to obtain a full understanding of the origins of this enhancement, some hypotheses can be put forward by an examination of the structural relationship of the Ni-Mo-oxide catalysts. The presence of oxygen vacancies in these transition metal oxides has been found to narrow the band gap and subsequently improve electrocatalytic activity [136, 137]. While the previous hypothesis only considers the influence of electronic density and structure on the intrinsic electrocatalytic activity of the cathodes, the 'spillover' process has also been used to interpret the synergism of transition metal-based HER alloys, and might be extrapolated (however, without experimental evidence) to oxides.

Most of the work on the development of nanostructured cathodes for the HER report the electrocatalytic activity concerning the electrode geometric area, as it was done above in Figure 4.5. This gives information on the extrinsic electrocatalytic activity of the electrode. Nevertheless, in order to evaluate the true (intrinsic) electrocatalytic activity of the material, the current density must be expressed in terms of the true electrochemically-active surface area of the electrode. The results discussed above, thus, cannot offer a definite conclusion if the observed electrocatalytic activity trend is either a result of only the variation in the surface area of the electrodes, or the change in intrinsic (electronic) electrocatalytic properties of the electrode material, or a combination of the two. Therefore, in order to investigate which of the electrocatalysts is intrinsically the best material for the HER, the Tafel curves were normalized to the true electrochemically-active surface area of the electrocatalyst (which was evaluated using the cyclic voltammetry method described in the experimental part of the paper and the corresponding results are presented in Table 1) [12]. Then, the results displayed in Figure 4.5 were normalized to the corresponding true electrochemically-active area of the electrodes and presented in Figure 4.6.

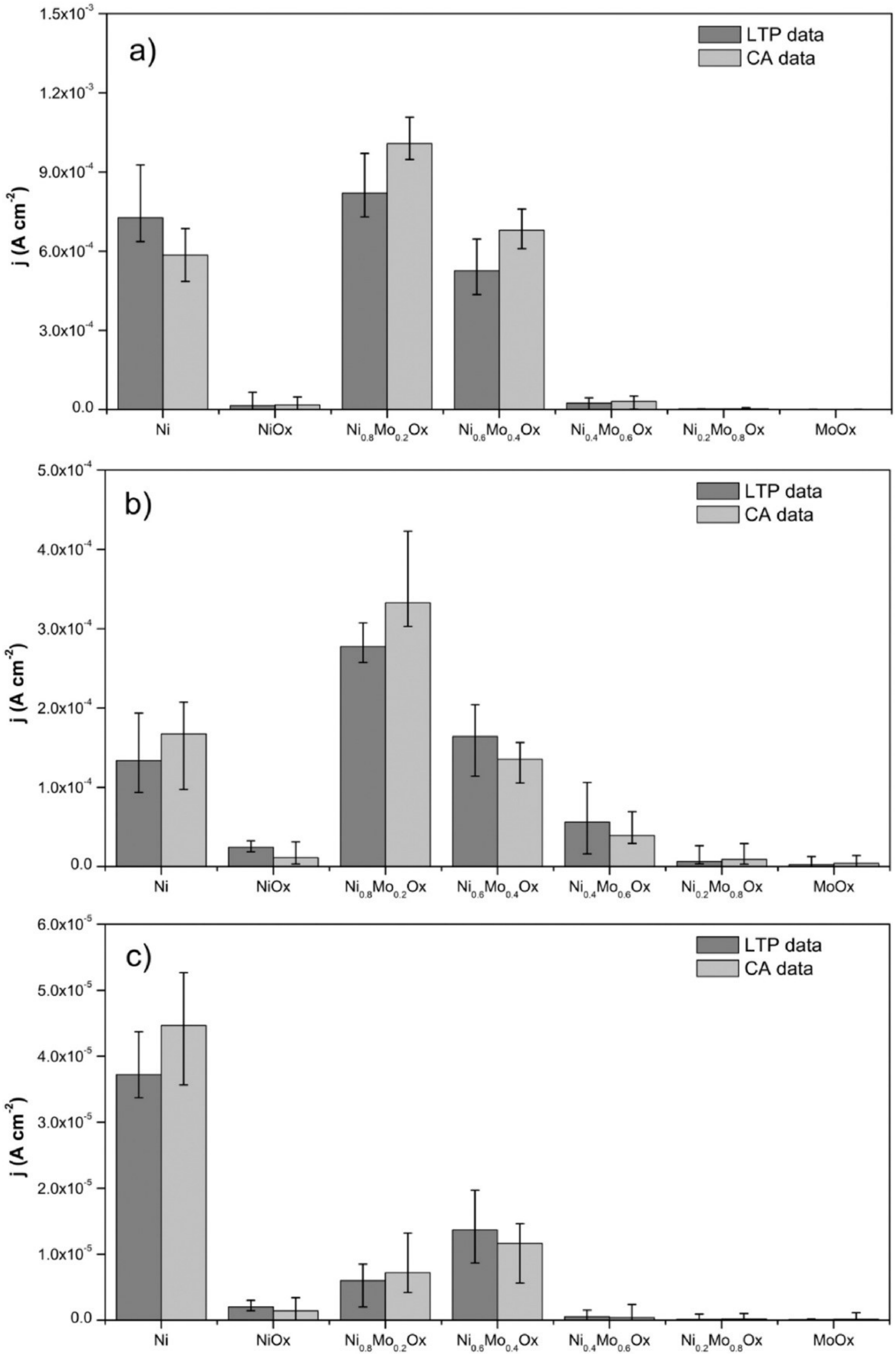

Figure 4.6: Comparison of the electrocatalytic activity of the investigated electrode materials in the HER in terms of current density expressed per true electrochemically-active area of the electrode and measured at overpotential of −30 0 mV in a) 0.5 M H_2SO_4, b) 1 M NaOH, and c) 0.6 M NaCl.

By comparing Figures 4.5 and 4.6, one can see that the trend in intrinsic electrocatalytic activity (Figure 4.6) is different from the trend in extrinsic electrocatalytic activity (Figure 4.5). In the acidic medium (Figure 4.6a), there is no statistically significant difference among pure Ni control, $Ni_{0.8}Mo_{0.2}$-oxide, and $Ni_{0.6}Mo_{0.4}$-oxide. However, the use of pure Ni-oxide and the three Mo-rich oxides ($Ni_{0.4}Mo_{0.6}$-oxide, $Ni_{0.2}Mo_{0.8}$-oxide, and Mo-oxide) results in a rather poor intrinsic electrocatalytic activity of the cathodes. The trend in activity among the oxide electrodes when used in the alkaline (Figure 4.6b) and NaCl neutral electrolyte (Figure 4.6c) is similar to that in the acidic environment (Figure 4.6a). Nonetheless, in the alkaline environment, the $Ni_{0.8}Mo_{0.2}$-oxide cathode displays the highest intrinsic electrocatalytic activity in the HER, ca. twice that of pure Ni control, indicating that alkaline water electrolyzers could benefit from using the $Ni_{08}Mo_{0.2}$-oxide cathode instead of currently-used Ni electrodes. The situation in the neutral NaCl electrolyte is different; here the Ni control shows the highest intrinsic electrocatalytic activity in the HER.

4.4.3 Long-term stability

The long-term stability of selected $Ni_xMo_{(1-x)}$-oxide electrodes was tested by running linear Tafel polarization (LTP) and chronopotentiometry (CP) measurements consecutively in the following order: LTP on freshly-prepared electrodes, CP (electrolysis) at 0.5 $A\,cm^{-2}$ for 24 hours, and LTP on the 'used' electrodes. These experiments were performed on the three $Ni_xMo_{(1-x)}$-oxide electrodes that displayed the highest extrinsic electrocatalytic activity ($Ni_{0.8}Mo_{0.2}$-oxide, $Ni_{0.6}Mo_{0.4}$-oxide, $Ni_{0.4}Mo_{0.6}$-oxide) and on the control sample (Ni), all in aggressive 0.5 M H_2SO_4. The corresponding results of electrocatalytic activity evaluated at overpotential of -300 mV are presented in Figure 4.7. It can be seen that there is no statistical difference in the activity of the electrodes before and after the 24-hour electrolysis, indicating that the materials are stable under the experimental conditions employed. Nevertheless, it should be noted that a significantly longer electrolysis time is needed in order to evaluate the true stability of the Ni-Mo-oxide electrodes as a number of factors could influence their HER activity over a prolonged period of time (deactivation by metal and other impurities present in the electrolyte, mechanical damage of the electrode due to the action of hydrogen bubbles and electrolyte flow, etc.).

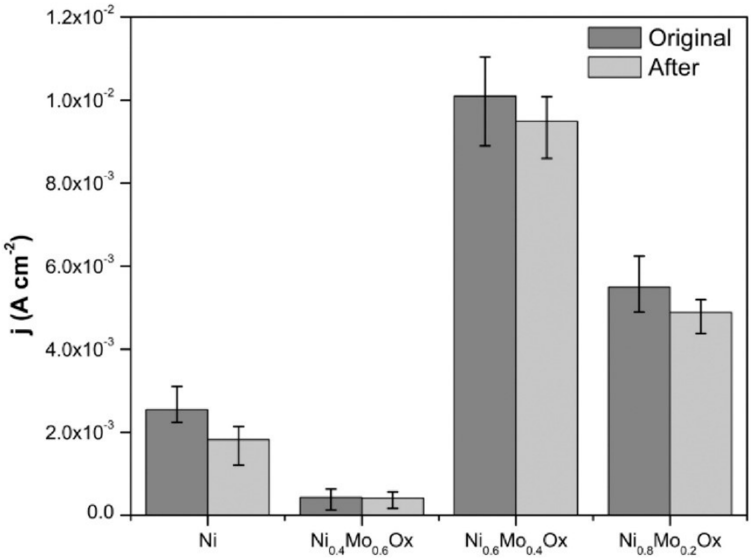

Figure 4.7: Comparison of the electrocatalytic activity of the investigated electrode materials in the HER in terms of current density expressed per geometric area of the electrode and measured at overpotential of −300 mV in 0.5 M H_2SO_4, before and after 24 hours of electrolysis at 0.5 A cm^{-2}.

4.5 Conclusions

Nickel-molybdenum oxides coatings of different compositions were formed on a titanium substrate and their electrocatalytic activity for the hydrogen evolution reaction was investigated in acidic, alkaline, and neutral media. The SEM analysis showed that the surface morphology of the metal oxide coatings depends on their chemical composition. All the coatings displayed a certain degree of surface roughness, ranging from a surface factor value of 5 to 52. The crystalline structure of the coatings was also found to be dependent on their chemical composition. While the single-metal-oxides displayed crystalline structure, the binary Ni-Mo-oxide coatings were characterized by a certain degree of amorphousness.

Electrochemical measurements revealed that the electrocatalytic activity of the coatings is dependent on both the coating composition (intrinsic effect) and coating roughness (i.e., true electrochemically-active area). The most extrinsically active coating was the $Ni_{0.6}Mo_{0.8}$-oxide coating (in all three electrolytes), while this coating showed the highest intrinsic activity in the neutral electrolyte. In the acidic and alkaline electrolyte, the $Ni_{0.8}Mo_{0.2}$-oxide coating was found to be most intrinsically active.

The results presented in the paper demonstrate that Ni-Mo-oxides could potentially be used as good HER electrocatalysts in the acidic, alkaline and neutral environment. Nevertheless, further work should be done to evaluate their long-term stability, fouling susceptibility and re-activation capability. Additionally, in order to use them in PEM electrolyzers, the metal oxides should be produced as nanoparticles.

Acknowledgement

Grateful acknowledgment is made to the McGill University through the McGill Engineering Doctoral Award (MEDA) program, and the Natural Sciences and Engineering Research Council of Canada (NSERC) for support of this research.

Chapter 5

5 The Influence of Addition of Iridium-Oxide to Nickel-Molybdenum-Oxide Cathodes on the Electrocatalytic Activity Towards Hydrogen Evolution in Acidic Medium and on the Cathode Fouling Resistance

5.1 Preface

This chapter presents an article that has been published in *Electrochimica Acta*. The citation of the published article is:

> A. Gomez Vidales, L. Dam-Quang, A. Hong, S. Omanovic, *Electrocatalytic Performance of Mixed Nickel-Molybdenum-Iridium-Oxide Cathodes for acidic water electrolysis and the Effect of Contamination of Copper and Iron Impurities*. Electrochimica Acta, 302 (2019) 198.

The contributions of each author were the following: Abraham Gomez Vidales (the Ph.D. candidate) designed the experiments, performed the physical characterization of the electrodes, analyzed results, and wrote the manuscript. Liem Dam-Quang (a McGill undergraduate student) prepared the electrodes and conducted the initial electrochemical tests of them. Anlan Hong (a McGill undergraduate student) executed the experiments related to the deactivation/reactivation of the electrodes. Prof. Sasha Omanovic was responsible for the supervision of the work, contributed to the interpretation and discussion of results, and corrected the manuscript. In the results and discussion section, each data point and the corresponding deviation presented in figures represent an average of 9-15 measurements: between 3 to 5 separate samples, each tested 3 times.

Ir is known to be an excellent HER catalyst, as already stated in the background section of the thesis. However, this noble metal due to its scarcity, is expensive. For this reason, this research work aimed to investigate if the addition of Ir-oxide to $Ni_{0.6}$-$Mo_{0.4}$-oxide coating (best performing composition obtained from our previous study, see Chapter 4) would result in improvement of the electrocatalytic activity towards the hydrogen evolution. Furthermore, it was also essential to determine the relationship between Ir-oxide content in the coating and the resulting activity is in order to determine its economic feasibility. Finally, fouling experiments were done to prove if these tailor-made oxides have better stability than the nickel control sample.

In order to achieve the previous objectives, in this article, the electrocatalytic activity of the Ni-Mo-Ir-oxide coatings for the hydrogen evolution reaction was evaluated using linear Tafel polarization and chronoamperometry techniques. In addition, several physicochemical properties of the coatings such morphology, surface roughness and composition of the coatings were determined. Finally, the deactivation and reactivation of the cathodes in the presence of the most common impurities (Cu, Fe, and Cu + Fe) was done. Resulting in all the cases, that the Ni-Mo-Ir-oxide have a better performance in comparison to the control sample (Ni).

This article is dedicated to my friend Jose Alberto Gomez Roldan.

Electrocatalytic Performance of Mixed Nickel-Molybdenum-Iridium-Oxide Cathodes for Acidic Water Electrolysis: The Effect of Contamination of Copper and Iron Impurities

Abraham Gomez Vidales, Liem Dam-Quang, Anlan Hong, Sasha Omanovic
Department of Chemical Engineering, McGill University, 3610 University St., Montreal, Quebec, H3A 0C5, Canada

Keywords: Hydrogen; Water electrolysis; Nickel; Molybdenum; Iridium; Metal oxides; Cathodes; Deactivation/reactivation.

* Corresponding author: abraham.gomezvidales@mail.mcgill.ca

Abstract

The influence of addition of Ir-oxide into Ni-Mo-oxide cathodes on the electrocatalytic activity of the hydrogen evolution reaction in acidic media was investigated. It was found that as the Ir-oxide content increased, the electrocatalytic activity towards hydrogen evolution also increased. This was attributed to the following two effects: the increase in the number of Ir surface sites and to the possible modification of the electronic structure of the material. Long-term electrolysis experiments confirmed high deactivation resistance of the Ni-Mo-Ir-oxide cathodes. It was also demonstrated that it is possible to *in-situ* reactivate the electrodes, making them potentially good cathode candidates for water electrolysis in the acidic medium.

5.2 Introduction

In light of the environmental and geopolitical impacts of the fossil fuel-based energy systems, the need for a renewable energy economy is stronger than ever [138]. Hydrogen is increasingly being considered as an alternative medium of energy storage and production due to its lack of carbon dioxide emissions when produced through water electrolysis. However, in order to become economically competitive, commercial-scale hydrogen production costs must be further reduced, with the U.S. Department of Energy targeting a 50% reduction in production costs per kg by 2020 compared to 2015 [139]. Hydrogen can be produced in electrolyzers by splitting water through the hydrogen evolution reaction (HER) at the cathode. If the electricity used to drive these reactions is generated from a carbon-neutral source, then hydrogen can be created and stored without any significant greenhouse gas emissions.

The catalyst of choice for electrochemical hydrogen evolution is Pt, due to its high catalytic activity and stability [140, 141]. Nevertheless, the use of Pt introduces high investment costs, due to the high price of the metal. Additionally, Pt tends to deactivate in acidic conditions, such as those found in proton exchange membrane (PEM) water electrolyzers, which are increasingly being considered as the technology of choice for water electrolysis [142]. The main advantages of PEM electrolysis over the conventional alkaline electrolysis (in which nickel and its alloys are used as the cathode) are the much higher current densities (1 - 3 A cm^{-2} compared to 0.2 A cm^{-2}), the more significant energy efficiency of the process, and the purity of the produced hydrogen [143, 144]. Moreover, PEM electrolyzers can work at higher (differential) pressures, allowing internal compression of the hydrogen required for its transport. Hence, PEM electrolyzers are ideal for small and remote plants and households with low and erratic energy consumption [145].

In the search for new materials and their applications, recent research studies and patents have claimed good performances of oxide electrodes for the cathodic evolution of hydrogen [71, 143, 144, 146-149]. The reported advantage of such electrodes is that, unlike their metallic counterparts, they are much less prone to poisoning by (underpotential) deposition of metals present as impurities in the electrolytes [71, 150, 151]. The effectiveness of transition metal oxides (TMOs) as catalysts for the HER was first reported in the 1980s [150]. Transition metal oxides have since emerged as one of the leading alternatives to noble metal electrodes. Although not as suitable as pure metals due to their lower activity, oxides are notable for being highly stable, even in harsh operating conditions. For example, there are few publications on the performance of iridium oxide (IrO_2) as a cathode. IrO_2 exhibits excellent corrosion resistance, excellent electrical conductivity, and high electrocatalytic activity toward hydrogen evolution reaction [71, 146, 152]. Furthermore, IrO_2 is widely used in the preparation of mixed oxide electrodes [71, 84, 153, 154]. Despite its widespread use as a component of oxide electrodes in technological applications, no recent information whatsoever is available on the performance of iridium oxide as a cathode.

Given the number of advantages of PEM water electrolyzers over currently-used alkaline electrolyzers and considering that expensive Pt is still being used as a cathode in PEM electrolyzers, there is a strong incentive to replace Pt by cheaper electrocatalyst materials, while still maintaining high electrocatalytic activity and improving the deactivation resistance of the cathode [90, 155, 156]. Previous studies have demonstrated that Ni-Mo oxides can be used as cost-effective electrocatalysts for the HER [148]. Adding Ir to these mixtures could potentially increase the catalytic performance while remaining economically competitive. In this research paper, we present initial results on the effect of the addition of Ir to $Ni_{0.6}$-$Mo_{0.4}$-oxide on the resulting HER kinetics and deactivation/reactivation of the electrodes. $Ni_{0.6}$-$Mo_{0.4}$-oxide was chosen as the base cathode material since our previous results [148] demonstrated that this Ni/Mo ratio yielded the highest electroactivity in the HER in the acidic medium among the investigated Ni-Mo-oxide compositions.

5.3 *Experimental procedure*

5.3.1 Electrode preparation

The electrodes were prepared by coating titanium buttons (1.27 cm diameter, 0.2 cm thickness, purity 99.2%, Alfa Aesar, USA) with a metal oxide coating using a thermal-salt-decomposition method. Nickel, molybdenum, and iridium precursor solutions were prepared from dissolving salts $NiCl_2 \times 6H_2O$ (purity 99.9%, Sigma-Aldrich, Canada), $Na_2MoO_4 \times 2H_2O$ (purity 99.5 wt.%, Sigma-Aldrich, Canada) and $IrCl_3 \times 3H_2O$ (purity 99.9 wt.%, Sigma Aldrich, Canada) in a mixture of 50 vol.% HCl (37 wt.%, Fisher Scientific, Canada) and 50 vol.% nanopure water (resistivity 18.2 MΩ cm). Titanium buttons were polished to a uniform finish using 600 grit sandpaper, followed by etching in the boiling HCl solution of the concentration quoted above for 30 minutes and drying with argon gas (MEGS Specialty Gases Inc., 99.998 wt.% pure, Canada). Nickel and molybdenum salts were mixed in a 60:40 molar metal-based ratio, while the percentage of iridium was varied with each set of samples, from 2 up to 60 mol.%. A 100% iridium-oxide electrode was also prepared. The analysis by electron dispersive spectroscopy (EDS) confirmed that the actual surface composition of the coatings is very similar to the nominal composition and that the elements were homogenously distributed on the surface of the coatings. For comparison proposes, a flat Ni (purity: 99.9%) foil was used as a control cathode.

The Ti buttons were coated on one side with the prepared solution of the desired composition using standard paint brushes. After applying the metal-precursor solution on the Ti surface, the samples were first dried in an oven to 368 K for five minutes to evaporate the solvent and subsequently transferred into a furnace to 773 K for fifteen minutes. The samples were then removed and allowed to cool at room temperature for ten minutes. Next, another coating layer was applied, and the process was repeated five times, for a total of six coatings. After applying the final coat, the buttons were kept in the furnace for one hour to convert metals into their oxides. Finally, the back side of the buttons was polished using 600 grit sandpaper to serve as the contact for the electrical circuit.

5.3.2 Physical characterization

The surface structure, composition, and morphology of the electrodes were studied by X-ray diffraction (XRD), electron dispersive spectroscopy (EDS), scanning electron microscopy (SEM) and stylus profilometry. The XRD patterns were recorded with a D8 Discover Bruker 2 Theta X-ray diffractometer equipped with a Cu source. The diffraction data were collected over an angle range of $2\theta = 20 - 90$ using GADDS software. The XRD generator was operated at 40 kV and 30 mA. The surface roughness was measured using a DektakXT stylus (Bruker, USA) surface profilometer. The measured area was 0.8 mm × 1.5 mm, and three measurements were conducted for an average value. SEM/EDS measurements were performed on a Hitachi SU-3500 Variable Pressure SEM (Hitachi, Japan) *microscope* (software: PC_SEM) with EDS detector (software: *AZtecEnergy EDS).*

5.3.3 Electrochemical characterization

Electrochemical techniques of Tafel polarization (TP), chronoamperometry (CA), chronopotentiometry (CP) were done to evaluate the performance of the electrodes in the HER, while electrochemical impedance spectroscopy (EIS) was used to measure the electrolyte resistance for the *jR-drop* correction and to obtain the real electrochemically-active surface area (EASA). These experiments were carried out using a typical three-electrode cell at room temperature 293 ± 2 K and atmospheric pressure. The working electrode (WE) had a geometrical area of 0.68 cm^2. A graphite rod was used as the counter electrode (CE), and it was placed inside a glass frit (Ace Glass Inc., USA) to avoid interfering with the HER. A saturated calomel electrode (SCE) (Accumet electrode, Fisher Scientific, USA) was used as the reference electrode (RE). The acidic electrolyte was prepared with H_2SO_4 (96 wt.% pure, Fisher Scientific, Canada), and nanopure water. The electrolyte in the cell was deaerated with argon for 30 minutes before measurements, and argon was passed over the top of the solution during the experiment to keep an oxygen-free electrolyte solution. Before each electrochemical LTP and CA measurement, the electrode was stabilized at -1.0 V for 30 minutes and the polarization was then started in the positive-going direction followed by performing an EIS measurement at 0.45 V in order to determine resistance for the jR-drop correction. Data acquisition and analysis were carried out with a potentiostat/galvanostat Autolab PGSTAT30 with NOVA software (v. 2.1; Metrohm, Netherlands). All the potentials are given versus the SCE, and all the polarization curves were corrected for the jR-drop.

5.3.4 Deactivation and activation of the electrodes

The same standard three-electrode electrochemical cell described above was used for investigating the susceptibility of electrodes towards deactivation and their capability towards re-activation. However, in this case, a platinum/rhodium wire (composition Pt 80 wt.% and Rh 20 wt.%, 0.5 mm diameter, Sigma-Aldrich, USA) was used as the counter electrode (CE). The electrolyte solution used as reference was 0.5 M H_2SO_4. All the solutions were prepared with nanopure water. Three metal-ion solutions with Cu or Fe or Cu + Fe ions dissolved in 0.5 M H_2SO_4 were made to examine the degree of deactivation of the cathodes by these metals. Cu in the form of $CuSO_4 \cdot 5H_20$ (98% pure Sigma-Aldrich, Canada) and Fe was introduced in the form of $FeSO_4 \cdot 7H_2O$ (99% pure, Sigma-Aldrich, Canada). The amount of dissolved Cu and Fe was 10 ppm, which is around 20 times higher than the concentration in the industrial electrolyzers (this was done to accelerate the deactivation process and make the deactivation condition harsher). The prepared solutions were sonicated for 30 minutes to enhance dissolution of the salts fully. After assembling the cell, argon gas was used to purge the solution for 30 minutes before any electrochemical measurements were taken and the solution was continued to be purged throughout the deactivation experiment.

The following methodology was executed in order to evaluate the effect of electrode deactivation (deposition of metals on the electrode surface) and its subsequent re-activation. First, the cathode was stabilized at a potential of -1.0 V in *pure* 0.5 M H_2SO_4 for 30 minutes. Next, EIS was done at 0.45 V to determine resistance for the *jR-drop* correction. After this, LTP in the hydrogen evolution region was performed, which gave the result on the freshly-prepared electrode HER activity. Then, the electrode was transferred into the "contaminated" solution, and galvanostatic polarization was performed for 24 hours at a constant current density of -100 mA cm^{-2}; this resulted in the deactivation of the electrode due to deposition of Cu and/or Fe on its surface. Hereafter, the electrode was rinsed with nanopure water, followed by a LTP measurement in *pure* 0.5 M H_2SO_4 in the hydrogen evolution region to assess the degree of electrode deactivation. Next, the electrode was re-activated by polarizing it galvanostatically in the anodic region at 100 mA cm^{-2} for 30 minutes in *pure* 0.5 M H_2SO_4. Finally, LTP was repeated in a freshly-prepared *pure* 0.5 M H_2SO_4 solution to assess the degree of re-activation of the electrode, followed by EIS measurement needed for the *jR*-drop correction.

In order to determine the influence of reactivation on the dissolution of Cu, Fe, Ni, Mo, and Ir, the electrolyte solution after reactivation was analyzed using a TraceScan Inductively Coupled Plasma – Optical Emission Spectroscopy (ICP-OES, iCAP 6500 dual view, Thermo Scientific, USA) system. The instrument was calibrated prior to the measurements using the standard solutions of the above-specified elements.

5.4 Results and discussion

5.4.1 Electrocatalytic activity in the HER

In order to evaluate the relative electrocatalytic activity of the produced electrode compositions in the HER, linear Tafel polarization curves were recorded. For comparison, the response of pure Ir-oxide and pure metallic Ni is also shown in Figure 5.1a. Furthermore, steady-state polarization curves obtained from CA measurements are also presented in Figure 5.1b, for comparison and validation purposes. The agreement between both sets of curves employing two different electrochemical techniques is excellent. These curves show the relationship between the overpotential (energy input) versus the current density (amount of hydrogen produced obtained through the Faraday law). As expected, with an increase in Ir content in the Ni-Mo-oxide coating, the hydrogen evolution current at a constant potential also increases. It is also important to mention that all the oxide-based electrodes display a significantly higher catalytic activity than pure metallic Ni, currently used in alkaline electrolyzers as a cathode (note that the results in Figure 5.1 were recorded in an acidic medium, and the Ni curve is shown only for comparison purposes, despite this metal not being used in PEM electrolyzers). In addition, the HER onset potential decreased appreciably on the oxide electrodes in comparisons to pure metal nickel.

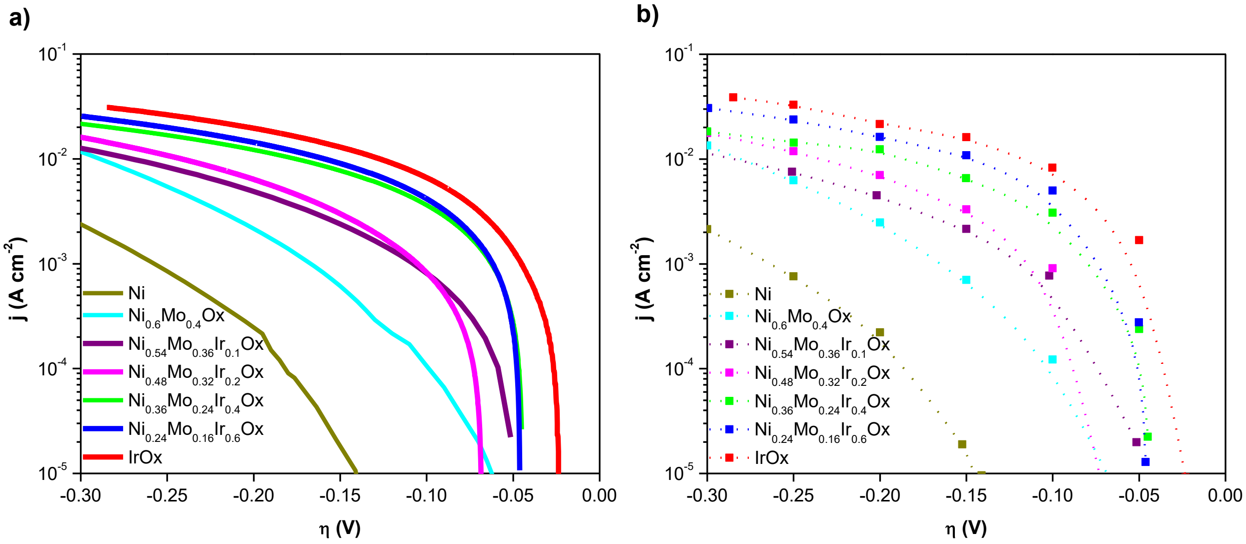

Figure 5.1: a) Linear Tafel polarization curves recorded in the hydrogen evolution region in 0.5 M H_2SO_4 on selected electrodes. Scan rate was 10 mVs^{-1}, b) Steady-state polarization curves recorded under the same conditions employing CA measurements.

As can be seen in Figure 5.1, the polarization curves corresponding to the response of electrodes that contain iridium deviate from the common Tafelian behavior (there is no defined linear Tafel region) and a semi-plateau region is reached at relatively low overpotential values. This effect can be attributed to the gradually-increasing electrode surface blockage by generated hydrogen bubbles (bubbles stick on the surface, reducing the electrochemically active surface area), and/or to the formation of hydrides on the surface layer (which can modify the electronic and structural properties of the coating) and/or to a local increase in pH at the electrode/electrolyte interface [152]. These results are similar to the ones from literature data reported recently for pure and other mixed Ir-oxide prepared by thermal decomposition [144, 145, 157].

A convenient way of evaluating the electrocatalytic activity of HER cathodes is by comparing the current density at a given overpotential. In the current case, this was done at an overpotential of -200 mV, and the results are presented in Figure 5.2 using data obtained from LTP and CA measurements.

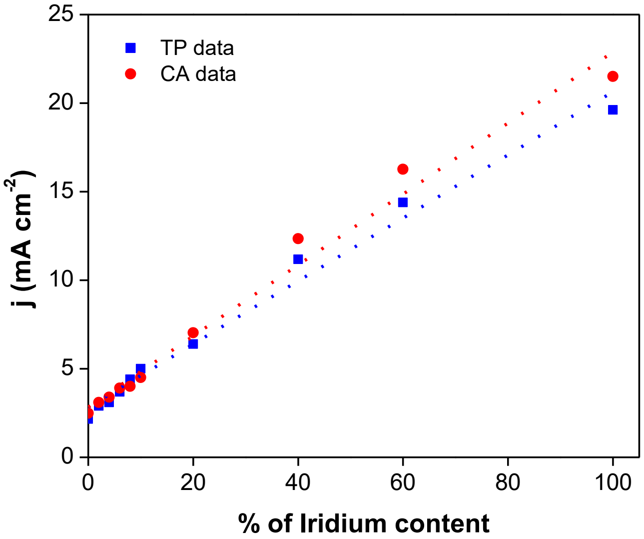

Figure 5.2: Dependence of hydrogen evolution current density recorded at overpotential of -200 mV as a function of iridium content in the metal-oxide electrode.

When comparing the HER activity of pure Ir, Ni, and Mo metals, Ir sits on top of the HER volcano curve, two orders of magnitude higher than Ni and four orders of magnitude above Mo [44]. Although the electrodes investigated here are not pure metals, but rather their oxides, it could still be expected from Ir-oxide to offer higher HER electrocatalytic activity than the Ni-Mo-oxide electrode. The result in Figure 5.2 shows that this is, indeed, the case. With an increase in Ir content in the Ni-Mo-oxide, the activity towards hydrogen evaluation increases linearly. Considering that these electrodes are much more complex than pure metal electrodes, the fundamental explanation for the trend observed in Figure 5.2, based on the electrode (metal-oxide)-hydrogen bond strength only (volcano curve [44]), cannot be employed here. The linear trend indicates that the HER kinetics is, at least to a certain extent, proportional to the number of Ir-oxide active sites on the electrode surface.

5.4.2 Morphology and surface roughness of the electrodes

Figure 5.3 shows the SEM images of the selected cathodes investigated in this work. The micrographs evidence that addition of Ir to the Ni-Mo-oxide results in a change in the surface morphology of the coating. While the surface that does not contain Ir (Figure 5.3a) shows a porous structure characterized by globules of ca. 1 - 3 μm in diameter, the surfaces that contain Ir (Figure 5.3b-f) display a cracked-mud morphology, which is characteristic of most metal-oxide coatings produced by thermal decomposition of their salts. This surface morphology is very similar to those observed with Ir, and Ir-oxide surfaces reported in the literature [137, 158]. It was determined that the average thickness of the metal coatings is 5 ± 2 μm.

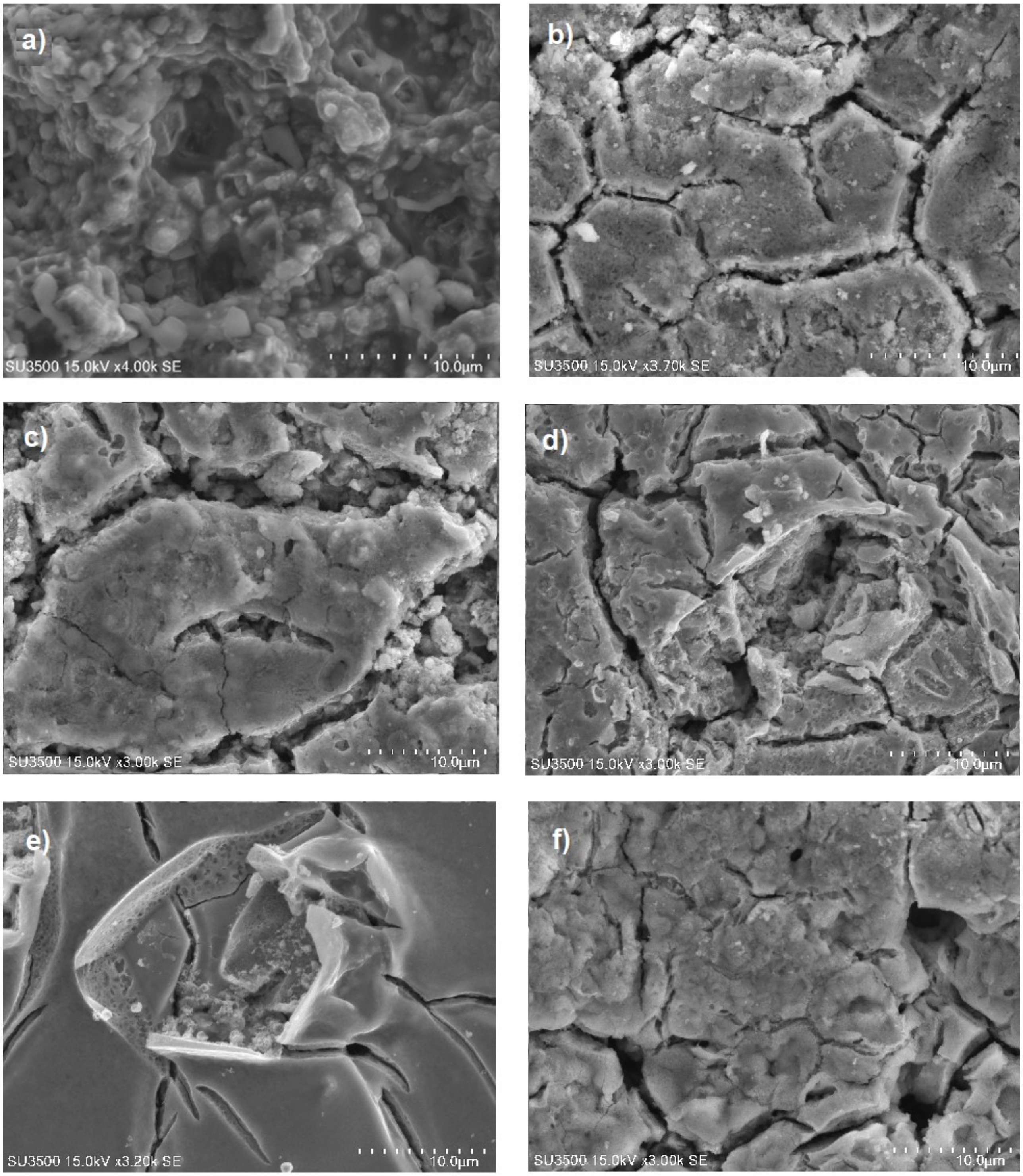

Figure 5.3: SEM images of a) $\mathrm{Ni}_{0.6}$ $\mathrm{Mo}_{0.4}$-oxide, b) $\mathrm{Ni}_{0.54}$ $\mathrm{Mo}_{0.36}\mathrm{Ir}_{0.1}$-oxide, c) $\mathrm{Ni}_{0.48}$ $\mathrm{Mo}_{0.32}\mathrm{Ir}_{0.2}$-oxide, d) $\mathrm{Ni}_{0.36}$ $\mathrm{Mo}_{0.24}\mathrm{Ir}_{0.4}$-oxide,e) $\mathrm{Ni}_{0.24}$ $\mathrm{Mo}_{0.16}\mathrm{Ir}_{0.6}$-oxide, and f) Ir-oxide coating. The overall scale length on the images is 10 μm.

Next, the surface roughness, in this case, the arithmetic average of the roughness profile, *Ra* (µm), was determined using a stylus profilometer, and the values are presented in Table 5.1. The control surface, a flat metallic nickel plate, was characterized by the lowest surface roughness value. Producing an oxide electrode resulted in an increase in surface roughness; the base electrode material, $Ni_{0.6}Mo_{0.4}$-oxide, displayed a surface roughness roughly twice of that presented by metallic nickel. The addition of Ir into the metal oxide coating resulted in a further increase in surface roughness; with an increase in Ir content, the surface roughness, in general, also increases, indicating an increase in the surface area of the cathode available for the HER.

Table 5.1: Measured roughness of the surface electrodes Ni, Ni-Mo-oxide, and Ni-Mo-Ir-oxide.

Sample	**Roughness Ra (um)**
Ni	0.26 ± 0.01
$Ni_{0.6}Mo_{0.4}Ox$	0.46 ± 0.02
$Ni_{0.54}Mo_{0.36}Ir_{0.1}Ox$	0.68 ± 0.05
$Ni_{0.48}Mo_{0.32}Ir_{0.2}Ox$	0.64 ± 0.07
$Ni_{0.36}Mo_{0.24}Ir_{0.4}Ox$	1.25 ± 0.11
$Ni_{0.24}Mo_{0.16}Ir_{0.6}Ox$	1.29 ± 0.13
IrOx	1.93 ± 0.10

Next, in order to estimate the true electrochemically-active surface area (EASA) of the electrode exposed to the electrolyte, electrochemical impedance spectroscopy (EIS) measurements were performed [12]. Figure A.2 in the supplementary material document shows an example of the EIS spectra recorded on the $Ni_{0.48}Mo_{0.32}Ir_{0.2}$-oxide coating. The spectra were modeled using an electrical equivalent circuit (EEC) presented in Figure A.3 in the supplementary material document. The agreement between the experimental (symbols) and modeled (line) data is good. The same procedure was employed to analyze spectra recorded on other electrode compositions, and the representative EEC parameters are listed in Table A.1. Then, using the Brug equation [12, 159], Equation A.3 in the supplemental material document, the electrode double layer capacitance was calculated, and the values are presented in Table 5.2. From this, the true electrochemically-active surface area (EASA) of the electrode was estimated by dividing these values by the theoretical electrochemical double-layer capacitance value of 20 μF cm^{-2}. Similarly to the trend of surface roughness values in Table 5.1, the EASA values also increase with the increase in Ir content in the oxide coating. Both relative-increase trends (Tables 5.1 and 5.2) are linear, with the corresponding slopes of 0.056 ($R^2 = 0.961$) for the surface roughness values, and 0.168 ($R^2 = 0.997$) for the EASA values. Given that profilometry can provide information only on the surface topography roughness at the micron scale, while EIS can provide information on the true electrochemically-active area that takes into account the coating porosity down to the nano-level, the relative comparison of the two slopes indicates that by increasing the Ir content in the oxide coating, the nano-level porosity increases significantly more than the micro-level surface roughness.

Considering the EASA values in Table 5.2, the linear trend in Figure 5.2, which shows the extrinsic electrocatalytic activity of the cathodes, can be normalized for the surface-area effect to estimate the relative *intrinsic* activity of the catalysts. The resulting trend is presented in Figure 5.4. With an increase in Ir content in the coating, the intrinsic activity of the cathode increases up to the Ir content of 40%, and then reaches a plateau. Although the trend is not linear as that one in Figure 5.2, it still shows that the actual intrinsic HER activity of the cathodes depends strongly on the amount of Ir in the coating up to a certain relative Ir content (40%). The trends in Figures 5.2 and 5.4 also indicate that the contribution to the intrinsic activity does not come only through the increase in Ir surface sites, but also through a possible modification of the electronic structure of the electrode; otherwise, the trend in Figure 5.4 would be the same as that one in Figure 5.2, taking into account that the Ir content on the top coating surface also increases in the same manner as that one in the bulk of the coating (which is the case, which has been verified by XPS – see Table A.2 in the supplementary material).

Table 5.2: Double layer capacitance and electrochemically-active surface area of the investigated coatings obtained from the EIS data.

Sample	**C_{DL} (F cm^{-2})**	**EASA (cm^2)**
Ni	$(6.60 \pm 0.5) \times 10^{-5}$	3.3
$Ni_{0.6}Mo_{0.4}Ox$	$(4.20 \pm 0.7) \times 10^{-4}$	21
$Ni_{0.54}Mo_{0.36}Ir_{0.1}Ox$	$(5.85 \pm 0.3) \times 10^{-4}$	29
$Ni_{0.48}Mo_{0.32}Ir_{0.2}Ox$	$(6.48 \pm 0.5) \times 10^{-4}$	32
$Ni_{0.36}Mo_{0.24}Ir_{0.4}Ox$	$(8.96 \pm 1.6) \times 10^{-4}$	45
$Ni_{0.24}Mo_{0.16}Ir_{0.6}Ox$	$(1.12 \pm 0.6) \times 10^{-3}$	56
IrOx	$(1.54 \pm 0.9) \times 10^{-3}$	77

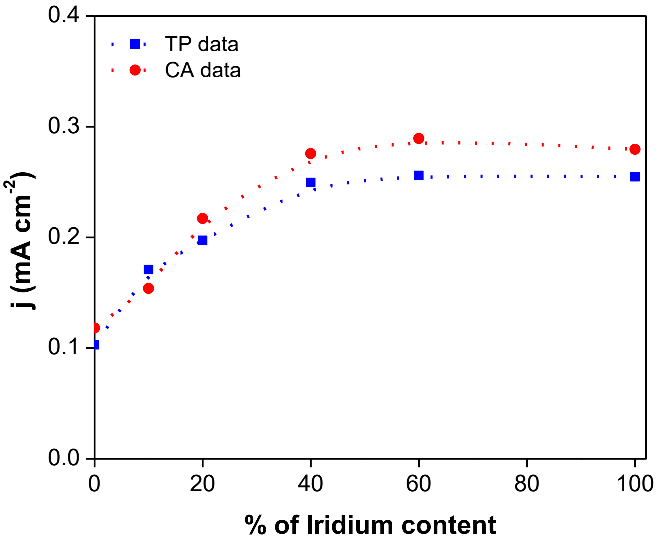

Figure 5.4: Dependence of hydrogen evolution current density normalized by the the true electrochemically-active surface area recorded at overpotential of -200 mV as a function of iridium content in the metal-oxide electrode.

5.4.3 Structural characterization

The XRD patterns of selected electrodes are displayed in Figure 5.5. The metallic Ni-control sample is presented as a reference, showing the corresponding characteristic phases of Ni and NiO, and a crystalline structure. The base oxide material, $Ni_{0.6}Mo_{0.4}$-oxide, is also presented, exposing a slightly amorphous structure and the existence of Ni, NiO, Ni_2O_3, Mo, and MoO_3. In the case of the Ni-Mo-Ir-oxide coatings, the characteristic peaks of Ni, NiO, MoO_2, and IrO_2 are visible, indicating that molybdenum and nickel oxidative states decreased from +6 to +4 and from +3 to +2, respectively, when the precursor Ir solution was incorporated into the coating. Moreover, all the Ni-Mo-Ir-oxide coatings presented a crystalline structure. Finally, the Ir-oxide sample contains IrO_2, and TiO_2 (the last oxide probably a consequence of the employed substrate) and the structure is crystalline.

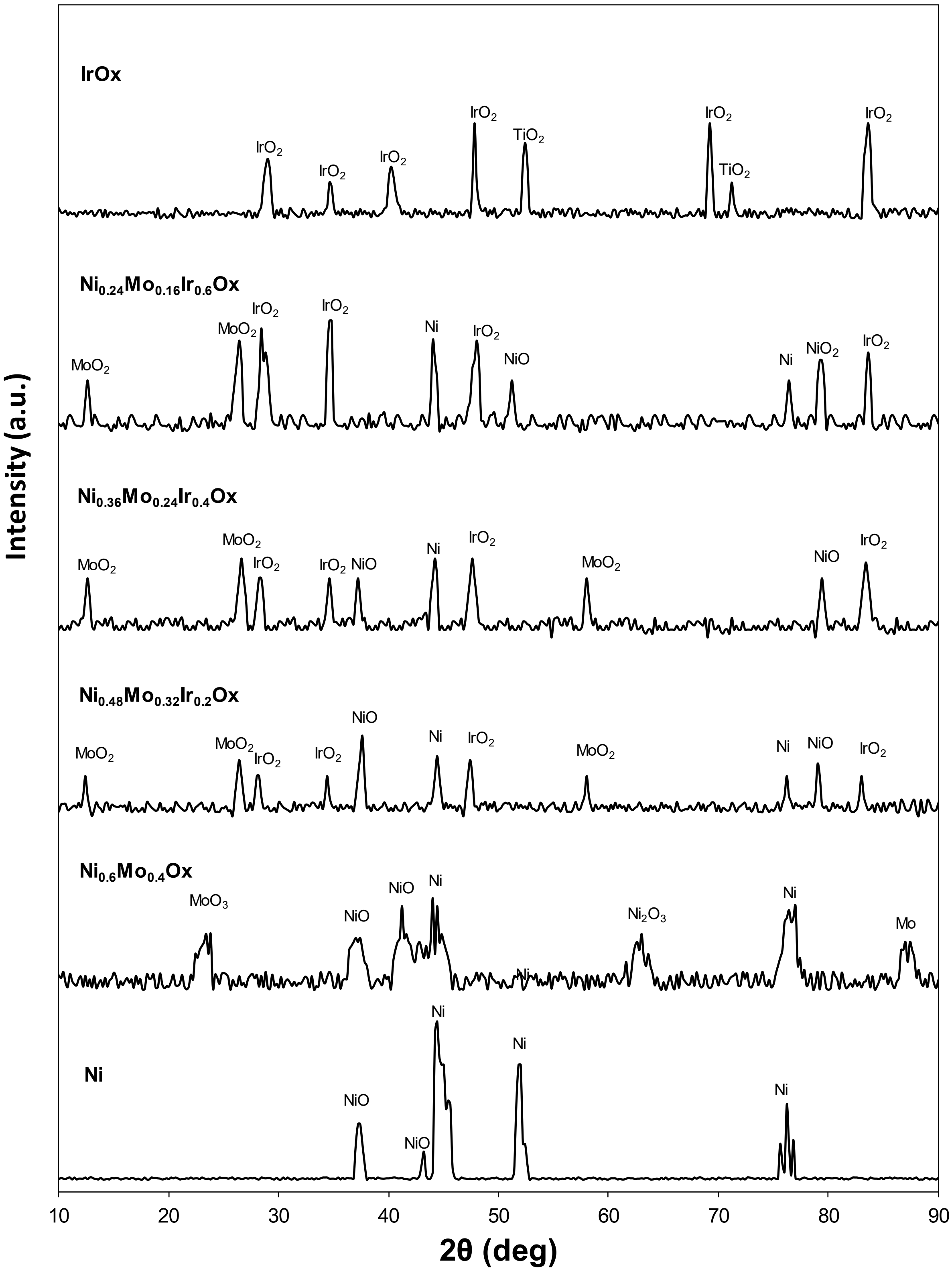

Figure 5.5: XRD spectra of Ni, Ni-Mo-oxide and Ni-Mo-Ir-oxide coatings deposited on a titanium substrate.

5.4.4 Long-term stability of the electrodes

It is expected from good electrocatalysts to yield stable performance over a long-term service. Although the goal of the current work was not to fabricate electrodes that would offer long-term stable electrocatalytic performance, but only to investigate the influence of addition of Ir into the Ni-Mo-oxide structure on the HER kinetics, it was interesting to examine the performance of the electrocatalysts over a four-day period of time of constant electrolysis of water. For this purpose, 40%, 60%, and 100% Ir-containing electrodes were tested by performing hydrogen production at a current density of -500 mA cm^{-2} for a period of 96 hours in 0.5 M H_2SO_4. For comparison, the electrocatalytic performance of pure metallic nickel was also investigated.

During the electrolysis process at this high current density, the potential of the Ni-Mo-Ir-oxide electrodes did not change significantly indicating their stable electrocatalytic performance. Nevertheless, for metallic nickel, the cathodic overpotential increased substantially with time, evidencing deactivation of the cathode. On completion of the electrolysis experiment, Tafel polarization curves were recorded and compared with those recorded on the freshly-prepared electrodes, prior electrolysis, in order to calculate the percentage of remaining activity. These results are presented in Figure 5.6. As it is seen, the electrocatalytic activity of metallic Ni decreased to half of the initial activity, ca. 53%, while the three Ir-containing oxide coatings kept the activity between 85%-90% of the initial value. Since the electrodes were used as cathodes, the loss in activity was most-likely due to their deactivation by deposition of trace metals present in the electrolysis electrolyte, rather than their corrosion/dissolution. These results indicate that the Ni-Mo-Ir-oxide coatings are less susceptible to deactivation, which makes them good candidates for HER in PEM electrolyzers.

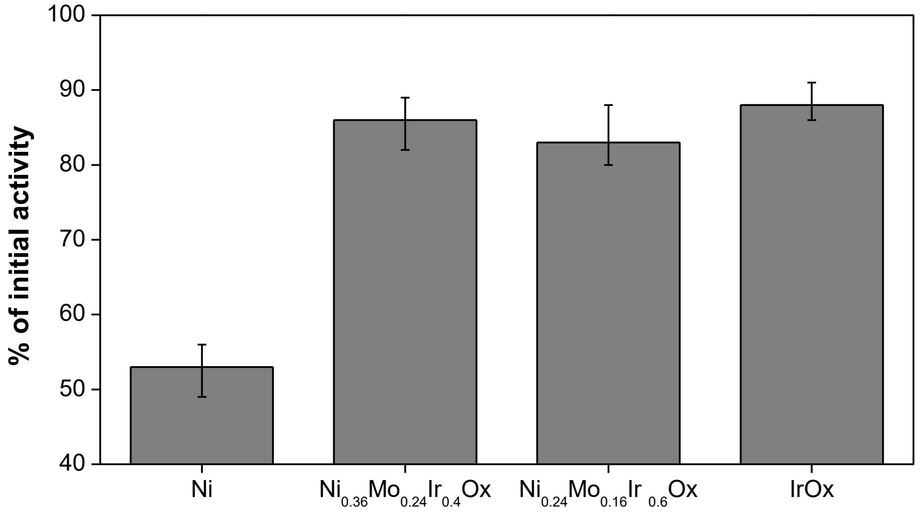

Figure 5.6: Percentage of remaining electrocatalytic activity in the HER of selected electrodes measured at an overpotential of -100 mV in 0.5 M H_2SO_4 after 96 hours of electrolysis at -500 mA cm^{-2}.

Studies on the influence of impurities present in the electrolyte on the behavior of HER cathodes have been carried out at constant current densities [160-162], and it was found that there is a marked loss in electrocatalytic activity with time. Various impurities deposited on the cathode surface could also reduce the electrical conductivity of the electrode. Electrolytes used in industrial hydrogen-production processes usually contain dissolved metal ions, such as Cu, and Fe (around 0.5 - 1 ppm for each), which are gradually electrodeposited on the cathode and in that way affect the electrode performance in the HER [163].

The experiments presented in Figure 5.6 show that there is a loss of activity during a four-day electrolysis period in 0.5 M H_2SO_4 electrolyte prepared using nanopure water, most likely due to the deactivation by impurities present in traces in the electrolyte. To more closely investigate the deactivation resistance of the prepared cathodes, a better-controlled set of deactivation experiments were performed and under much more severe conditions, followed by investigating a possibility of cathode re-activation.

The two most active Ni-Mo-Ir-oxides (corresponding to the samples 40% and 60% of Ir content), and the nickel control sample were deactivated by performing electrolysis at -100 A cm^{-2} for 24 hours in the electrolyte containing 10 ppm Cu or Fe, or 20 ppm Cu + Fe. The degree of electrode deactivation was calculated by comparing the hydrogen evolution current density at overpotentials of -150, -200 and -250 mV before and after the deactivation, and the results are presented in Figure 5.7a.

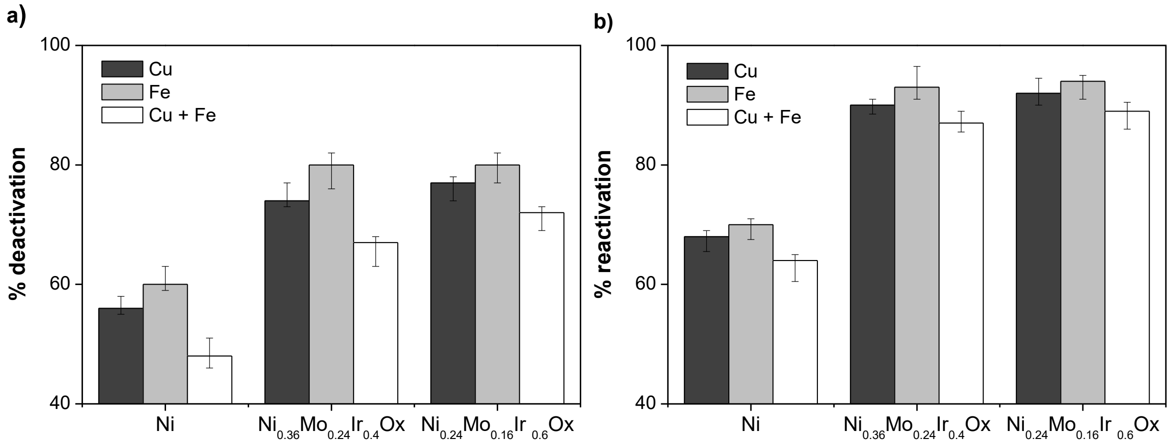

Figure 5.7: a) Percentage of remaining electrocatalytic activity in the HER of selected electrodes after deactivation in 0.5M H_2SO_4 containing 10 ppm of dissolved Cu, Fe or 20 ppm Cu + Fe. b) Percentage of restored initial electrocatalytic activity after applying an in-situ re-activation method.

Nickel displays the poorest performance, similarly to the result in Figure 5.6. In contrast, both metal oxide electrodes maintained a relatively high activity, evidencing their significantly higher resistance towards deactivation. The mechanism of deactivation is by electrodeposition of the metals on the cathode surface, effectively converting the Ni-Mo-Ir-oxide surface into Cu, Fe or Cu + Fe and thus altering the HER kinetics [162]. EDS confirmed the presence of Cu and Fe on the Ni-Mo-Ir-oxide surfaces. For the solution containing Cu, it was found that Cu almost entirely covered the surface of all the electrodes investigated. The thickness of the Cu layer was 10 ± 2 nm. Furuya et al. [66] showed that by increasing Cu concentration in the electrolyte (0.5 M H_2SO_4) up to $3x10^{-6}$ mol L^{-1}, there was a significant decrease in the rate of hydrogen production on the Pt cathode. Cobourn et al. [162] obtained similar results increasing the concentration of Cu up to 10 ppm, and they found a 50 % decrease of the current density in comparison with the pure electrolyte solution (0.5 M H_2SO_4) when Pt/C cathodes were employed.

In the case of electrolyte containing Fe, the amount of Fe on the surface was lower, and Fe did not cover the whole cathode surface; the thickness of this layer was 5 ± 1 nm. This was reflected by a smaller degree of deactivation, in comparisons to that one with Cu (Figure 5.7a). In similar studies, but in alkaline media (employing an electrolyte solution of 30 wt.% KOH at 343 K), Huot and Brossard [160] reported a decremental of the electrocatalytic activity on the nickel cathode when the solution contained 0.5 ppm Fe, based on the increase of the overpotential from -362 mV to -541 mV (an increment of around 50%) between a period of 60 s and 33.7×10^4 s at a constant current density of -250 mV cm^{-2}.

Finally, when the deactivation was done in the electrolyte containing both 10 ppm Cu and 10 ppm Fe, the degree of deactivation was larger than that with Cu (Figure 5.7a), which was to expect due to the higher total (sum) concentration of the two metals (20 ppm). EDS revealed that Cu was preferentially deposited on the surface, with a Cu + Fe ratio of 3/2. The preferential deposition of Cu is to expect since Cu has a more positive standard potential than Fe. The thickness of the bi-metal layer was found to be 13 ± 3 nm.

As it is inevitable for HER cathodes to deactivate with time, it would be desirable to re-activate them *in-situ*, rather than to either replace them or perform re-activation externally, which would require disassembly of the electrolyzer. A convenient way to perform *in-situ* re-activation would be to switch the electrolyzer polarity and dissolve metal (and other) impurities by anodic oxidation, flush out the dissolved impurities and continue with the electrolyzer operation by re-switching back the polarity. A simple simulation of this scenario was done in this research. Namely, after deactivating the cathodes (Figure 5.7a), they were then polarized in 0.5 M H_2SO_4 as anodes at 100 mA cm^{-2} for 30 minutes, followed by testing of their HER activity in a fresh 0.5 M H_2SO_4 electrolyte by LTP. The degree of electrode re-activation was then calculated by comparing the recorded hydrogen evolution current density at overpotentials of -150, -200 and -250 mV to the values obtained with the freshly-prepared electrodes (before deactivation), and the results are presented in Figure 5.7b. The re-activation procedure had the smallest effect on the Ni cathode, while the two Ni-Mo-Ir-oxide cathodes achieved ca. 90% of the original activity. It can be assumed that by optimizing the reactivation conditions (which was not the goal of this study), even a higher degree of re-activation could be achieved. Nonetheless, the experiments presented in Figure 5.7 demonstrate that the Ni-Mo-Ir-oxide cathodes are significantly more resistant to deactivation than the Ni electrode and that it is possible to *in-situ* reactivate them, at least to a certain degree.

In order to investigate if the reactivation results in dissolution of Ni, Mo or Ir, ICP analysis of the spent reactivation H_2SO_4 electrolyte (after reactivation) was done; however, for these experiments in order to increase the concentration of dissolved elements, reactivation was done over a period of four hours, rather than over a period of 30 minutes as in the case of reactivation results presented in Figure 5.7b. ICP analysis confirmed a significant increase in Cu, Fe, and Cu + Fe in the reactivation electrolyte as a result of dissolution of these metal impurities. No Ir was detected, while a negligible increase in Ni was detected (the Cu and Fe salts already contained trace amounts of Ni, and a relative increase in dissolved Ni by 4×10^{-8} wt.% was detected as the consequence of reactivation). Mo was also detected at a very low concentration (5.61×10^{-6} wt. %). This indicates that some negligible dissolution of Ni and Mo occurs during the reactivation procedure, which could potentially limit the applicability of the procedure over a longer period of time (higher number of reactivation cycles). Nevertheless, the extrapolation of the reactivation single-period time (one four-hour cycle) to the same time length done over multiple reactivation cycles might not be straightforward as the initial dissolution of metals from the deactivated electrode occurs primarily through the dissolution of Cu and Fe, rather than that of Ni and/or Mo. Thus, further studies are needed for more conclusive data and to optimize the reactivation procedure (temperature, current density, time) in order to maximize the dissolution of Cu and Fe, and minimize degradation of the electrode through the dissolution of base Ni and Mo components.

5.5 Conclusion

The results demonstrate that the Ni-Mo-Ir-oxide cathodes prepared by thermal decomposition exhibit good performance for the HER in the acidic medium. The cathodes were found to be crystalline and exhibit a cracked-mud surface morphology of increasing surface roughness with Ir content increase. The electrochemical activity of the Ni-Mo-Ir-oxides was found to be dependent on the amount of Ir, which contributed to the increase in intrinsic activity due to both the increase in number of Ir surface sites and possible modification of the electronic structure of the material. Long-term electrolysis experiments confirmed significantly higher fouling resistance of the oxide electrodes in comparison to the pure metal Ni electrode. It was also demonstrated that it is possible to *in-situ* re-activate all the electrodes; however, the degree of re-activation of Ni-Mo-Ir-oxide electrodes was found to be much higher. The results presented here, thus, show that Ni-Mo-Ir-oxide could represent good candidates for cathodes for water electrolysis in the acidic medium, potentially in PEM electrolyzers. However, for the later, further investigation is needed in the direction of fabricating nanoparticulate Ni-Mo-Ir-oxide electrodes and investigating their performance in a real PEM cell.

Acknowledgement

Financial support from McGill University through the McGill Engineering Doctoral Award (MEDA) program, the Eugenie Ulmer Lamothe Endowment, the National Research Council of Canada (NRC), and the National Council of Science and Technology of Mexico (CONACYT) is gratefully acknowledged.

Chapter 6

6 $Ni_{0.6-x}Mo_{0.4-x}Ir_x$-oxide as an Electrode Material for Supercapacitors: Investigation of the Influence of Iridium content on the Charge Storage/Delivery

6.1 Preface

This chapter presents an article that was submitted to the Journal of the Electrochemical Society. The citation of the article is the following:

> A. Gomez Vidales, S. Omanovic. *$Ni_{0.6-x}$ $Mo_{0.4-x}Ir_x$-oxide as an Electrode Material for Supercapacitors: Investigation of the Influence of Ir content on the Charge Storage/Delivery*. Submitted to the Journal of the Electrochemical Society (2019).

The contributions of each author were the following: Abraham Gomez Vidales (the Ph.D. candidate) designed experiments, prepared samples, performed the experimental work, analyzed results and wrote the manuscript. Prof. Sasha Omanovic provided guidance, helped in interpretation and discussion of results and reviewed the manuscript. In the results and discussion section, each data point and the corresponding deviation presented in figures represent an average of 9-15 measurements: between 3 to 5 separate samples, each tested 3 times.

When evaluating the electrochemical properties of the Ni-Mo-Ir-oxide coatings developed in Chapter 5, it was discovered that these electrodes have an excellent capacitance, which allows them to be used as potential supercapacitor materials. Considering the previous information, the following chapter presents a research study of the electrochemical properties of the Ni-Mo-Ir-oxides coatings as potential electrodes for energy storage applications (supercapacitors). Focusing mainly on the influence of the iridium content on the charge storage capacity. The experimental work concentrated in the surface characterization (morphology, composition, and structure), the charge storage/delivery capacity, and the long-term stability of the coatings. Appendix III display preliminary results in acidic medium which were not published on the submitted version of the paper.

This article is dedicated to my friends Pablo Diaz Gomez Maqueo and Mayra Rosario Martinez Gonzalez. Thank you!

$Ni_{0.6-x}Mo_{0.4-x}Ir_x$-oxide as an Electrode Material for Supercapacitors: Investigation of the Influence of Ir content on the Charge Storage/Delivery

Abraham Gomez Vidales*, Sasha Omanovic

Department of Chemical Engineering, McGill University, 3610 University St., Montreal, Quebec, H3A 0C5, Canada

Keywords: Supercapacitors; Molybdenum; Nickel; Iridium; Metal oxides.

* Corresponding author: abraham.gomezvidales@mail.mcgill.ca

Abstract

$Ni_{0.6-x}Mo_{0.4-x}Ir_x$-oxide coatings were fabricated with the purpose of investigating the influence of Ir content on their charge storage/delivery capability when used as an electrode for electrochemical supercapacitor. Experimental work in alkaline medium confirmed that the amount of Ir in the Ni-Mo-oxide significantly influences the material's charge storage capacity. The highest overall capacitance (108 ± 2 mF cm^{-2} at 1 mA cm^{-2}) was obtained for the composition containing 40 mol.% of Ir ($Ni_{0.36}Mo_{0.24}Ir_{0.4}$-oxide), while the best candidates in terms of the intrinsic (surface-area-independent) charge storage/delivery are the compositions containing 20 and 40 mol.% of Ir (no statistical difference). $Ni_{0.36}Mo_{0.24}Ir_{0.4}$-oxide was found to retain ca. 86% of its initial capacitance after 2500 charging/discharging cycles, at 1 mA cm^{-2}.

6.2 Introduction

Efficient, affordable, sustainable, and clean sources of energy production and storage are required to address the current energy crisis and global warming [164]. Electrochemical supercapacitors (ES) are promising energy storage devices that have garnered much interest due to their high power density, fast charge-discharge rate, and long-life cycling capability [103, 165]. In addition, they can complement or even replace batteries in some instances, especially when high power delivery is needed [166]. ES have attracted much attention due to their application in portable electric devices and electric vehicles. In recent years, extensive work has focused on ways to increase their specific energy density and lower their production costs.

ES are classified into two types based on their charge storage mechanisms: electrical double-layer capacitors (EDLCs) based on the double-layer capacitance where electrostatic forces store energy at the electrode/electrolyte interface, and pseudocapacitors also known as a faradaic supercapacitors, which are based on the pseudocapacitance arising from fast reversible faradaic reactions occurring at the (sub)electrode surface [167]. In general, both energy storage mechanisms, electrostatic and faradaic, coexist in a supercapacitor, although it is always one of the two that determines their overall behavior.

For ES, the capacitance relies heavily upon the electrode materials that are used. Three types of electrode materials are usually employed in ES: carbon materials, conducting polymers, and metal oxides [168, 169]. Carbon-based materials, used mainly in EDLCs, exhibit a low charge storage capacity, which in turn limits their practical applications in certain cases. On the other hand, conducting polymers and metal oxides, commonly used as electrode materials for pseudocapacitors, yield a significantly higher specific capacitance when compared to EDLCs [170-172]. Specifically, transition metal oxides (TMOs) have been recognized as the most promising electrode materials to use in ES [173, 174] due to their relatively good conductivity, large specific capacitance, and much longer life cycles in comparison to conducting polymers [85, 173, 175-177]. TMOs such as ruthenium, iridium, manganese, nickel, and molybdenum oxides can provide high energy density and a superior capacitance due to the several oxidation states which facilitate redox reactions [102, 103, 178].

Iridium oxide was found to be a promising material as an electrochemical supercapacitor electrode due to its high specific capacitance, high conductivity, and excellent electrochemical reversibility [103, 166, 179]. Even with its unique properties as an electrode for ES applications, its high cost has restricted its extensive utilization. Therefore, alternative electrode materials, such as nickel and molybdenum oxides, which are inexpensive and exhibit excellent pseudocapacitive behavior, have been explored [169]. Specifically, nickel oxide has been employed recently in rechargeable batteries and electrochemical supercapacitors, owing to its low cost and availability [167, 180, 181]. Furthermore, it is known that the combination of nickel oxides with other oxides not only reduces the cost but also improves the electrode stability [148, 149, 182] and could enhance the power capability due to its amorphous nature and porous structure, which significantly improves the charge transfer and capacitance of an electrode [180, 183].

Taking into account, on one side, that Ir-oxide offers high specific capacitance but is a rather expensive material, and, on the other side, that Ni-based oxide materials also offer relatively high specific capacitance values, but are significantly cheaper, in this research study, we report results on the investigation of combining Ir- and a Ni-Mo-based oxide to produce a high-capacitance and cost-effective electrode material for supercapacitors. More specifically, the influence of Ir-oxide content on the charge storage/delivery capability of $Ni_{0.6-x}$ $Mo_{0.4-x}Ir_x$-oxide electrodes was investigated. It should be noted that the aim of this study was only to screen (compare) potential electrode combinations for their charge storage/delivery, rather than designing a nanostructured combination of the same and their three-dimensional structure optimization for testing in a two-electrode (electrochemical supercapacitor) cell, which is the next step of our project.

6.3 Experimental Procedure

6.3.1 Material synthesis

Ni-Mo-Ir-oxide coatings were prepared by dissolving $NiCl_2 \times 6H_2O$ (purity 99.9%, Sigma-Aldrich, Canada), $Na_2MoO_4 \times 2H_2O$ (purity 99.5 wt.%, Sigma-Aldrich, Canada) and $IrCl_3 \times 3H_2O$ (purity 99.9 wt.%, Sigma Aldrich, Canada) in an equivolume mixture of HCl (37 wt.%, Fisher Scientific, Canada) and nanopure water (resistivity 18.2 MΩ cm). Ni and Mo were always mixed in a 60:40 molar ratio, while the percentage of Ir was varied from 0 to 100 mol.% (relative to the Ni/Mo amount). Titanium buttons (1.27 cm diameter, 0.2 cm thickness, purity 99.2%, Alfa Aesar, USA) were used as a substrate. First, the Ti buttons were polished with 600 grit polishing paper (Anamet, Canada). The Ti substrates were then sonicated in deionized water for 10 min to remove any residue. Next, they were etched in a mixture HCl and nanopore water (1:1 by volume) for 30 minutes and dried with argon gas (MEGS Specialty Gases Inc., 99.998 wt.% pure, Canada). The coating solution was applied uniformly on one side of the prepared substrate using a standard paintbrush. The substrates were placed in the oven at 373 K for five minutes to vaporize the solvent and then annealed for fifteen minutes at 773 K in a furnace. The samples were then cooled to ambient temperature for ten minutes. The procedure was repeated until six coatings had been applied. For the last coating, the plate was annealed in the furnace for one hour (at 773 K) to oxidize the metal coating. Finally, the resulting electrode was sonicated for ten minutes in a nanopure water bath and dried with argon.

6.3.2 Material characterization

Scanning electron microscope (SEM) was used to investigate the surface morphology and structure of the samples. Energy dispersive spectroscopy (EDS) was conducted to quantify the content of the elements in the coating. Both measurements were performed on a Hitachi SU-3500 Variable Pressure SEM (Hitachi, Japan) microscope with EDS detector. X-ray photoelectron spectroscopy (XPS) was used to examine the surface chemical composition of the coatings employing the Thermo Scientific K-Alpha X-ray Photoelectron Spectrometer (ThermoFisher Scientific, USA). A goniometer model OCA 15EC equipped with a CCD camera (Data Physics, USA) was used to measure the contact angle. Finally, the surface roughness and coating thickness were measured using a DektakXT stylus (Bruker, USA) surface profilometer.

6.3.3 Electrochemical characterization

The electrochemical behavior of electrodes was characterized using cyclic voltammetry (CV) and galvanostatic charge/discharge (GCD) cycling to evaluate their performance and potential suitability as supercapacitor electrodes. A two-electrode cell was employed. The cell configuration included two Ni-Mo-Ir-oxide working electrodes (WEs) with the coated side facing each other, separated by a filter paper (P5 Grade, Fisher Scientific, USA) immersed in aqueous 6 M KOH electrolyte. The geometric area of the electrode exposed to the electrolyte solution was 1.27 cm^2. All electrochemical measurements were performed using a potentiostat/galvanostat analyzer (Autolab PGSTAT30, Metrohm, the Netherlands) controlled by the NOVA software (v. 2.1.3; Metrohm, the Netherlands).

6.4 Results and discussion

6.4.1 Physical characterization of the Ni-Mo-Ir-oxides

Figure 6.1 depicts the morphology of the Ni-Mo-Ir-oxide coatings. The prepared coatings have a uniform morphological distribution with an average thickness of 5 ± 2 μm. It is noted that the addition of Ir to the Ni-Mo-oxide change the surface morphology of the coatings. The coating without Ir (Figure 6.1a) has a porous structure. Meanwhile, the coatings that contain Ir (Figure 6.1b-f) have a cracked-mud/cauliflower-like morphology. This cracked-mud structure which prevails in Figure 6.1b), e), and f) provide easy mobility for ions to access the electrode/electrolyte interface, which is a crucial factor for the surface redox reactions. The cauliflower-like structure which is more distinctive in Figure 6.1c) and d) contributes a more active surface area, which prevents particulate (ion) aggregation. According to literature, these surface morphologies are commonly observed in the Ir-oxide, and Ni-oxide surfaces produced by thermal decomposition [137, 158].

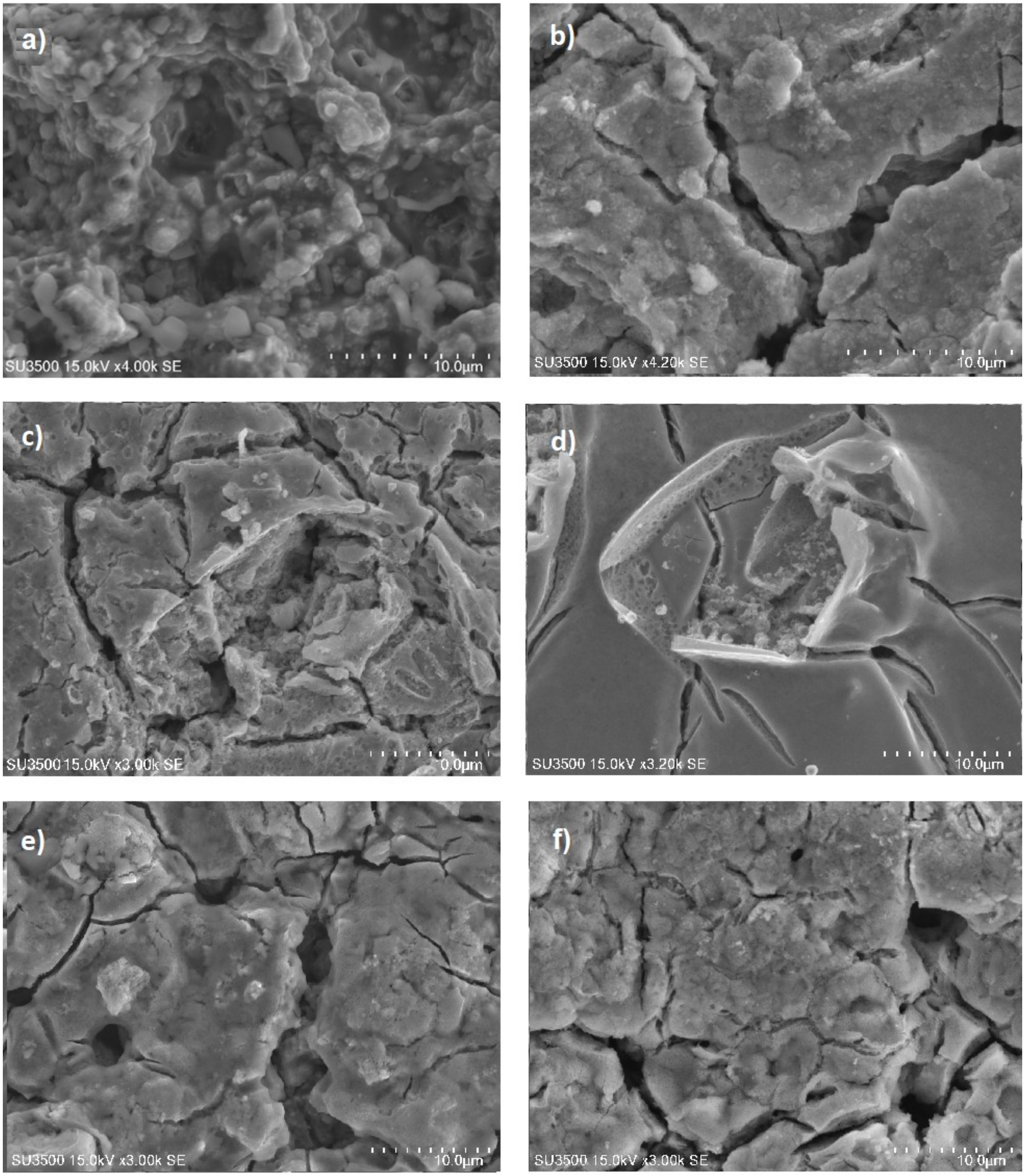

Figure 6.1: SEM images of a) $Ni_{0.6}Mo_{0.4}$-oxide, b) $Ni_{0.48}Mo_{0.32}Ir_{0.2}$-oxide, c) $Ni_{0.36}Mo_{0.24}Ir_{0.4}$-oxide, d) $Ni_{0.24}Mo_{0.16}Ir_{0.6}$-oxide, e) $Ni_{0.12}Mo_{0.08}Ir_{0.8}$-oxide, and f) Ir-oxide coatings. The overall scale length on the images is 10 µm.

The surface roughness *Ra* (µm) was determined using a stylus profilometer, and the values are presented in Table 6.1. In general, producing an oxide electrode results in an increase in surface roughness. Moreover, the addition of Ir into the base metal oxide coating ($Ni_{0.6}Mo_{0.4}$-oxide) resulted in a further increase in surface roughness. This effect may indicate that the addition of Ir increases the active surface area of the electrode, which has a positive impact on the capacitance.

Table 6.1: Measured roughness of the surface electrodes Ni-Mo-oxide, and Ni-Mo-Ir-oxide coatings.

Sample	Roughness Ra (um^{-2})
$Ni_{0.6}Mo_{0.4}Ox$	0.46 ± 0.02
$Ni_{0.48}Mo_{0.32}Ir_{0.2}Ox$	0.64 ± 0.07
$Ni_{0.36}Mo_{0.24}Ir_{0.4}Ox$	1.25 ± 0.11
$Ni_{0.24}Mo_{0.16}Ir_{0.6}Ox$	1.29 ± 0.13
$Ni_{0.12}Mo_{0.08}Ir_{0.8}Ox$	1.42 ± 0.09
IrOx	1.63 ± 0.10

Electron dispersive spectroscopy (EDS) was used to estimate the elemental composition of the Ni-Mo-Ir-oxide coatings. In all the coatings, peaks characteristic of Ni, Mo, and Ir were obtained. This proves the presence of these metals on the electrode surface. Table 6.2 shows the normalized results obtained from this study. The nominal values are very similar to the resulted EDS-determined values. This confirms that the desired composition of coatings is achieved excellently through the thermal-salt decomposition method. Moreover, since the measurements were done in different sections of the coating, this also demonstrates that the elements were homogenously distributed.

Table 6.2: Relative atomic percentage of Ni, Mo, and Ir in oxide coatings (excluding the contribution of oxygen and other impurities in the coatings) obtained by EDS.

Nominal	**Results**
$\mathbf{Ni_{0.6}Mo_{0.4}Ox}$	$Ni_{0.63}Mo_{0.37}Ox$
$\mathbf{Ni_{0.48}Mo_{0.32}Ir_{0.2}Ox}$	$Ni_{0.50}Mo_{0.26}Ir_{0.24}Ox$
$\mathbf{Ni_{0.36}Mo_{0.24}Ir_{0.4}Ox}$	$Ni_{0.45}Mo_{0.20}Ir_{0.35}Ox$
$\mathbf{Ni_{0.24}Mo_{0.16}Ir_{0.6}Ox}$	$Ni_{0.38}Mo_{0.13}Ir_{0.51}Ox$
$\mathbf{Ni_{0.12}Mo_{0.08}Ir_{0.8}Ox}$	$Ni_{0.18}Mo_{0.10}Ir_{0.72}Ox$
IrOx	IrOx

To confirm the top-surface composition of the oxide coatings produced, X-ray photoelectron spectroscopy (XPS) measurements were carried out on selected compositions. The surface of each sample was examined at three different locations to ensure the reliability of results. The binding energy scale was referenced to the C 1s signal at 284.5 eV. XPS wide-scan (survey) spectra of the selected coatings are shown in Figure 6.2. Typical survey spectra for ternary oxide revealed that all electrode-composition elements are present at the surface with the Ni, Mo, and Ir photoelectron peaks found at 870–850, 235–225, and 70–55 eV respectively. Additional peaks corresponding to oxygen (lattice oxygen and hydroxides), Na and Cl, (precursor salts), Ti (substrate) and C (contamination) were also present. Table 6.3 shows the relative atomic percentage of the elements present in the coatings, which agree with the previous results obtained by EDS.

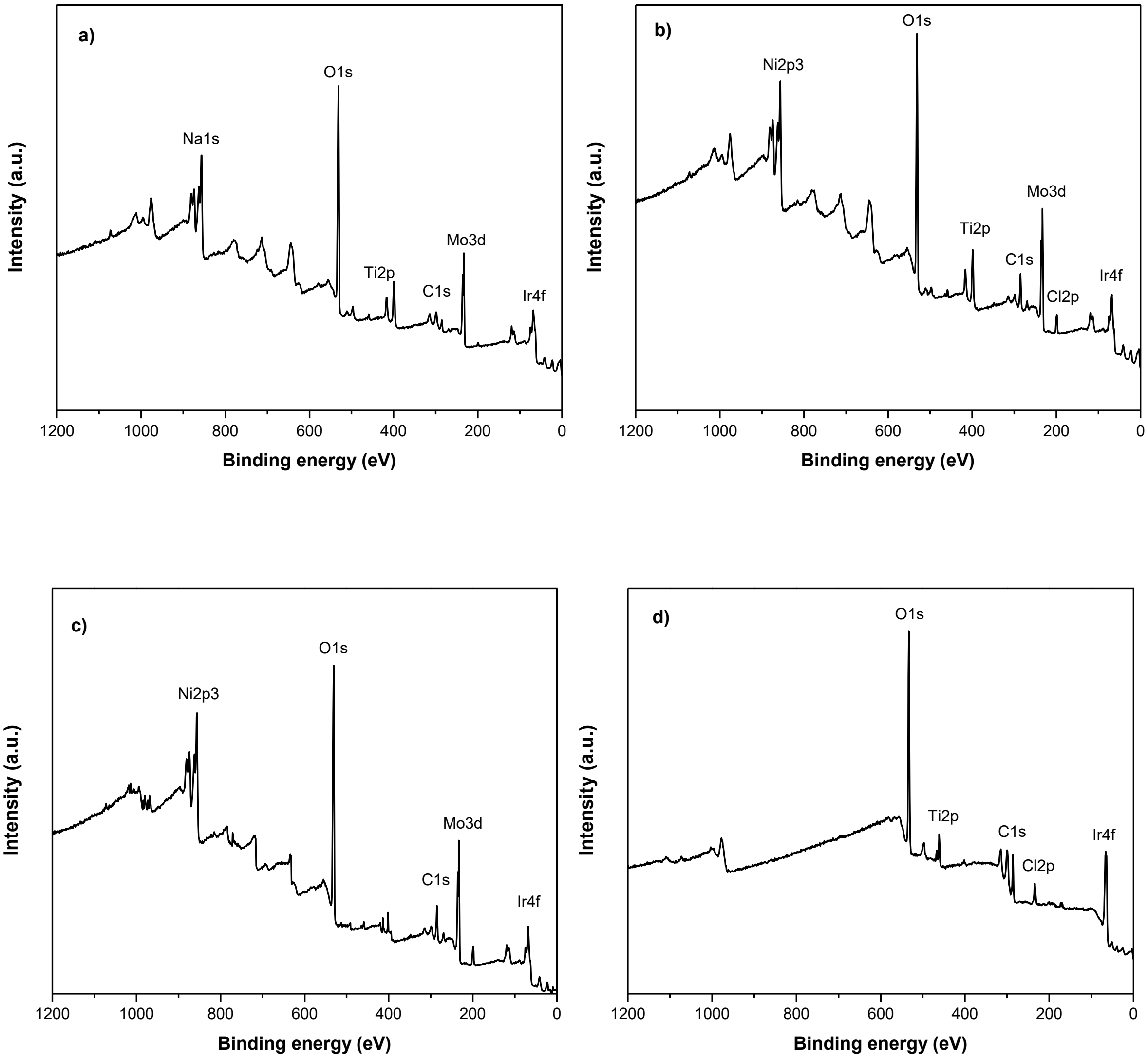

Figure 6.2: XPS analysis of selected samples a) $Ni_{0.6}Mo_{0.4}$-oxide, b) $Ni_{0.48}Mo_{0.32}Ir_{0.2}$-oxide, c) $Ni_{0.36}Mo_{0.24}Ir_{0.4}$-oxide, and d) Ir-oxide.

Table 6.3: Relative atomic percentage of Ni, Mo, and Ir in oxide coatings (excluding the contribution of oxygen and other impurities in the coatings) obtained by XPS in selected electrodes.

Nominal	Results
$Ni_{0.6}Mo_{0.4}Ox$	$Ni_{0.58}Mo_{0.42}Ox$
$Ni_{0.48}Mo_{0.32}Ir_{0.2}Ox$	$Ni_{0.47}Mo_{0.25}Ir_{0.28}Ox$
$Ni_{0.36}Mo_{0.24}Ir_{0.4}Ox$	$Ni_{0.34}Mo_{0.20}Ir_{0.46}Ox$
IrOx	IrOx

After the general scan was made, high-resolution binding energy spectra for Ni 2p, Mo 3d, Ir 4f, and O 1s regions were performed on the $Ni_{0.36}Mo_{0.24}Ir_{0.4}$-oxide coating (the sample that yielded the highest capacitance, as shown later in the text). Figure 6.3a) shows the Ni 2p spectrum; the Ni $2p_{3/2}$ photoelectron peak is visible at 854 eV and a satellite peak at 862 eV. Besides, Ni $2p_{1/2}$ photoelectron peak at 871 and a satellite peak at 880 eV is also visible on the spectrum. The spectrum confirms the presence of nickel oxides, NiO and Ni_2O_3, on the coating surface. Figure 6.3b) presents the Mo spectrum with peaks for 3 $d_{5/2}$ and 3 $d_{3/2}$, which suggests the presence of MoO_2 and MoO_3. Both oxides have characteristic peaks at 228 eV and 232 eV, respectively. Additionally, the spectrum evidences that MoO_2 is the predominant form of Mo-oxide on the outer part of the coating surface. Figure 6.3c) displays the spectrum for the Ir 4f region. The peaks located at binding energy values of 62 eV and 64 eV correspond to Ir $4f_{7/2}$ and Ir $4f_{5/2}$ levels of Ir^{4+}. These peaks confirm the presence of iridium in the IrO_2 form [184]. Finally, in Figure 6.3d) the O 1s spectrum is shown. The high-resolution binding energy spectrum can be deconvoluted into two types of components. The deconvoluted peak at 528 eV represents oxygen in a crystal lattice (O^{2-}), while the peak at 531 eV represents oxygen in the hydroxyl group (OH^-) [185]. Hence, the coating compounds are metal oxides and metal hydroxides existing in an approximate ratio of 1.5:1. As a result, it can be assumed that the capacitance not only depends on the oxides but is also increased by the presence of metal hydroxides [186].

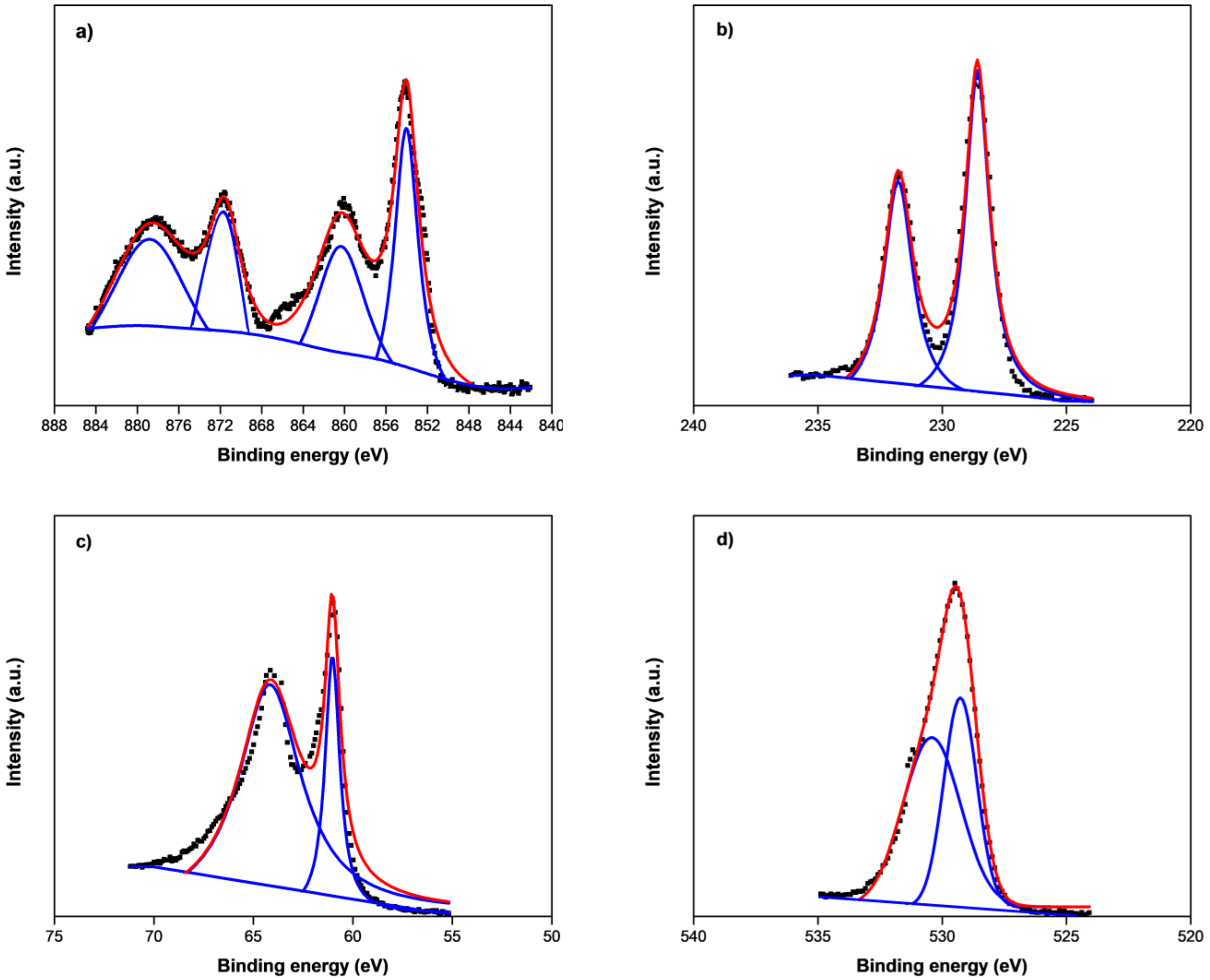

Figure 6.3: a) Ni 2p XPS spectrum, b) Mo 3d XPS spectrum, c) Ir 4f XPS spectrum, and e) O1s XPS spectrum of the Ni-Mo-Ir oxide sample. The black points represent experiment data, the red line represents the corresponding simulated spectrum, and the blue lines represent deconvoluted contributions of the major peaks.

6.4.2 Electrochemical performance of the Ni-Mo-Ir-oxides as supercapacitors

Cyclic voltammetry (CV) was employed to evaluate the capacitive behavior of the Ni-Mo-Ir-oxides as supercapacitors in alkaline medium in a two-electrode cell (similar preliminary studies were done in acidic medium in a three-electrode cell; see Appendix III). As an example, CVs of the $Ni_{0.36}$ $Mo_{0.24}Ir_{0.4}$-oxide electrode recorded at several scan rates are displayed in Figure 6.4. The voltammograms exhibit a semi-rectangular shape characteristic of electrochemical-double-layer capacitors. Redox peaks associated with the mixed oxides produced on the coatings are not clearly visible in the CV. Instead, the CVs are composed of several overlapping redox peaks.

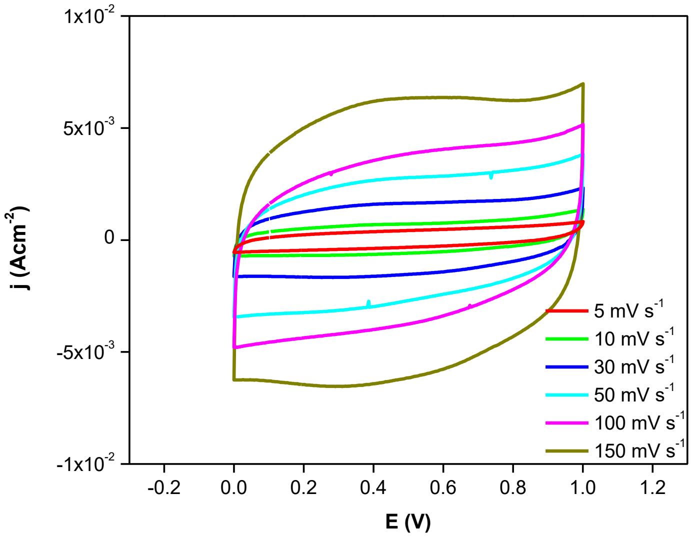

Figure 6.4: Cyclic voltammograms of the $Ni_{0.36}Mo_{0.24}Ir_{0.4}$-oxide electrode recorded in 6 M KOH.

The similarity in the shape of the CVs for all scan rates suggests a high efficiency in the capacitive characteristics at the electrode/electrolyte interphase [167]. However, at a high scan rates the CV curve was distorted since there is not sufficient time for the electrolyte cations to diffuse into/from the bulk of the solution when the scan direction is changed, and only the outer active surface is utilized for charge storage, whereas at low scan rates, the entire active surface area can be used for charge storage, which leads to a higher specific capacitance [172, 177, 181]. Similar behavior is reported in the literature for various electrode materials [103, 170]. In the case of an IrO_2 supercapacitor, this effect is attributed to the increment of the ionic resistance inside the pores and the weak electric contact between the electrolyte/electrode [187, 188].

To calculate the capacitance of the metal oxide electrodes produced, from CV measurements, the following equation can be used [166]:

$$C = \frac{\int IdV}{2A\Delta ES} \tag{6.1}$$

where C is the capacitance (mF cm^{-2}), $\int IdV$ the integrated anodic or cathodic area enclosed in the CV curve (mA s), A is the geometric area of the electrode exposed to the electrolyte (cm^{-2}), ΔE is the scanned potential range (V), and S the scan rate (V s^{-1}). Figure 6.5 shows the corresponding variation of capacitance of the Ni-Mo-Ir-oxide electrodes investigated in this work as a function of scan rate. The observed capacitance values of the Ni-Mo-Ir-oxide electrodes are higher than the values reported for some inexpensive oxides such as NiO and MoO [175, 177, 180], but also than those for pure Ir-oxide.

As it is noted, the capacitance decreases with scan rate, which is commonly observed in the literature [85, 86, 94, 103, 151]. This is to expect since at higher scan rates the redox zone in the solid phase is 'shallower,' i.e., there is not sufficient time for the electrolyte cations to diffuse (intercalated) deeper under the oxide surface and compensate the metal redox charge change.

The lowest capacitances values were obtained with the $Ni_{0.6}$-$Mo_{0.4}$-oxide coating (no Ir content), while the next higher capacitance was obtained for pure Ir-oxide. All Ni-Mo-Ir-containing oxide compositions yielded higher capacitance values. When the Ir is added (20 wt.%) to the Ni-Mo-oxide coating, the capacitances increase around three times with respect to $Ni_{0.6}$-$Mo_{0.4}$-oxide. The highest capacitance was obtained when the Ir content reached 40 wt.%. After this concentration is achieved, the capacitance decreased gradually. This provides evidence that the behavior of the oxide coatings is significantly dependent on the coating composition and is not a linear function of Ir content.

Previous studies on Ir and Ir-oxide attributed the increase of the capacitance to the growth of the electrochemically active surface area [175]. As it can be seen in Table 6.1, with the increase of the Ir content, the surface roughness of the coatings increases linearly ($R^2 = 0.911$), which is a preliminary indication of the increment of the active surface area. Nevertheless, this linear trend could (potentially) explain the increase in capacitance from 0 to 40% of Ir in the coating, but not the decrease in capacitance after this composition; even the pure Ir-oxide sample (the roughest one) has lower capacitance values compared to all of the Ni-Mo-Ir-oxide coating. This proves that the addition of Ir to the Ni-Mo-oxides coatings improved the pseudocapacitive properties compared to pure Ir-oxide and the existence of a maximum (at 40% of Ir in the coating) also indicates that probably the combination of these three metal oxides produced a maximum synergetic effect at this composition. Therefore, the improved rate of the capacitance of the Ni-Mo-Ir oxides coatings could be due to the activation of non-stochiometric sites of the precursor's species in the oxide films, the increment of the electrical conductivity of the electrodes and ion diffusion rate, and not only to the enhancement of the electrochemical-active surface area (surface roughness) [103, 170, 189].

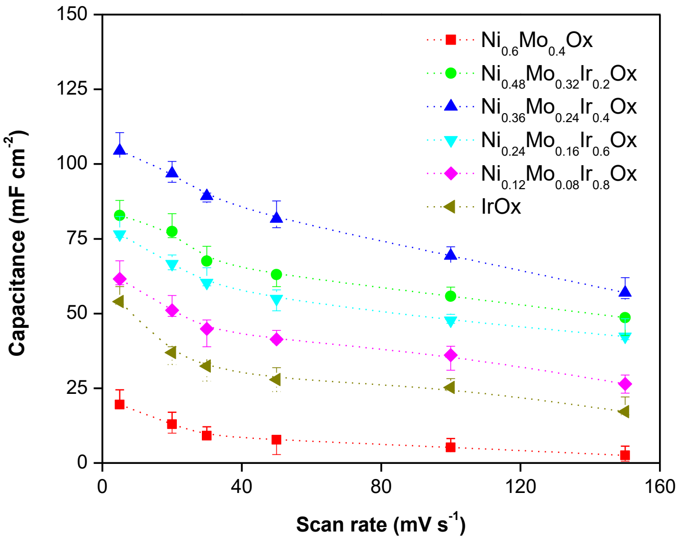

Figure 6.5: Variation of capacitance with scan rate calculated from CVs recorded on different Ni-Mo-Ir-oxide electrodes in 6 M KOH.

To further investigate the performance and cycle life of the Ni-Mo-Ir-oxide coatings, galvanostatic charge-discharge (GCD) experiments were performed [179]. Initial GCD measurements were conducted at different current densities (1, 3, 5, and 10 mA cm^{-2}) for 250 cycles in a 6 M KOH solution in a two-electrode cell. As a representative example, Figure 6.6 shows the GCD curves for the 250th cycle of the $Ni_{0.36}$ $Mo_{0.24}Ir_{0.4}$-oxide electrode at different charging/discharging current densities. All the electrodes have the triangular charge-discharge behavior traditionally observed in electrochemical supercapacitors. The slight deviation from linearity suggests a pseudocapacitive behavior which is the result of the electrochemical redox reactions occurring at the electrode-electrolyte interface and within the electrode sub-surface and is in accordance with CV measurements presented previously in the text [180]. As expected, with an increase in charging/discharging current, the GCD curves move to shorter times.

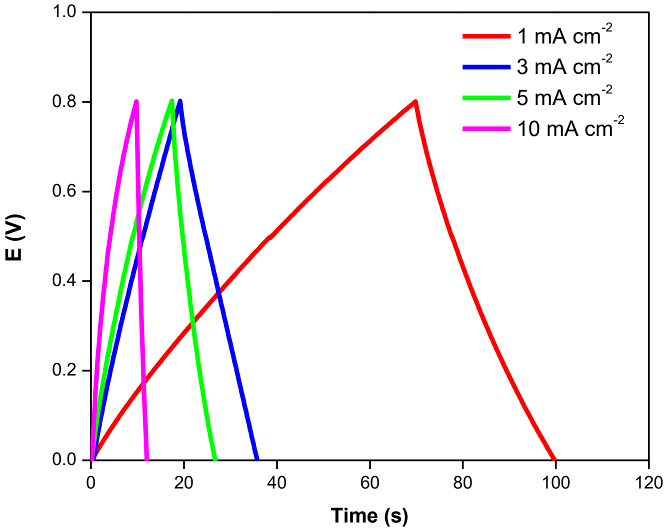

Figure 6.6: The 250th full charge-discharge cycle of $Ni_{0.36}$ $Mo_{0.24}Ir_{0.4}$-oxide coating recorded in 0.5 M H_2SO_4 at various current densities.

GCD curves were used to calculate the capacitance of the electrodes employing the following equation:

$$C = \frac{I\Delta t}{\Delta E A} \tag{6.2}$$

where C is the capacitance (mF cm^{-2}) I is the current applied for the charge/discharge (mA), Δt is the time elapsed for the charge/discharge cycle (s), A is the geometric area of the electrode exposed to the electrolyte (cm^{-2}), and ΔE (V) is the corresponding potential interval of the charge/discharge cycle (V) [190].

Figure 6.7 shows the capacitance of the Ni-Mo-Ir-oxide electrodes as a function of current density. The capacitance was determined by averaging the values recorded in the last 50 cycles after the capacitance was stabilized. As it was expected, the capacitance values follow the same trend as the ones obtained from CV and could be explained in the same manner. Again, the maximum capacitance was reached when the content of Ir was 40%. Research by Ullah et al. [101] examined the capacitance of several compositions of Ir_xRu_{1-x}-oxide coatings, and they also found a considerable increase (6-fold in their case) in capacitance when the Ir content reached 40% in this particular metal oxide. However, they obtained a lower capacitance, ca. 85 mF cm^{-2}, with $Ir_{0.4}$-$Ru_{0.6}$-oxide at a significantly lower current density, 0.1 mA cm^{-2}. This demonstrates that the $Ni_{0.36}Mo_{0.24}Ir_{0.4}$-oxide is an excellent candidate for supercapacitors.

In all the cases, a gradual decrease in capacitance occurs when the current density was increased. This behavior is reported in the literature on several metal-oxide-based supercapacitors electrodes [101, 191], and it is related to ion mass transport limitations, i.e., at high current densities the change in potential is so fast that the charging potential limit is reached before ions are capable of compensating the charge within narrow pores of the material and only the outer surface is thus utilized for the charge storage [190, 192].

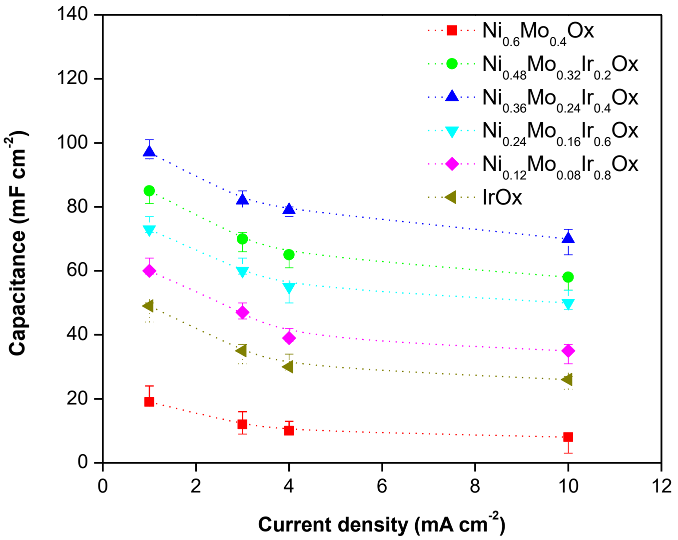

Figure 6.7: Capacitances as a function of charging/discharging current density of different Ni-Mo-Ir-oxide electrodes obtained from GCD curves recorded in 6 M KOH.

In general, the capacitive performance of the electrodes studied here was mainly related to both the inherent reactivity of the electroactive material and its accessible surface area [85].

Finally, the performance of the $Ni0._{38}Mo_{0.24}Ir_{0.4}$-oxide coating was investigated throughout 2500 charging/discharging cycles, Figure 6.8. Overall, the result evidences a decrease in capacitance, with total capacitance retention of 86% after 2500 cycles. As it can be seen, during the initial 500 cycles, the capacitance value decreased more sharply from 108 ± 2 to 95 ± 2 mF cm^{-2} and then gradually reached a value of 93 ± 2 mF cm^{-2}. Possible causes for the capacitance decline of the electrodes in the first 500 cycles can be related to the partial dissolution of the $Ni0._{38}Mo_{0.24}Ir_{0.4}$-oxide coating into the electrolyte, to a decrement of the surface area exposed to the electrolyte, or structural changes within the top-most part of the coating [190]. However, the percentage of retention obtained for this specific electrode is much higher than some reported in several studies on mixed-metal-oxide based electrodes [180, 191].

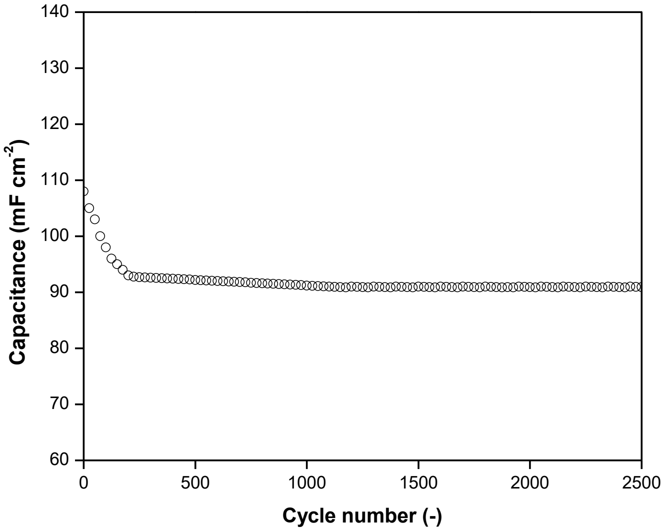

Figure 6.8: Dependence of capacitance of the $Ni_{0.38}Mo_{0.24}Ir_{0.4}$-oxide electrode on the number of charging-discharging cycles recorded in 6 M KOH at 1 mA cm^{-2}.

6.5 Conclusions

Ni-Mo-Ir-oxides exhibited a high specific capacitance, excellent cycling stability, and a fast charge/discharge rate making them promising electrode materials for supercapacitors. The highest capacitance was obtained for the composition that contained 40 mol.% of Ir ($Ni_{0.36}Mo_{0.24}Ir_{0.4}$-oxide). The coatings were found to yield good charge storage in both acidic and alkaline environment. The $Ni_{0.36}Mo_{0.24}Ir_{0.4}$-oxide was found to retain ca. 86% of its initial capacitance after 2500 charging/discharging cycles, at 1 mA cm^{-2}. Based on these findings, the authors' opinion is that the $Ni_{0.36}Mo_{0.24}Ir_{0.4}$-oxide composition is a suitable candidate material for fabrication of supercapacitor electrodes based on the metal-oxide nanoparticle/carbon composites.

Acknowledgment

This research was supported by the National Council on Science and Technology (CONACYT), the National Science and Engineering Research Council of Canada (NSERC), and McGill University through the McGill Engineering Doctoral Award (MEDA) program.

Chapter 7

7 *Conclusions*

This Ph.D. project focused on the development of mixed metal oxide coatings Ni-Co-oxide, Ni-Mo-oxide, and Ni-Mo-Ir-oxide) on a titanium substrate using a thermal-salt decomposition method for potential applications as cathodes for hydrogen production by electrochemical water splitting, and supercapacitor electrode materials.

The work presented over the course of this Ph.D. thesis in Chapter 3-6 lead to the development of several key conclusions which are summarized in the following sections:

Chapter 3: Nickel-cobalt-oxide cathodes for hydrogen production by water electrolysis in acidic and alkaline media

Mixed Ni-Co-oxide cathodes of various compositions were fabricated by a thermal-decomposition method and used as electrocatalysts for hydrogen production by water electrolysis in acidic and alkaline media. The main conclusions from this study are described below:

I. Stable phases of Ni-Co-oxide can be synthesized using the thermal decomposition method. The resulted oxide electrodes were found to be of a semi-crystalline structure, yielding the surface morphology characterized by relatively high surface roughness factor (up to 25).

II. The degree of amorphousness augmented with the increase in cobalt content in the coatings.

III. In all the cases, the electrochemically-active surface areas were determined to be considerably larger than the geometrical surface area of the electrocatalysts. Co-oxide electrode displayed the highest electrochemically active surface area, whereas the nickel control sample displayed the lowest active area.

IV. The Volmer reaction step (i.e., the electrochemical adsorption of hydrogen) controlled the kinetics of the hydrogen evolution on all the Ni-Co-oxide cathodes, and also on the pure metal Ni electrode.

V. The $Ni_{0.2}Co_{0.8}$-oxide was identified as the best electrode material candidate among the investigated metal oxides, which was associated with the surface-area effect. Nevertheless, its intrinsic activity was found to be lower than that of pure metallic Ni.

VI. Ni-Co-oxides were found to be significantly more fouling/deactivation-resistant than Ni during long-term testing (for 72 h, using 0.5 M H_2SO_4 as electrolyte, at a current density of -500 mA cm^{-2}).

VII. The effect of temperature on the kinetics of the HER on the $Ni_{0.2}Co_{0.8}$-oxide electrode was evaluated in the temperature range from 293 K to 323 K. The results showed that with an increase in temperature, the HER activity is enhanced. Moreover, it was corroborated that the HER kinetics on this oxide follows the Arrhenius law.

Chapter 4: Evaluation of nickel-molybdenum-oxides as cathodes for hydrogen evolution by water electrolysis in acidic, alkaline, and neutral media

Nickel-molybdenum oxides coatings of different compositions were formed on a titanium substrate employing a thermal-salt decomposition method, and their electrocatalytic activity for the hydrogen evolution reaction was investigated in acidic, alkaline, and neutral media. Several electrochemical and surface characterization techniques were employed for the characterization of the electrode and the main conclusions obtained were the following:

I. EDS confirmed the agreement between the nominal and experimental relative values of Ni and Mo in the coating. Furthermore, the surface mapping of Ni and Mo corroborated a uniform distribution of the elements on the surfaces of all the coatings and the presence of an amorphous mixed layer.

II. The SEM images indicated that the total surface area of the coatings is considerably larger than the corresponding geometric area for all the coatings.

Furthermore, the true electrochemically-active area of the coatings was determined using cyclic voltammetry in a ruthenium-complex solution. The $Ni_{0.2}Mo_{0.8}$-oxide coating yielded the largest electrochemical surface area, characterized by the surface roughness factor of 52.

III. XRD pattern displays a crystalline structure of the Ni plate and NiOx coating. Though, the addition of Mo in the oxide coating introduces some level of amorphousness.

IV. Tafel analysis revealed that the Volmer step (H^+ adsorption) is the rate determining mechanism controlling the HER on Ni-Mo cathodes for all the cases (all electrodes / all electrolytes). This was consistent with what others have determined using Ni and their alloys.

V. The most extrinsically active coating was the $Ni_{0.6}Mo_{0.4}$-oxide coating (in all three electrolytes), while this coating showed the highest intrinsic activity in the neutral electrolyte. The $Ni_{0.8}Mo_{0.2}$-oxide coating was found to be most intrinsically active in the acidic and alkaline electrolyte. This confirms that the actual HER activity of the oxides is more dependent on the cathode composition (intrinsic effect) rather than on the surface area (extrinsic effect).

VI. The Ni-Mo-oxides were stable for a long-term stability test of 24 hours at a current density of -500 mA cm^{-2} in acidic media (electrolyte 0.5 M H_2SO_4).

VII. The results presented in the paper demonstrate that Ni-Mo-oxides could potentially be used as good HER electrocatalysts in the acidic, alkaline and neutral environment.

Chapter 5: 5 The influence of addition of iridium-oxide to nickel-molybdenum-oxide cathodes on the electrocatalytic activity towards hydrogen evolution in acidic medium and on the cathode fouling resistance

The impact of the Ir content was evaluated in the fabrication of the mixed Ni-Mo-Ir-oxide cathodes used as electrocatalysts for hydrogen production by water electrolysis in acidic media.

I. All the oxide-based electrodes display a significantly higher catalytic activity than pure metallic Ni. The Ir content augmented the electrocatalytic activity for hydrogen evolution reaction linearly. This trend indicates that the HER kinetics is proportional to the number of Ir-oxide active sites on the electrode surface and that the influence of possible modification of the electronic structure of the oxide electrode is minor.

II. The addition of Ir to the Ni-Mo-oxide results in a change in the surface morphology of the coating. The surface that does not contain Ir shows a porous structure characterized by globules, the surfaces that contain Ir display a cracked-mud morphology. Moreover, the addition of Ir to the metal oxide coating increased surface roughness.

III. The long-term stability experiments were done in which the Ni-Mo-Ir-oxide cathodes showed steady performance for 96 hours in acidic media.

IV. The deactivation/reactivation of the of the cathodes was tested in the presence of Cu, Fe, and the higher degree of reactivation by in-situ anodic oxidation.

V. When the deactivation was done in the electrolyte containing both Cu and Fe, EDS revealed a that Cu was preferentially deposited on the surface, with a Cu/Fe ratio of 3/2. The preferential deposition of Cu could be due to both thermodynamics and due to kinetics.

VI. The in-situ regeneration by anodic oxidation had the smallest effect on the Ni cathode, while in the two Ni-Mo-Ir-oxide cathodes was successful since the electrocatalytic activity of these electrodes reached around 90%.

VII. These results confirm the Ni-Mo-Ir-oxide coatings have excellent catalytic properties combined with corrosion and mechanical stability, which make them outstanding candidates for HER in PEM electrolyzers.

Chapter 6: $Ni_{0.6-x}Mo_{0.4-x}Ir_x$-oxide as an Electrode Material for Supercapacitors: Investigation of the Influence of Ir content on the Charge Storage/Delivery

The influence of Ir-oxide content on the charge storage/delivery capability of $Ni_{0.6-x}Mo_{0.4-x}Ir_x$-oxide electrodes was investigated to evaluate their performance and potential suitability as supercapacitor electrodes.

I. The addition of Ir to the Ni-Mo-oxide change the surface morphology of the coatings. The coatings that contain Ir have a cracked-mud/cauliflower-like morphology which provides easy mobility for ions on the electrode/electrolyte interface.

II. EDS and XPS confirm that the desired composition of coatings and their homogeneity prepared through a thermal-salt decomposition method.

III. The behavior of the oxide coatings is significantly dependent on the coating composition. The highest capacitance (108 ± 2 mF cm^{-2}) was obtained for the composition containing 40 mol.% of Ir ($Ni_{0.36}Mo_{0.24}Ir_{0.4}$-oxide coating).

IV. The capacitance achieved in H_2SO_4 for the Ir-containing oxides is higher at all scan rates than that recorded in KOH. An acidic medium favors the electrosorption and intercalation of H^+ ions, and also provides a more conductive medium, thus increasing capacitance.

V. All the electrodes have the triangular charge-discharge behavior. The slight deviation from linearity suggests a pseudocapacitive behavior.

VI. The $Ni_{0.36}Mo_{0.24}Ir_{0.4}$-oxide was found to rain ca. 86% of its initial capacitance after 2500 charging/discharging cycles, at 1 mA cm^{-2}. Possible causes can be related to the partial dissolution of the oxide coatings into the electrolyte, or to a decrement of the surface area exposed to the electrolyte.

As a general conclusion, comparing the performance of the Ni-oxide-based electrodes employed in this research work, Ni-Co-oxide electrodes had a similar performance to metallic nickel (control) as an electrocatalyst for the hydrogen evolution reaction in both acidic and alkaline media. The enhancement of the activity in some compositions of this mixed-metal-oxide was mainly due to the increase of surface area. On the other hand, when Ni-Mo-oxide coatings were used for the same purpose, they had a better performance than both nickel and Ni-Co-oxide electrodes, in the whole pH range. This was related to both the enhancement of the electrochemically active surface area (extrinsic effect) and the intrinsic properties of the metal oxide coating (electronic structure of the material and bifunctional characteristic of Ni and Mo in the oxide). The addition of Ir into the Ni-Mo-oxide coatings further increased the activity for the HER due to a possible modification of the electronic structure of the coatings and excellent activity of Ir in the HER. One of the main advantages of the developed Ni-Mo-Ir-oxide electrodes for the hydrogen evolution was their electrocatalytic stability, i.e., an excellent resistance to deactivation and a high degree of reactivation, in comparison to the Ni control.

Addition of Ir into Ni-Mo-oxide coatings also resulted in a considerable increase in capacitance of the electrodes. This increment was dependent on the Ir content. Considering all the previous information, it is concluded that the nickel-oxide-based electrodes (Ni-Co, and especially Ni-Mo and Ni-Mo-Ir) prepared through a thermal-salt decomposition are good electrode for energy storage applications, namely for hydrogen evolution by water electrolysis and charge storage in supercapacitors.

Chapter 8

8 Original Contributions and Future Work

8.1 Original contributions to knowledge

This Ph.D. thesis confirmed that Ni-oxide-based electrodes could be synthesized using a cost-effective and simple thermal-decomposition technique to produce active electrodes for alternative energy storage devices, specifically for hydrogen production by water electrolysis and for supercapacitors. The following points outline the original contributions to the knowledge which were accomplished in this research work:

I. It was found that Ni-oxide-based electrodes are suitable materials for the production of hydrogen by water electrolysis. The main advantage of using these oxides, especially Ni-Mo-Ir-oxides, is their electrocatalytic-activity stability (high resistance to deactivation and high degree of re-activation).

II. It was found that Ni-Mo-oxide coatings can be used as cathodes material for the hydrogen evolution reaction in the whole pH scale, rendering them good cathode materials for PEM, sea-water and alkaline water electrolyzers.

III. It was found that the addition of Ir to the Ni-Mo-oxide coatings increases both the cathode electrocatalytic activity in the hydrogen evolution reaction and the charge storage/delivery capability.

8.2 Recommendations for future work

The work done in this thesis confirms the success of the mixed metal oxide (Ni-Co-oxide, Ni-Mo-oxide, and Ni-Mo-Ir-oxide) electrodes as potential alternative energy for the hydrogen production by water splitting and their use in supercapacitors. Though the application of oxide coatings has been studied for several decades, and additional work on the electrodes must be done to understand the properties of the produced coatings to employ them in different novel applications. For this purpose, the following aspects of research on the development of mixed metal oxide as energy storage applications are suggested:

I. The use of other transition metal oxides can be employed for the HER. There have been some studies related to the use of alloys such as Ni–Fe, Ni–W in their metallic forms, which show high electrochemical activity, and the same combinations can be used but this time with their oxide forms. Moreover, in this research, a ternary mixed metal oxide was prepared (Ni-Mo-Ir-oxide coating). It would be relevant to see the effect of adding a third component such as Fe, Co, W in preparing ternary mixed metal oxides (using inexpensive transition metals) to determine the influence of the third metal oxide component.

II. A thermal-salt decomposition has been employed in this thesis to form oxide coatings on a titanium substrate. It would be interesting to apply other coating deposition techniques such as spin coating, sol-gel, and physical vapor deposition to compare the performance of these methods.

III. For PEM-type electrolyzers, it is recommended to produce the mixed oxides in the form of nanoparticles, which could potentially increase the electrode electrical conductivity and also their electrochemical activity.

IV. The use of the mixed metal oxides as a catalyst support. Since these metal oxides showed better stability than metals, they could be used as a support of active catalyst such as platinum or ruthenium which can be introduced in the form of nanoparticles.

V. Optimize the reactivation procedure based on the anodic polarization of the electrodes. For the specific case of the Ni-Mo-Ir-oxides, a deactivation/reactivation procedure was done (for more information, please see chapter 5). Nonetheless, this procedure was not optimized. It would be interesting to increase the time of reactivation and/or the current density applied to determine if the electrodes can achieve a higher degree of reactivation.

VI. The long-term stability, fouling susceptibility and re-activation capability of the mixed metal oxides should be evaluated taking into account different conditions, in particular in alkaline media. Nowadays, alkaline electrolyzers are the most commonly used in industry. For this reason, the metal oxides should be tested in the actual conditions (electrolyte-type, temperature, flow, and pressure) to determine if they can be employed with the current type of electrolyzers.

VII. Due to the stability demonstrated as cathodes for HER, these metal oxide coatings could potentially be used as anodes for the oxygen evolution reaction (OER).

VIII. The use of the mixed metal oxide coatings on carbon nanofibers for supercapacitors, including the use of Ni-Mo and Ni-Co-oxides or combinations thereof. In order to evaluate the use of these mixed metal oxide coatings and their impact on the pseudocapacitance of the electrodes.

:

Appendix I

LTP is a useful technique for determining the kinetics of HER on an electrocatalyst and it will be used throughout this project.

In a LTP measurement, the current density of an electrode is recorded as its potential is varied. A plot of the logarithm of the current density as a function of potential yields the well-known Tafel curve, exemplified in Figure A.1. The applied overpotential (difference between the applied and reversible potential) presented on the abscissa represents the driving force for the electron transfer in the HER, i.e., the input energy, while the current density presented on the ordinate represents the corresponding HER kinetics, i.e., the amount of H_2 produced. If the linear region is extrapolated to the current density axis, the intercept yields the exchange current density.

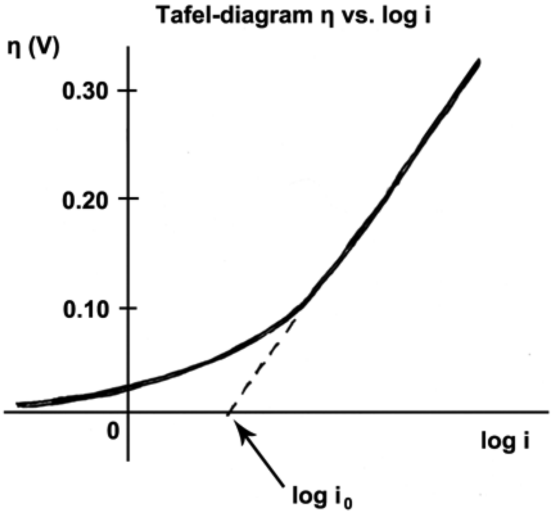

Figure A.1 A schematic representation of a typical Tafel plot. The current density intercept represents the exchange current density, log j_0.

The Tafel slope b, indicates the shift in electrode potential (in mV) for each decade of current applied. In addition, it is useful for determining the mechanism under which HER occurs. For example, if b = 120 mV decade^{-1}, the Volmer reaction is a rate determining step (rds). Similarly, if b = 40 mV decade^{-1}, then the Tafel step is rate limiting, and if b = 30 mV decade^{-1}, the Heyrovsky reaction is the rds. In terms of the HER, a large exchange current density implies low resistance and a small Tafel slope characterize a good catalyst.

Using equations A.1 and A.2 different parameters can be obtained such as the Tafel slope and the transfer coefficient (concepts which were explained in Chapter 2 and 3 of this thesis)

$$\eta = a + blog(j) \tag{A.1}$$

$$b = \frac{2.3\ RT}{\alpha nF}\log(j_0) \tag{A.2}$$

Where:
η = Overpotential (V)
b = Tafel slope (mV dec^{-1})
j = Current density (A cm^{-2})
j_0 = Exchange current density (A cm^{-2})
R = Gas constant (8.314 J K^{-1} mol^{-1})
T = Temperature (K)
α = Transfer coefficient (-)
n = number of electrons exchanged (-)
F = Faraday constant (96 485 J)

Appendix II

Supplementary material Chapter 5: The influence of addition of iridium-oxide to nickel-molybdenum-oxide cathodes on the electrocatalytic activity towards hydrogen evolution in acidic medium and on the cathode fouling resistance

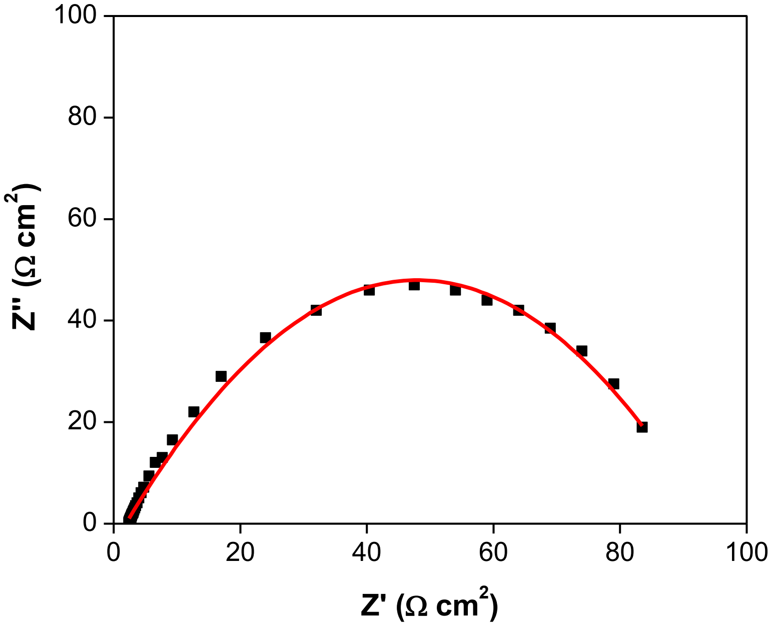

Figure A.2: Nyquist plot for the $Ni_{0.48}Mo_{0.32}Ir_{0.2}$*-oxide coating recorded in 0.5 M* H_2SO_4 *at* $\eta = -150$ *mV. Symbols represent the experimental data and the solid line represent the modeled data.*

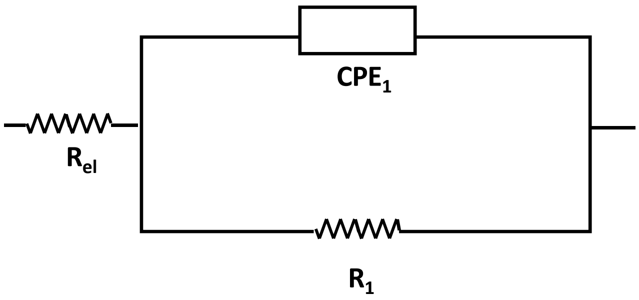

Figure A.3: One-time constant electric equivalent circuit (EEC) model used to model the electrochemical impedance spectroscopy (EIS) response of the investigated Ni-Mo-Ir-oxide coatings.

Table A.1: EEC parameters obtained by fitting EIS experimental spectra recorded at η =-150 on the investigated coatings using the EEC model presented in Figure A.3.

Sample	**R_{el} (Ω cm^2)**	**CPE (F s^{n-1} cm^{-2})**	**n (-)**	**R_1 (Ω cm^2)**
Ni	2.01	6.90×10^{-4}	0.93	78
$Ni_{0.6}Mo_{0.4}Ox$	2.45	8.68×10^{-4}	0.94	60
$Ni_{0.54}Mo_{0.36}Ir_{0.1}Ox$	2.24	9.60×10^{-4}	0.94	90
$Ni_{0.48}Mo_{0.32}Ir_{0.2}Ox$	3.03	2.18×10^{-3}	0.85	103
$Ni_{0.36}Mo_{0.24}Ir_{0.4}Ox$	2.69	1.91×10^{-3}	0.91	49
$Ni_{0.24}Mo_{0.16}Ir_{0.6}Ox$	2.12	3.07×10^{-3}	0.88	83

Equation A.3: Brug equation used to determine the double layer capacitance.

$$C_{DL} = \left[\frac{CPE}{(R_{el}^{-1} + R_1^{-1})^{(1-n)}}\right]^{n^{-1}} \qquad (A.3)$$

Where:

CPE is the constant phase element (F s^{n-1} cm^{-2})

R_{el} is the electrolyte resistance (Ω cm^2)

R_1 is the charge-transfer resistance (Ω cm^2)

n is the CPE exponent (-)

C_{DL} is the double layer capacitance (F cm^{-2})

Table A.2: Relative atomic percentage of Ni, Mo, and Ir in oxide coatings (excluding the contribution of oxygen and other impurities in the coatings) obtained by XPS in selected electrodes.

Nominal	**Results**
$Ni_{0.6}Mo_{0.4}Ox$	$Ni_{0.58}Mo_{0.42}Ox$
$Ni_{0.48}Mo_{0.32}Ir_{0.2}Ox$	$Ni_{0.47}Mo_{0.25}Ir_{0.28}Ox$
$Ni_{0.36}Mo_{0.24}Ir_{0.4}Ox$	$Ni_{0.34}Mo_{0.20}Ir_{0.46}Ox$
IrOx	IrOx

Appendix III

Preliminary experiments were done in acidic medium to evaluate the capacitance of the Ni-Mo-Ir-oxide electrodes. For this medium, electrochemical measurements were conducted in a standard three-electrode cell using 0.5 M H_2SO_4 (96 % assay; Fisher Scientific, USA) as the electrolyte solution at 295 ± 2 K and atmospheric pressure. Ni-Mo-Ir-oxide coatings of various compositions were used as the working electrodes (WE). The geometric area of the electrode exposed to the electrolyte was 0.68 cm^2. A saturated calomel electrode (SCE; Accumet electrode, Fisher Scientific, USA) was used as the reference electrode (RE), and a graphite rod was employed as a counter electrode (CE). The graphite rod was separated from the main cell body by a glass frit (porosity C, Ace Glass, Inc., USA). All the potential values reported are presented versus SCE. To maintain an oxygen-free electrolyte, argon was bubbled for 30 minutes before electrochemical measurements and continuously during the measurements. The electrochemical behavior of the electrodes was characterized by cyclic voltammetry (CV) performed in a potentiostat/galvanostat analyzer (Autolab PGSTAT30, Metrohm, the Netherlands) controlled by the NOVA software (v. 2.1.3; Metrohm, the Netherlands).

CVs of the $Ni_{0.36}$ $Mo_{0.24}Ir_{0.4}$-oxide electrode recorded at several scan rates are displayed in Figure A.1. The voltammograms exhibit two broad peaks/shoulders appearing at around 0.7 V in the anodic scan and at 0.5 V in the cathodic redox. These broad peaks have multiple transitions that overlap, possibly from several redox reactions of the involved oxides.

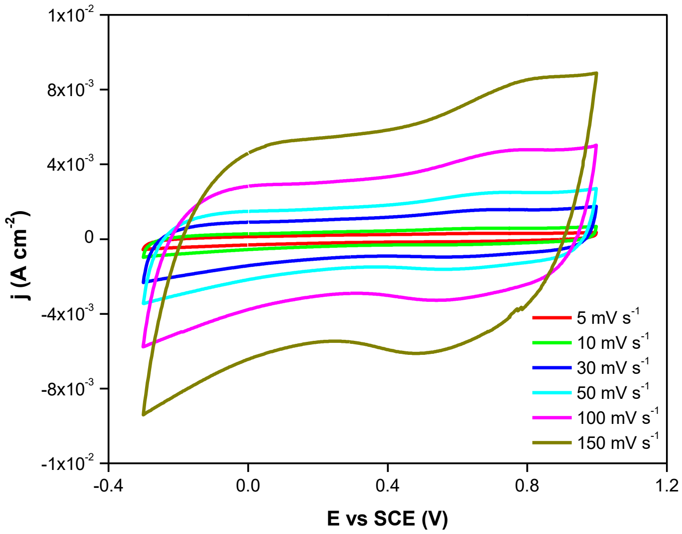

Figure A.4: Cyclic voltammograms of the $Ni_{0.36}Mo_{0.24}Ir_{0.4}$*-oxide electrode recorded in 0.5 M* H_2SO_4*.*

Figure A.4 shows the corresponding variation of capacitance of the Ni-Mo-Ir-oxide electrodes as a function of scan rate. The results follow the same trend when using an alkaline electrolyte (see Figure 6.5 in the thesis). All Ni-Mo-oxide compositions containing Ir yielded higher capacitance values in comparison to $Ni_{0.6}$-$Mo_{0.4}$-oxide and pure Ir-oxide, with the Ir content of 40 wt.% yielding the highest capacitance. A detailed explanation of the possible causes for this is discussed in Chapter 6.

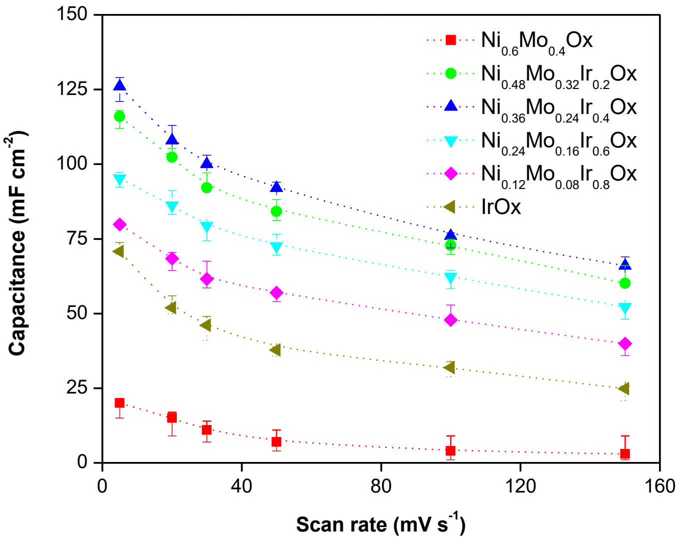

Figure A.5: Variation of capacitance with scan rate calculated from CVs recorded on different Ni-Mo-Ir-oxide electrodes in 0.5 M H_2SO_4.

From Figure A.5 can be seen that the highest capacitance obtained is 122 ± 2 $mF\,cm^{-2}$ for the composition containing 40 mol.% of Ir. Furthermore, it is important to mention that the capacitance achieved in H_2SO_4 for the Ir-containing oxides is higher at all scan rates than that recorded in KOH (see Figure 6.5). Similarly, a research study by Saji et al. [193] demonstrated that an acidic medium favors the electrosorption and intercalation of H^+ ions, and also provides a more conductive medium, thus increasing capacitance.

References

1. Change, I.P.o.C., *Climate change 2014: Mitigation of climate change*. Vol. 3. 2015: Cambridge University Press.

2. Mueller-Langer, F., et al., *Techno-economic assessment of hydrogen production processes for the hydrogen economy for the short and medium term*. International Journal of Hydrogen Energy, 2007. **32**(16): p. 3797-3810.

3. Turner, J.A., *A realizable renewable energy future*. Science, 1999. **285**(5428): p. 687-689.

4. Hijikata, T., *Research and development of international clean energy network using hydrogen energy (WE-NET)*. International Journal of Hydrogen Energy, 2002. **27**(2): p. 115-129.

5. Kruger, P., *Electric power requirement for large-scale production of hydrogen fuel for the world vehicle fleet*. International Journal of Hydrogen Energy, 2001. **26**(11): p. 1137-1147.

6. Mitsugi, C., A. Harumi, and F. Kenzo, *WE-NET: Japanese hydrogen program*. International Journal of Hydrogen Energy, 1998. **23**(3): p. 159-165.

7. Pletcher, D., X. Li, and S. Wang, *A comparison of cathodes for zero gap alkaline water electrolysers for hydrogen production*. international journal of hydrogen energy, 2012. **37**(9): p. 7429-7435.

8. De Souza, R.F., et al., *Electrochemical hydrogen production from water electrolysis using ionic liquid as electrolytes: towards the best device*. Journal of Power Sources, 2007. **164**(2): p. 792-798.

9. Ni, M., M.K. Leung, and D.Y. Leung, *Energy and exergy analysis of hydrogen production by a proton exchange membrane (PEM) electrolyzer plant*. Energy conversion and management, 2008. **49**(10): p. 2748-2756.

10. Zhang, L., et al., *In situ growth of ruthenium oxide-nickel oxide nanorod arrays on nickel foam as a binder-free integrated cathode for hydrogen evolution*. Journal of Power Sources, 2015. **274**: p. 114-120.

11. LeRoy, R., *Industrial water electrolysis: present and future.* International Journal of Hydrogen Energy, 1983. **8**(6): p. 401-417.

12. Navarro-Flores, E., Z. Chong, and S. Omanovic, *Characterization of Ni, NiMo, NiW and NiFe electroactive coatings as electrocatalysts for hydrogen evolution in an acidic medium.* Journal of Molecular Catalysis A: Chemical, 2005. **226**(2): p. 179-197.

13. Jaksic, M.M., *Hypo–hyper-d-electronic interactive nature of interionic synergism in catalysis and electrocatalysis for hydrogen reactions.* International journal of hydrogen energy, 2001. **26**(6): p. 559-578.

14. Kirk, D., S. Thorpe, and H. Suzuki, *Ni-base amorphous alloys as electrocatalysts for alkaline water electrolysis.* International journal of hydrogen energy, 1997. **22**(5): p. 493-500.

15. Zeng, K. and D. Zhang, *Recent progress in alkaline water electrolysis for hydrogen production and applications.* Progress in Energy and Combustion Science, 2010. **36**(3): p. 307-326.

16. Trasatti, S., *Hydrogen evolution on oxide electrodes*, in *Modern chlor-alkali technology*. 1992, Springer. p. 281-294.

17. Shibli, S. and J. Sebeelamol, *Development of Fe 2 O 3–TiO 2 mixed oxide incorporated Ni–P coating for electrocatalytic hydrogen evolution reaction.* International Journal of Hydrogen Energy, 2013. **38**(5): p. 2271-2282.

18. Tavares, A. and S. Trasatti, *Ni+ RuO 2 co-deposited electrodes for hydrogen evolution.* Electrochimica acta, 2000. **45**(25): p. 4195-4202.

19. Veggetti, E., I. Kodintsev, and S. Trasatti, *Hydrogen evolution on oxide electrodes: Co 3 O 4 in alkaline solution.* Journal of Electroanalytical Chemistry, 1992. **339**(1): p. 255-268.

20. Trasatti, S., *Electrocatalysis: understanding the success of DSA®.* Electrochimica Acta, 2000. **45**(15): p. 2377-2385.

21. Kodintsev, I. and S. Trasatti, *Electrocatalysis of H 2 evolution on RuO 2+ IrO 2 mixed oxide electrodes.* Electrochimica acta, 1994. **39**(11): p. 1803-1808.

22. Vijh, A.K., *Electrolytic hydrogen evolution reaction on aluminum, oxide-covered electrodes.* The Journal of Physical Chemistry, 1969. **73**(3): p. 506-513.

23. Leonard, K.C., M.I. Tejedor-Anderson, and M.A. Anderson, *Nanoporous oxide coatings on stainless steel to enable water splitting and reduce the hydrogen evolution overpotential.* international journal of hydrogen energy, 2012. **37**(24): p. 18654-18660.

24. Raj, I.A., *Nickel-based, binary-composite electrocatalysts for the cathodes in the energy-efficient industrial production of hydrogen from alkaline-water electrolytic cells.* Journal of materials science, 1993. **28**(16): p. 4375-4382.

25. Trasatti, S., *Physical electrochemistry of ceramic oxides.* Electrochimica Acta, 1991. **36**(2): p. 225-241.

26. Kötz, E. and S. Stucki, *Ruthenium dioxide as a hydrogen-evolving cathode.* Journal of applied electrochemistry, 1987. **17**(6): p. 1190-1197.

27. Colton, R.J., A.M. Guzman, and J.W. Rabalais, *Electrochromism in some thin-film transition-metal oxides characterized by x-ray electron spectroscopy.* Journal of Applied Physics, 1978. **49**(1): p. 409-416.

28. Esswein, A.J., et al., *Size-dependent activity of Co3O4 nanoparticle anodes for alkaline water electrolysis.* The Journal of Physical Chemistry C, 2009. **113**(33): p. 15068-15072.

29. Highfield, J., E. Claude, and K. Oguro, *Electrocatalytic synergism in Ni/Mo cathodes for hydrogen evolution in acid medium: a new model.* Electrochimica acta, 1999. **44**(16): p. 2805-2814.

30. Pal, B., M. Sharon, and G. Nogami, *Preparation and characterization of TiO 2/Fe 2 O 3 binary mixed oxides and its photocatalytic properties.* Materials Chemistry and Physics, 1999. **59**(3): p. 254-261.

31. McKone, J.R., et al., *Earth-abundant hydrogen evolution electrocatalysts.* Chemical Science, 2014. **5**(3): p. 865-878.

32. Brey, J., et al., *Designing a gradual transition to a hydrogen economy in Spain.* Journal of power sources, 2006. **159**(2): p. 1231-1240.

33. Momirlan, M. and T.N. Veziroglu, *The properties of hydrogen as fuel tomorrow in sustainable energy system for a cleaner planet.* International journal of hydrogen energy, 2005. **30**(7): p. 795-802.

34. Owen, K. and T. Coley, *Automotive fuels reference book.* 1995.

35. Haryanto, A., et al., *Current status of hydrogen production techniques by steam reforming of ethanol: a review.* Energy & Fuels, 2005. **19**(5): p. 2098-2106.

36. Baykara, S.Z., *Hydrogen as fuel: a critical technology?* International journal of hydrogen energy, 2005. **30**(5): p. 545-553.

37. Ewan, B. and R. Allen, *A figure of merit assessment of the routes to hydrogen.* International Journal of Hydrogen Energy, 2005. **30**(8): p. 809-819.

38. Christopher, K. and R. Dimitrios, *A review on exergy comparison of hydrogen production methods from renewable energy sources.* Energy & Environmental Science, 2012. **5**(5): p. 6640-6651.

39. Brown, L.F., *A comparative study of fuels for on-board hydrogen production for fuel-cell-powered automobiles.* International Journal of Hydrogen Energy, 2001. **26**(4): p. 381-397.

40. Prins, M.J., K.J. Ptasinski, and F.J. Janssen, *From coal to biomass gasification: comparison of thermodynamic efficiency.* Energy, 2007. **32**(7): p. 1248-1259.

41. Sankaranarayanan, K., *Efficiency and Sustainability in the Energy and Chemical Industrial.* 2010.

42. Kreuter, W. and H. Hofmann, *Electrolysis: the important energy transformer in a world of sustainable energy.* International Journal of Hydrogen Energy, 1998. **23**(8): p. 661-666.

43. Trasatti, S., *Electronegativity, work function, and heat of adsorption of hydrogen on metals.* Journal of the Chemical Society, Faraday Transactions 1: Physical Chemistry in Condensed Phases, 1972. **68**(0): p. 229-236.

44. Trasatti, S., *Work function, electronegativity, and electrochemical behaviour of metals: III. Electrolytic hydrogen evolution in acid solutions.* Journal of Electroanalytical Chemistry and Interfacial Electrochemistry, 1972. **39**(1): p. 163-184.

45. Wang, S., S.P. Jiang, and X. Wang, *Polyelectrolyte functionalized carbon nanotubes as a support for noble metal electrocatalysts and their activity for methanol oxidation*. Nanotechnology, 2008. **19**(26): p. 265601.

46. Wang, S., et al., *Controlled synthesis of dendritic Au@ Pt core–shell nanomaterials for use as an effective fuel cell electrocatalyst*. Nanotechnology, 2009. **20**(2): p. 025605.

47. Novakovic, J., et al., *Electroless NiP–TiO 2 composite coatings: Their production and properties*. Surface and Coatings Technology, 2006. **201**(3): p. 895-901.

48. Dunn, S., *Hydrogen futures: toward a sustainable energy system*. International journal of hydrogen energy, 2002. **27**(3): p. 235-264.

49. Barbir, F., *PEM electrolysis for production of hydrogen from renewable energy sources*. Solar energy, 2005. **78**(5): p. 661-669.

50. Bennett, J., *Electrodes for generation of hydrogen and oxygen from seawater*. International Journal of Hydrogen Energy, 1980. **5**(4): p. 401-408.

51. Jiang, N., et al., *Study on Ni–Fe–C cathode for hydrogen evolution from seawater electrolysis*. International Journal of Hydrogen Energy, 2010. **35**(15): p. 8056-8062.

52. Niu, X., et al., *Robust and stable ruthenium alloy electrocatalysts for hydrogen evolution by seawater splitting*. Electrochimica Acta, 2016. **208**: p. 180-187.

53. Baniasadi, E., I. Dincer, and G.F. Naterer, *Electrochemical analysis of seawater electrolysis with molybdenum-oxo catalysts*. International Journal of Hydrogen Energy, 2013. **38**(6): p. 2589-2595.

54. Kirk, D. and A. Ledas, *Precipitate formation during sea water electrolysis*. International Journal of Hydrogen Energy, 1982. **7**(12): p. 925-932.

55. Meier, K., *Hydrogen production with sea water electrolysis using Norwegian offshore wind energy potentials*. International Journal of Energy and Environmental Engineering, 2014. **5**(2): p. 104.

56. Smolinka, T., *PEM Water Electrolysis - Present Status of Research and Development*. 2010.

57. Md Mamoon Rashid, M.K.A.M., Hamid Naseem, Mohd Danish, *Hydrogen Production by Water Electrolysis: A Review of Alkaline Water Electrolysis, PEM Water Electrolysis and High Temperature Water Electrolysis*. 20115.

58. Miles, M. and M. Thomason, *Periodic variations of overvoltages for water electrolysis in acid solutions from cyclic voltammetric studies.* Journal of The Electrochemical Society, 1976. **123**(10): p. 1459-1461.

59. Jakšić, M.M., *Hypo–hyper-d-electronic interactive nature of synergism in catalysis and electrocatalysis for hydrogen reactions.* Electrochimica Acta, 2000. **45**(25): p. 4085-4099.

60. Metikoš-Huković, M. and A. Jukić, *Correlation of electronic structure and catalytic activity of Zr–Ni amorphous alloys for the hydrogen evolution reaction.* Electrochimica acta, 2000. **45**(25): p. 4159-4170.

61. Highfield, J., K. Oguro, and B. Grushko, *Raney multi-metallic electrodes from regular crystalline and quasi-crystalline precursors: I. Cu-stabilized Ni/Mo cathodes for hydrogen evolution in acid.* Electrochimica acta, 2001. **47**(3): p. 465-481.

62. Marozzi, C. and A. Chialvo, *Development of electrode morphologies of interest in electrocatalysis: part 2: hydrogen evolution reaction on macroporous nickel electrodes.* Electrochimica acta, 2001. **46**(6): p. 861-866.

63. Damian, A. and S. Omanovic, *Ni and Ni Mo hydrogen evolution electrocatalysts electrodeposited in a polyaniline matrix.* Journal of Power Sources, 2006. **158**(1): p. 464-476.

64. McArthur, M., et al., *Synthesis and characterization of 3D Ni nanoparticle/carbon nanotube cathodes for hydrogen evolution in alkaline electrolyte.* Journal of Power Sources, 2014. **266**: p. 365-373.

65. Chul Shin, S., et al., *Carbon nanowalls as platinum support for fuel cells.* Journal of Applied Physics, 2011. **110**(10): p. 104308.

66. Furuya, N. and S. Motoo, *The electrochemical behavior of ad-atoms and their effect on hydrogen evolution: Part I. Order-disorder rearrangement of copper ad-atoms on platinum.* Journal of Electroanalytical Chemistry and Interfacial Electrochemistry, 1976. **72**(2): p. 165-175.

67. *1 Year Nickel Prices and Price Charts, InfoMine.* 2016 [cited 2016; Available from: http://www.infomine.com/investment/metal-prices/nickel/1-year/.

68. Zheng, Y., et al., *Advancing the Electrochemistry of the Hydrogen-Evolution Reaction through Combining Experiment and Theory.* Angewandte Chemie International Edition, 2015. **54**(1): p. 52-65.

69. Krstajic, N. and S. Trasatti, *Cathodic behaviour of RuO2-doped Ni/Co3O4 electrodes in alkaline solutions: hydrogen evolution.* Journal of applied electrochemistry, 1998. **28**(12): p. 1291-1297.

70. Kawashima, A., et al., *Characterization of sputter-deposited Ni-Mo and Ni-W alloy electrocatalysts for hydrogen evolution in alkaline solution.* Materials Science and Engineering: A, 1997. **226**: p. 905-909.

71. Kodintsev, I. and S. Trasatti, *Electrocatalysis of H2 evolution on RuO2+ IrO2 mixed oxide electrodes.* Electrochimica acta, 1994. **39**(11-12): p. 1803-1808.

72. Suffredini, H., et al., *Recent developments in electrode materials for water electrolysis.* International Journal of Hydrogen Energy, 2000. **25**(5): p. 415-423.

73. Janjua, M. and R. Le Roy, *Electrocatalyst performance in industrial water electrolysers.* International Journal of Hydrogen Energy, 1985. **10**(1): p. 11-19.

74. Jaksic, M.M., *Interionic nature of synergism in catalysis and electrocatalysis.* Solid State Ionics, 2000. **136**: p. 733-746.

75. Bou-Saleh, Z. and S. Omanovic, *Nickel-Based 3D Electrocatalyst Layers for Production of Hydrogen by Water Electrolysis in an Acidic Medium.* Journal of nanoscience and nanotechnology, 2009. **9**(4): p. 2469-2479.

76. Jakśić, M., *Towards the reversible electrode for hydrogen evolution in industrially important electrochemical processes.* International journal of hydrogen energy, 1986. **11**(8): p. 519-532.

77. Jakšić, J., M. Vojnović, and N. Krstajić, *Kinetic analysis of hydrogen evolution at Ni–Mo alloy electrodes.* Electrochimica Acta, 2000. **45**(25): p. 4151-4158.

78. Jaksic, M., *Volcano plots along the Periodic table, their causes and consequences on electrocatalysis for hydrogen electrode reactions.* Journal of New Materials for Electrochemical Systems, 2000. **3**(2): p. 167-182.

79. Dotson, R.L. and K.J. O'leary, *Electrolytic production of high purity alkali metal hydroxide*. 1977, Google Patents.

80. Nicolas, E. and L. Merckaert, *Cathode for the electrolytic production of hydrogen and its use*. 1985, Google Patents.

81. Cairns, J.F., D.A. Denton, and P.A. Izzard, *Cathode for use in electrolytic cell*. 1986, Google Patents.

82. Hayfield, P., *Development of the noble metal/oxide coated titanium electrode*. Platinum metals review, 1998. **42**(2): p. 46-55.

83. Shibli, S. and V. Dilimon, *Effect of phosphorous content and TiO2-reinforcement on Ni–P electroless plates for hydrogen evolution reaction*. International Journal of Hydrogen Energy, 2007. **32**(12): p. 1694-1700.

84. Blouin, M. and D. Guay, *Activation of ruthenium oxide, iridium oxide, and mixed RuxIr1− x oxide electrodes during cathodic polarization and hydrogen evolution*. Journal of the electrochemical society, 1997. **144**(2): p. 573-581.

85. Conway, B.E., *Electrochemical supercapacitors: scientific fundamentals and technological applications*. 2013: Springer Science & Business Media.

86. Kötz, R. and M. Carlen, *Principles and applications of electrochemical capacitors*. Electrochimica acta, 2000. **45**(15-16): p. 2483-2498.

87. Christen, T. and M.W. Carlen, *Theory of Ragone plots*. Journal of power sources, 2000. **91**(2): p. 210-216.

88. Berradi, S., F. Moutaouakkil, and H. Medromi, *Hybrid Electrical Architecture for Vertical Takeoff and Landing Unmmaned Aerial Vehicule*, in *Advances in Ubiquitous Networking*. 2016, Springer. p. 439-448.

89. Burke, A., *Ultracapacitors: why, how, and where is the technology*. Journal of power sources, 2000. **91**(1): p. 37-50.

90. Garche, J., et al., *Encyclopedia of electrochemical power sources*. 2013: Newnes.

91. Aslani, M., *Electrochemical double layer capacitors (supercapacitors)*. Standford University, 2012.

92. Sharma, P. and T. Bhatti, *A review on electrochemical double-layer capacitors.* Energy conversion and management, 2010. **51**(12): p. 2901-2912.

93. Schneuwly, A. and R. Gallay, *Properties and applications of supercapacitors: From the state-of-the-art to future trends.* Rossens, Switzerland, 2000.

94. Conway, B., V. Birss, and J. Wojtowicz, *The role and utilization of pseudocapacitance for energy storage by supercapacitors.* Journal of Power Sources, 1997. **66**(1-2): p. 1-14.

95. contributors, W., *Double-layer capacitance.* Wikipedia, The Free Encyclopedia, 2018.

96. Obreja, V.V., *On the performance of supercapacitors with electrodes based on carbon nanotubes and carbon activated material—a review.* Physica E: Low-dimensional Systems and Nanostructures, 2008. **40**(7): p. 2596-2605.

97. Michell, D., D. Rand, and R. Woods, *A study of ruthenium electrodes by cyclic voltammetry and X-ray emission spectroscopy.* Journal of Electroanalytical Chemistry and Interfacial Electrochemistry, 1978. **89**(1): p. 11-27.

98. Delahay, P. and K. Holub, *Coupling of charging and faradaic processes: Electrode admittance for reversible processes.* Journal of Electroanalytical Chemistry and Interfacial Electrochemistry, 1968. **16**(2): p. 131-136.

99. Gerischer, H., *The impact of semiconductors on the concepts of electrochemistry.* Electrochimica Acta, 1990. **35**(11-12): p. 1677-1699.

100. Hu, C.-C., M.-J. Liu, and K.-H. Chang, *Anodic deposition of hydrous ruthenium oxide for supercapacitors.* Journal of Power Sources, 2007. **163**(2): p. 1126-1131.

101. Ullah, N., M.A. McArthur, and S. Omanovic, *Iridium-ruthenium-oxide coatings for supercapacitors.* The Canadian Journal of Chemical Engineering, 2015. **93**(11): p. 1941-1948.

102. Deng, L., et al., *RuO2/graphene hybrid material for high performance electrochemical capacitor.* Journal of Power Sources, 2014. **248**: p. 407-415.

103. Simon, P. and Y. Gogotsi, *Materials for electrochemical capacitors*, in *Nanoscience And Technology: A Collection of Reviews from Nature Journals*. 2010, World Scientific. p. 320-329.

104. Hu, C.-C. and K.-H. Chang, *Cyclic voltammetric deposition of hydrous ruthenium oxide for electrochemical capacitors: effects of codepositing iridium oxide.* Electrochimica Acta, 2000. **45**(17): p. 2685-2696.

105. McKeown, D.A., et al., *Structure of hydrous ruthenium oxides: implications for charge storage.* The Journal of Physical Chemistry B, 1999. **103**(23): p. 4825-4832.

106. Bullard, G., et al., *Operating principles of the ultracapacitor.* IEEE Transactions on magnetics, 1989. **25**(1): p. 102-106.

107. Zhang, Z.J., et al., *Hydrothermal synthesis and self-assembly of magnetite (Fe3O4) nanoparticles with the magnetic and electrochemical properties.* Journal of crystal growth, 2008. **310**(24): p. 5453-5457.

108. Castro, E., S. Real, and L.P. Dick, *Electrochemical characterization of porous nickel–cobalt oxide electrodes.* International journal of hydrogen energy, 2004. **29**(3): p. 255-261.

109. Prentice, G., *Electrochemical engineering principles*. 1991.

110. Ezaki, H., et al., *Hydrogen overpotential for intermetallic compounds, TiAl, FeAl and NiAl, containing 3d transition metals.* Electrochimica acta, 1994. **39**(11-12): p. 1769-1773.

111. Rosalbino, F., et al., *Electrocatalytic behaviour of Co–Ni–R (R= Rare earth metal) crystalline alloys as electrode materials for hydrogen evolution reaction in alkaline medium.* International Journal of Hydrogen Energy, 2008. **33**(22): p. 6696-6703.

112. Cao, B., et al., *Mixed close-packed cobalt molybdenum nitrides as non-noble metal electrocatalysts for the hydrogen evolution reaction.* Journal of the American Chemical Society, 2013. **135**(51): p. 19186-19192.

113. Zhao, Z., et al., *A High-Performance Binary Ni–Co Hydroxide-based Water Oxidation Electrode with Three-Dimensional Coaxial Nanotube Array Structure.* Advanced Functional Materials, 2014. **24**(29): p. 4698-4705.

114. Yan, X., et al., *Converting CoMoO4 into CoO/MoO x for Overall Water Splitting by Hydrogenation.* ACS Sustainable Chemistry & Engineering, 2016. **4**(7): p. 3743-3749.

115. Wang, Y., J.G. Limon-Petersen, and R.G. Compton, *Measurement of the diffusion coefficients of [Ru (NH 3) 6] 3+ and [Ru (NH 3) 6] 2+ in aqueous solution using microelectrode double potential step chronoamperometry*. Journal of Electroanalytical Chemistry, 2011. **652**(1): p. 13-17.

116. Limon-Petersen, J.G., et al., *Quantitative Voltammetry in Weakly Supported Media. Chronoamperometric Studies on Diverse One Electron Redox Couples Containing Various Charged Species: Dissecting Diffusional and Migrational Contributions and Assessing the Breakdown of Electroneutrality*. The Journal of Physical Chemistry C, 2010. **114**(5): p. 2227-2236.

117. Sreenivas, G., et al., *Fabrication and Characterization of Sputtered-Carbon Microelectrode Arrays*. Analytical Chemistry, 1996. **68**(11): p. 1858-1864.

118. Keeley, G.P., et al., *Electrochemical ascorbic acid sensor based on DMF-exfoliated graphene*. Journal of Materials Chemistry, 2010. **20**(36): p. 7864-7869.

119. Gomez Vidales, A. and S. Omanovic, *Evaluation of nickel-molybdenum-oxides as cathodes for hydrogen evolution by water electrolysis in acidic, alkaline, and neutral media*. Electrochimica Acta, 2018. **262**: p. 115-123.

120. Wen, X., et al., *Nanosized carbon black combined with Ni2O3 as "universal" catalysts for synergistically catalyzing carbonization of polyolefin wastes to synthesize carbon nanotubes and application for supercapacitors*. Environmental science & technology, 2014. **48**(7): p. 4048-4055.

121. Richardson, J.T., R. Scates, and M.V. Twigg, *X-ray diffraction study of nickel oxide reduction by hydrogen*. Applied Catalysis A: General, 2003. **246**(1): p. 137-150.

122. Bagotsky, V.S., *Fundamentals of electrochemistry*. Vol. 44. 2005: John Wiley & Sons.

123. Savadogo, O. and E. Ndzebet, *Influence of SiW 12 O 40 4− on the electrocatalytic behaviour of Pt–Co alloy supported on carbon for water electrolysis in 3 M KOH aqueous solution*. International journal of hydrogen energy, 2001. **26**(3): p. 213-218.

124. Parsons, R., *The rate of electrolytic hydrogen evolution and the heat of adsorption of hydrogen*. Transactions of the Faraday Society, 1958. **54**: p. 1053-1063.

125. Metikoš-Huković, M., et al., *Sputter deposited nanocrystalline Ni and Ni-W films as catalysts for hydrogen evolution.* Journal of Molecular Catalysis A: Chemical, 2006. **249**(1): p. 172-180.

126. Krstajić, N., et al., *Non-noble metal composite cathodes for hydrogen evolution. Part I: the Ni–MoO x coatings electrodeposited from Watt's type bath containing MoO 3 powder particles.* international journal of hydrogen energy, 2011. **36**(11): p. 6441-6449.

127. Krstajić, N., et al., *Non-noble metal composite cathodes for hydrogen evolution. Part II: The Ni–MoO 2 coatings electrodeposited from nickel chloride–ammonium chloride bath containing MoO 2 powder particles.* international journal of hydrogen energy, 2011. **36**(11): p. 6450-6461.

128. Lačnjevac, U., et al., *RuO x nanoparticles deposited on TiO 2 nanotube arrays by ion-exchange method as electrocatalysts for the hydrogen evolution reaction in acid solution.* Electrochimica Acta, 2015. **168**: p. 178-190.

129. Trasatti, S., *Electrocatalysis in the anodic evolution of oxygen and chlorine.* Electrochimica Acta, 1984. **29**(11): p. 1503-1512.

130. Chen, S., et al., *A graphene–MnO 2 framework as a new generation of three-dimensional oxygen evolution promoter.* Chemical Communications, 2014. **50**(2): p. 207-209.

131. Chassaing, E., et al., *Characterisation of electrodeposited nanocrystalline Ni–Mo alloys.* Journal of applied electrochemistry, 2004. **34**(11): p. 1085-1091.

132. Stilling, J., N. Ullah, and S. Omanovic, *Ir-Ni oxide as a promising material for nerve and brain stimulating electrodes.* Journal of Electrochemical Science and Engineering, 2014. **4**(3): p. 85-96.

133. Battisti, A.D., et al., *Preparation and characterization of oxide film electrodes.* Canadian journal of chemistry, 1997. **75**(11): p. 1759-1765.

134. Compton, R.G. and C.E. Banks, *Understanding voltammetry.* 2007: World Scientific.

135. Tavares, M., S. Machado, and L. Mazo, *Study of hydrogen evolution reaction in acid medium on Pt microelectrodes.* Electrochimica Acta, 2001. **46**(28): p. 4359-4369.

136. Naldoni, A., et al., *Effect of nature and location of defects on bandgap narrowing in black TiO2 nanoparticles.* Journal of the American Chemical Society, 2012. **134**(18): p. 7600-7603.

137. Lei, F., et al., *Oxygen Vacancies Confined in Ultrathin Indium Oxide Porous Sheets for Promoted Visible-Light Water Splitting.* Journal of the American Chemical Society, 2014. **136**(19): p. 6826-6829.

138. Energy Information, A., *International Energy Outlook 2016.* 2016.

139. *DOE Technical Targets for Hydrogen Production from Electrolysis | Department of Energy.*

140. Walter, M.G., et al., *Solar Water Splitting Cells.* Chemical Reviews, 2010. **110**(11): p. 6446-6473.

141. Trasatti, S., *Work function, electronegativity, and electrochemical behaviour of metals.* Journal of Electroanalytical Chemistry and Interfacial Electrochemistry, 1972. **39**(1): p. 163-184.

142. Cherevko, S., et al., *Dissolution of Platinum in the Operational Range of Fuel Cells.* ChemElectroChem, 2015. **2**(10): p. 1471-1478.

143. Millet, P., M. Pineri, and R. Durand, *New solid polymer electrolyte composites for water electrolysis.* Journal of Applied Electrochemistry, 1989. **19**(2): p. 162-166.

144. Rasten, E., G. Hagen, and R. Tunold, *Electrocatalysis in water electrolysis with solid polymer electrolyte.* Electrochimica acta, 2003. **48**(25-26): p. 3945-3952.

145. Slavcheva, E., et al., *Sputtered iridium oxide films as electrocatalysts for water splitting via PEM electrolysis.* Electrochimica Acta, 2007. **52**(12): p. 3889-3894.

146. Boodts, J. and S. Trasatti, *Hydrogen evolution on iridium oxide cathodes.* Journal of applied electrochemistry, 1989. **19**(2): p. 255-262.

147. Chen, L., D. Guay, and A. Lasia, *Kinetics of the Hydrogen Evolution Reaction on RuO2 and IrO2 Oxide Electrodes in H 2 SO 4 Solution: An AC Impedance Study.* Journal of The Electrochemical Society, 1996. **143**(11): p. 3576-3584.

148. Vidales, A.G. and S. Omanovic, *Evaluation of nickel-molybdenum-oxides as cathodes for hydrogen evolution by water electrolysis in acidic, alkaline, and neutral media.* Electrochimica Acta, 2018.

149. Vidales, A.G., K. Choi, and S. Omanovic, *Nickel-cobalt-oxide cathodes for hydrogen production by water electrolysis in acidic and alkaline media.* International Journal of Hydrogen Energy, 2018.

150. Kötz, E.R. and S. Stucki, *Ruthenium dioxide as a hydrogen-evolving cathode.* Journal of Applied Electrochemistry, 1987. **17**(6): p. 1190-1197.

151. *International Energy Outlook 2016 - Energy Information Administration.*

152. Cherevko, S., et al., *Oxygen and hydrogen evolution reactions on Ru, RuO2, Ir, and IrO2 thin film electrodes in acidic and alkaline electrolytes: A comparative study on activity and stability.* Catalysis Today, 2016. **262**: p. 170-180.

153. Balko, E. and P. Nguyen, *Iridium-tin mixed oxide anode coatings.* Journal of applied electrochemistry, 1991. **21**(8): p. 678-682.

154. Reetz, M.T., et al., *Preparation of colloidal nanoparticles of mixed metal oxides containing platinum, ruthenium, osmium, and iridium and their use as electrocatalysts.* The Journal of Physical Chemistry B, 2003. **107**(30): p. 7414-7419.

155. Zeng, M. and Y. Li, *Recent advances in heterogeneous electrocatalysts for the hydrogen evolution reaction.* Journal of Materials Chemistry A, 2015. **3**(29): p. 14942-14962.

156. Edwards, P.P., et al., *Hydrogen and fuel cells: towards a sustainable energy future.* Energy policy, 2008. **36**(12): p. 4356-4362.

157. Pauporté, T. and R. Durand, *Impedance spectroscopy study of electrochromism in sputtered iridium oxide films.* Journal of applied electrochemistry, 2000. **30**(1): p. 35-41.

158. Topalov, G., et al., *Preparation and properties of thin Pt–Ir films deposited by dc magnetron co-sputtering.* International Journal of Hydrogen Energy, 2011. **36**(23): p. 15437-15445.

159. Brug, G., et al., *The analysis of electrode impedances complicated by the presence of a constant phase element.* Journal of electroanalytical chemistry and interfacial electrochemistry, 1984. **176**(1-2): p. 275-295.

160. Huot, J. and L. Brossard, *Time dependence of the hydrogen discharge at 70 C on nickel cathodes.* International journal of hydrogen energy, 1987. **12**(12): p. 821-830.

161. Brossard, L. and J.-Y. Huot, *Influence of iron impurities on the time dependence of the hydrogen evolution reaction on platinum cathodes during electrolysis of 30 w/o KOH.* Journal of applied electrochemistry, 1989. **19**(6): p. 882-888.

162. Cobourn, S.L. and E.B. Easton, *The effect of copper contamination at the cathode of Cu-Cl/HCl electrolyzers.* International Journal of Hydrogen Energy, 2017. **42**(47): p. 28157-28163.

163. Brossard, L., *Electrocatalytic performance for alkaline water electrolysis of Ni electrodes electrocoated with Fe or Fe/Mo.* International Journal of Hydrogen Energy, 1991. **16**(1): p. 13-21.

164. McArthur, M., et al., *A binder-free multi-walled carbon nanotube electrode containing oxygen functionalities for electrochemical capacitors.* Electrochimica Acta, 2015. **162**: p. 245-253.

165. Cho, M.-Y., et al., *Electrochemical performance of hybrid supercapacitor fabricated using multi-structured activated carbon.* Electrochemistry Communications, 2014. **47**: p. 5-8.

166. Chen, Y.-M., et al., *A nanostructured electrode of IrOx foil on the carbon nanotubes for supercapacitors.* Nanotechnology, 2011. **22**(35): p. 355708.

167. Inamdar, A., et al., *Chemically grown, porous, nickel oxide thin-film for electrochemical supercapacitors.* Journal of Power Sources, 2011. **196**(4): p. 2393-2397.

168. Pang, S.C., M.A. Anderson, and T.W. Chapman, *Novel electrode materials for thin-film ultracapacitors: comparison of electrochemical properties of sol-gel-derived and electrodeposited manganese dioxide.* Journal of the Electrochemical Society, 2000. **147**(2): p. 444-450.

169. Ganesh, V., V. Lakshminarayanan, and S. Pitchumani, *Assessment of liquid crystal template deposited porous nickel as a supercapacitor electrode material.* Electrochemical and Solid-State Letters, 2005. **8**(6): p. A308-A312.

170. Mastragostino, M., C. Arbizzani, and F. Soavi, *Conducting polymers as electrode materials in supercapacitors.* Solid state ionics, 2002. **148**(3-4): p. 493-498.

171. Xia, X.-h., et al., *Self-supported hydrothermal synthesized hollow Co3O4 nanowire arrays with high supercapacitor capacitance.* Journal of Materials Chemistry, 2011. **21**(25): p. 9319-9325.

172. Shakir, I., et al., *Ultra-thin solution-based coating of molybdenum oxide on multiwall carbon nanotubes for high-performance supercapacitor electrodes.* Electrochimica Acta, 2014. **118**: p. 138-142.

173. Nelson, P.A. and J.R. Owen, *A high-performance supercapacitor/battery hybrid incorporating templated mesoporous electrodes.* Journal of The Electrochemical Society, 2003. **150**(10): p. A1313-A1317.

174. Nam, K.-W., et al., *Synthesis and Electrochemical Investigations of Ni1− x O Thin Films and Ni1− x O on Three-Dimensional Carbon Substrates for Electrochemical Capacitors.* Journal of the Electrochemical Society, 2005. **152**(11): p. A2123-A2129.

175. Nam, K.-W. and K.-B. Kim, *A study of the preparation of NiO x electrode via electrochemical route for supercapacitor applications and their charge storage mechanism.* Journal of the Electrochemical Society, 2002. **149**(3): p. A346-A354.

176. Xie, Y., et al., *Supercapacitor application of nickel oxide–titania nanocomposites.* Composites Science and Technology, 2009. **69**(13): p. 2108-2114.

177. Shakir, I., et al., *Ultrahigh-energy and stable supercapacitors based on intertwined porous MoO3–MWCNT nanocomposites.* Electrochimica Acta, 2011. **58**: p. 76-80.

178. Poonguzhali, R., et al., *Effect of Fe doping on the electrochemical capacitor behavior of MnO2 nanocrystals.* Journal of Power Sources, 2015. **293**: p. 790-798.

179. Thind, S.S., et al., *High-performance supercapacitor based on tantalum iridium oxides supported on tungsten oxide nanoplatelets.* Electrochemistry Communications, 2016. **67**: p. 1-5.

180. Yuan, C.-Z., B. Gao, and X.-G. Zhang, *Electrochemical capacitance of NiO/Ru0. 35V0. 65O2 asymmetric electrochemical capacitor.* Journal of Power sources, 2007. **173**(1): p. 606-612.

181. Lang, X., et al., *Nanoporous metal/oxide hybrid electrodes for electrochemical supercapacitors.* Nature nanotechnology, 2011. **6**(4): p. 232.

182. Vidales, A.G., et al., *The influence of addition of iridium-oxide to nickel-molybdenum-oxide cathodes on the electrocatalytic activity towards hydrogen evolution in acidic medium and on the cathode deactivation resistance.* Electrochimica Acta, 2019.

183. Chang, J., et al., *Liquid-phase synthesized mesoporous electrochemical supercapacitors of nickel hydroxide.* Electrochimica Acta, 2008. **53**(15): p. 5016-5021.

184. Kötz, R., H. Neff, and S. Stucki, *Anodic Iridium Oxide Films XPS-Studies of Oxidation State Changes and.* Journal of The Electrochemical Society, 1984. **131**(1): p. 72-77.

185. Dupin, J.-C., et al., *Systematic XPS studies of metal oxides, hydroxides and peroxides.* Physical Chemistry Chemical Physics, 2000. **2**(6): p. 1319-1324.

186. Li, H., et al., *Amorphous nickel hydroxide nanospheres with ultrahigh capacitance and energy density as electrochemical pseudocapacitor materials.* Nature communications, 2013. **4**: p. 1894.

187. Chuang, C.-M., et al., *Effects of carbon nanotube grafting on the performance of electric double layer capacitors.* Energy & Fuels, 2010. **24**(12): p. 6476-6482.

188. Chuang, C.-M., et al., *Hydrothermally synthesized RuO2/Carbon nanofibers composites for use in high-rate supercapacitor electrodes.* Composites Science and Technology, 2012. **72**(13): p. 1524-1529.

189. Frackowiak, E. and F. Beguin, *Carbon materials for the electrochemical storage of energy in capacitors.* Carbon, 2001. **39**(6): p. 937-950.

190. Jiang, F., et al., *MoO3/PANI coaxial heterostructure nanobelts by in situ polymerization for high performance supercapacitors.* Nano Energy, 2014. **7**: p. 72-79.

191. McArthur, M.A., et al., *A binder-free Ir0. 4Ru0. 6-oxide/functionalized multi-walled carbon nanotube electrode for possible applications in supercapacitors*. The Canadian Journal of Chemical Engineering, 2018. **96**(1): p. 74-82.

192. Rakhi, R., et al., *Substrate dependent self-organization of mesoporous cobalt oxide nanowires with remarkable pseudocapacitance*. Nano letters, 2012. **12**(5): p. 2559-2567.

193. Saji, V.S. and C.-W. Lee, *Potential and pH dependent pseudocapacitance of Mo/Mo oxides-An impedance study*. Electrochimica Acta, 2014. **137**: p. 647-653.